



International scoping study of a future Neutrino Factory and super-beam facility

RAL-TR-2007-24

Detectors and flux instrumentation for future neutrino facilities

T. Abe^a, H. Ahara^a, C. Andreopoulos^b, A. Ankowski^{a,j}, A. Badertscher^c, G. Battiston^d,
A. Blondel^e, J. Bouchez^f, A. Bross^h, A. Buenoⁱ, L. Camilleri^g, J.E. Campana^j, A. Cazes^k,
A. Cervera-Villanueva^l, G. De Lellis^m, F. DiCapua^m, M. Ellis^h, A. Ereditatoⁿ,
L.S. Esgosito^o, C. Fukushima^p, E. Gschwendtner^g, J.J. Gomez-Cadenas^l, M. Iwasaki^h,
K. Kaneyuki^h, Y. Karadzhov^q, V. Kashikhin^h, Y. Kawaf^r, M. Komatsu^s, E. Kozlovskaya^t,
Y. Kudenko^u, A. Kusaka^a, H. Kusunoki^r, A. Longhin^v, A. Marchionni^f, A. Marotta^m,
C. McGrew^w, S. Menary^{h,x}, A. Meregaglia^c, M. Mezzetto^v, P. Migliozzi^m, N.K. Mondal^y,
C. Montanari^z, T. Nakadaira^{aa}, M. Nakamura^s, H. Nakumoto^a, H. Nakayama^a, J. Nelson^{ab},
J. Nowak^{ak}, S. Ogawa^p, J. Peltoniemi^{f,c}, A. Pla-Dalmáu^h, S. Ragazzi^{ad}, A. Rubbia^c,
F. Sanchez^{ae}, J. Sarkamo^{ac}, O. Sato^s, M. Selvi^f, H. Shibuya^p, M. Shozawa^a, J. Sobczyk^{aj},
F.J.P. Soler^{ag}, P. Strolin^m, M. Suyama^r, M. Tanaka^{aa}, F. Terranova^k, R. Tesnov^q,
Y. Uchida^{ah}, A. Weber^{ai,b}, A. Zlobin^h

^a ICRR, University of Tokyo, Tokyo, Japan

^b CCLRC, Rutherford Appleton Laboratory, UK

^c ETH, Zurich, Switzerland

^d INFN Sezione di Milano, Milano, Italy

^e University of Geneva, Geneva, Switzerland

^f CEA/DAPNIA-Saclay & APC Paris

^g CERN, Geneva, Switzerland

^h FNAL, USA

ⁱ University of Granada, Granada, Spain

^j LAL, Univ Paris-Sud, IN2P3/CNRS, Orsay, France

^k Laboratori Nazionali di Frascati dell'INFN, Frascati (Roma), Italy

^l IFIC, University of Valencia and CSIC, Valencia, Spain

^m Università di Napoli Federico II and INFN, Napoli, Italy

ⁿ University of Bern, Bern, Switzerland

^o Laboratori Nazionali del Gran Sasso dell'INFN, Assergi (L'Aquila), Italy

^p Toho University, Funabashi 274-8510, Japan

^q University of Sofia, "St Kliment Ohridski"

^r Hamamatsu Photonics, Japan

^s Nagoya University, 464-01 Nagoya, Japan

^t Sodankylä Geophysical Observatory, University of Oulu, Oulu, Finland

^u INR, Moscow, Russia

^v Università di Padova and INFN, Padova, Italy

^w SUNY Stony Brook, NY, USA

^x York University, Toronto, Ontario, Canada

^y Tata Institute, Mumbai, India

^z Università di Pavia and INFN, Pavia, Italy

^{aa} KEK, Tsukuba, Japan

^{ab} College of William & Mary, Williamsburg, Virginia, USA

^{ac} Centre for Underground Physics Pyhasalmi, Univ of Oulu, Oulu, Finland

^{ad} Università di Milano and INFN, Milano, Italy

^{ae} IFAE, Barcelona, Spain

^{af} Università di Bologna and INFN, Italy

^{ag} University of Glasgow, Glasgow, Scotland, UK

^{ah} Imperial College, London, UK

^{ai} University of Oxford, Oxford, UK

^{aj} Inst. Th. Physics, University of Wrocław, Poland

^{ak} Louisiana State University, Louisiana, USA

The ISS Detector Working Group

Abstract

This report summarises the conclusions from the detector group of the International Scoping Study of a future Neutrino Factory and Super-Beam neutrino facility. The baseline detector options for each possible neutrino beam are defined as follows:

1. A very massive (Megaton) water Cherenkov detector is the baseline option for a sub-GeV Beta Beam and Super Beam facility.
2. There are a number of possibilities for either a Beta Beam or Super Beam (SB) medium energy facility between 1-5 GeV. These include a totally active scintillating detector (TASD), a liquid argon TPC or a water Cherenkov detector.
3. A 100 kton magnetized iron neutrino detector (MINN) is the baseline to detect the wrong sign muon final states (golden channel) at a high energy (20-50 GeV) neutrino factory from muon decay. A 10 kton hybrid neutrino magnetic emulsion cloud chamber detector for wrong sign tau detection (silver channel) is a possible complement to MINN, if one needs to resolve degeneracies that appear in the θ_{13} parameter space.

Contents

1	Introduction	1
1.1	Organization	1
1.2	Main beam and far detector options	1
1.3	Main achievements and open issues	3
2	Beam instrumentation	5
2.1	Flux Control and Resulting Constraints on the Decay Ring Design for the Neutrino Factory	5
2.1.1	Neutrino fluxes from muon decay	5
2.1.2	Absolute flux monitoring	6
2.1.3	Theoretical knowledge of the neutrino fluxes from muon decay	7
2.1.4	Muon polarisation	7
2.1.5	Neutrino fluxes and muon polarisation	10
2.1.6	Effect of beam divergence	11
2.1.7	Summary of uncertainties in the neutrino flux	13
2.2	Flux control for Beta Beams and Super Beams	15
3	Near detectors	16
3.1	Aims	16
3.2	Near detector at a Beta beam and Super Beam	18
3.3	Near detector at a Neutrino Factory	18
3.3.1	Flux normalization and control	19
3.3.2	Cross-sections and parton distribution functions	22
3.3.3	Charm measurements	24
3.3.4	Outlook	26

4	Far detectors	26
4.1	Tracking calorimeters	26
4.1.1	Magnetised iron calorimeters	27
4.1.2	Totally Active Scintillating Detectors	36
4.2	Large Water Cherenkov detectors	37
4.2.1	The present detector design	38
4.2.2	Large underground cavities	40
4.2.3	Photodetector R & D	40
4.3	Liquid Argon TPCs	41
4.3.1	The GLACIER project	43
4.3.2	O ⁻ -axis NuMI or Wide-band Superbeam Detector	45
4.4	Emulsion Cloud Chambers	46
4.4.1	Introduction	46
4.4.2	The Emulsion Cloud Chamber	47
4.4.3	The Magnetized Emulsion Cloud Chamber	48
4.4.4	Conclusion and outlook	54
4.5	Hybrid detectors	54
5	Baseline Detectors and Conclusion	55
A	R & D program	56
A.1	Magnetized Iron Neutrino Detector (MINOS) and Totally Active Scintillator Detector (TASD)	56
A.2	Water Cherenkov detector	57
A.3	Liquid Argon detector	58
A.4	Emulsion Cloud Chamber	58
A.5	Near Detectors	59
B	Large magnetic volumes	59
B.1	Introduction	59
B.2	Conventional Room Temperature Magnets	60
B.3	Conventional Superconducting Coils	61
B.4	High Temperature Magnets	62
B.5	Low Temperature Non-Conventional Superconducting Coils	63
B.6	Superconducting Transmission Line	63
B.7	STL Solenoid Power	65
B.8	Conclusions	65
C	Matter effects	66
D	Low energy cross sections	70
D.1	Neutral current elastic and charge current quasi-elastic interactions	72
D.2	Charge and Neutral Current resonance: single and multi pion production	72
D.3	Neutral and charged current multipion production and deep inelastic interactions	72
D.4	Charge and Neutral Current coherent pion production	73
D.5	The cross-section double ratio	73

1 Introduction

The International Scoping Study (ISS) for a future accelerator neutrino complex was carried out by the international community between NuFact05, Frascati, 21-26 June 2005, and NuFact06, Irvine, 24-30 August 2006. The physics case for the facility was evaluated and options for the accelerator complex and neutrino detection systems were studied. One of the novel characteristics of the ISS with respect to previous studies was the systematic investigation of detector options for future long base line neutrino experiments, as a necessary step towards optimizing the performance of the whole facility. In addition to the study of far detectors it was felt necessary to add a study of the near detectors and instrumentation for the primary beam line. These are crucial to understand the performance of the facilities from the point of view of systematic errors. This applies to the Beta-beam or Neutrino Factory storage ring, or to the Superbeam decay tunnel. Two additional topics of critical relevance for the choice of facility were added to the discussion: matter effect uncertainties and systematic errors due to uncertainties in the cross-sections and efficiencies of low energy neutrino interactions.

1.1 Organization

Following the initial guidelines given at NUFACT05 [1], the working groups have largely built on existing studies to delineate the main avenues where further investigations would be most beneficial, and initiated the required simulation work. The work was carried out in five working groups:

- Segmented magnetic detectors;

- Large Water Cherenkov detectors (WC);

- Large Liquid Argon TPCs (LArTPC);

- Emulsion-based detectors: Emulsion Cloud Chamber (ECC) and Magnetized ECC (MECC);

- Near detector and beam instrumentation.

The important issue of novel detector techniques of common interest (such as Silicon Photo Multipliers and large area photo-detectors) was treated in common dedicated sessions of the working group. Finally, the need of large magnetic volumes required for the neutrino factory detector was considered.

The mandate of the study was to establish a set of baseline detectors to be carried forward for further study. It is clear that accomplishing such a goal would require an extremely tight collaboration between the physics performance group and the detector design group. However a number of choices could be made from known feasibility/cost considerations.

1.2 Main beam and far detector options

The main far detector options are listed below:

1. Single flavour sub-GeV neutrino beams: low energy superbeam and beta-beam. This is the scenario advocated for instance for the ν_{μ} -axis beam from J-PARC,

the SPL superbeam and ${}^6\text{He}$ or ${}^{18}\text{Ne}$ beta-beams at CERN. In this energy range detectors need not be magnetized, quasi-elastic reactions dominate and pion production is small. A very massive water Cherenkov (WC) detector is the baseline option. The small and poorly understood cross-sections, and the low Q^2 of the interactions pose considerable systematic problems which make the design of the near detectors very critical. The possibility to use very large LArTPCs has been envisaged, but the relative merit would need to be better justified, and indications are that this is not the case.

2. Few GeV beams: on-axis and wide band beam and high energy beta-beam. This is what one would obtain with an on-axis NUMI beam or equivalent, wide-band pion/kaon decay beam (WBB) from a 20-50 GeV proton beam, or from a high energy beta-beam, either from high ${}^6\text{He}$ or ${}^{18}\text{Ne}$ or from accelerating higher Q (e.g. ${}^8\text{B}$ or ${}^8\text{Li}$) isotopes. Here the situation is more complex since multipion production becomes common and event identification requires more sophistication. This is not an easy energy domain to work at, and there is not a clear winner in this domain between the WC, the totally active scintillating detector (TASD) (a la NOA), a LArTPC or even an iron-scintillator sandwich.
3. High energy beams from muon decay (Neutrino Factory). Magnetic detectors are compulsory since two leptonic charges of neutrinos are present at the same time. The baseline detector here is the magnetized iron neutrino detector (MIND) for the wrong sign muon ν states, but the full exploitation of the richness of possible oscillation channels strongly motivates the study of other types of detectors: magnetized low Z ν grain detector (scintillator or LAr) for wrong-sign electron ν states, emulsion detector (ECC) for wrong-sign tau detection and magnetized emulsion (MECC) for all the above.

In all three scenarios appropriate near detectors and beam instrumentation are essential. Indeed, the precision era poses new challenges for the flux and cross-section monitoring systems. Appearance measurements require that the product of cross-section times acceptance be measured for the appearance channel in relation to that of initial neutrino flavour. This is a major difficulty for the conventional pion decay superbeam, since little instrumentation can be installed to monitor the secondary flux of mesons in a high intensity environment; there is a clear need for specific hadro-production experiments backed up with fine grained near detectors, to measure precisely $\sigma(\nu\mu)$, $\sigma(\nu e)$ and $\sigma(\bar{\nu}e)$, topological cross-sections. The issue is much easier for the beta-beam or the neutrino factory, where the stored parent beam can be monitored precisely and the known decay provides a potentially well known flux. In addition, purely leptonic reactions can be used as absolute candles. A new domain of precision cross-section measurements at the 10^{-3} level opens up. Of course a detailed simulation and study of the near detector station and of the associated near detectors and beam instrumentation is required to firm up these claims.

More details and the presentations can be found on the detector study web site [2]. The physics performance¹ and the sensitivity to the oscillation parameters of the different far detectors (and combinations) can be found in the ISS Physics Report [3].

¹Including signal and background efficiencies in some cases

1.3 Main achievements and open issues

Given that this study is not the first one, it is worthwhile emphasizing in this introduction what is the new information content, and what are the issues which remain open after its completion.

The main achievements or new information gathered through this study are as follows.

A Magnetized Iron Neutrino Detector (MIND) of 100 kton should be feasible for a hardware cost of 200 M €.

The threshold for muon detection in an optimised MIND can be lowered down to 1-3 GeV/c for a dominant background of wrong charge assignment of $O(10^{-3})$. The efficiency above 5 GeV can be set to 70%.

A large air-core coil can be envisaged to host 20-30 kton of fully active fine grained detector (scintillator, LAr or emulsion) for a reasonable cost ($O(100 \text{ M } \text{€})$).

The muon detection threshold can be further lowered down to 0.4 GeV=c using a Totally Active Scintillating Detector (TASD). This detector should be able to measure the charge of the muon with a negligible mis-identification rate ($O(10^{-5})$) for muons above 0.4 GeV=c.

A MECC of 10 kton can be designed, which, thanks to the exquisite space and angle resolution of the emulsion, can measure electron and muon charge and momentum up to 10 GeV.

The first studies of very large underground excavations have been pursued and cost estimates for a megaton WC detector have been given.

A revolution in photo-detection has been brought forward in the last few years with the appearance of new type of avalanche-photodiode-arrays (SiPMs of MPPCs).

In the context of the LArTPC-Glacier project the operation of a (small) LArTPC in a magnetic field was achieved and a commercial company has produced a feasibility study of a LNG tanker for 100 kton LAr. There is a very active R&D program to study i) a two phase detector with very long drift paths, ii) novel charge readout and HV supply and iii) drift properties at high pressure.

A large LArTPC (15 to 50 kton) is being considered in the US as the detector for a long-baseline ν_e appearance experiment. The efficiency for detecting ν_e 's in such a detector is 80-90% with a negligible neutral-current ν_0 event background. An ambitious R&D program was approved in 2005 and is underway.

Matter effects can be calculated rather precisely down to a matter density uncertainty of about 2% or better, but a dedicated geological study has to be foreseen once the site has been chosen. A few particular baselines encountering very irregular terrain should be avoided.

A first estimate was performed of the interplay of ν mass, nuclear effects, and non-isoscalar target (water) with the conclusion that at a few 100 MeV they impact measurements of CP asymmetries by several percent. This effect decreases with energy

for the quasi-elastic reaction, and at higher energy may affect also the pion production channel. Detector effects have not been studied yet.

The detectors can take alternative trains of neutrinos produced by stored positive and negative muons as long as the time distance between trains is above 100 ns.

Nevertheless many issues remain open for further study and R & D. A few outstanding points are listed below.

For what concerns the neutrino factory detectors:

Priority should be given to a solid study of performance, cost estimate and infrastructure requirements of the baseline detector for the neutrino factory (MIND) and of its variants (such as the Indian Neutrino Observatory, INO).

The performance of the TAsD detector against hadronic backgrounds should be computed. Pion decay and pion/muon mis-identification could be important given the low detector density.

The study of the large coils and associated infrastructure for the above has only started and this is clearly a field that motivates further studies. The super-conducting transfer line (STL) is probably the most promising option for large magnetic volumes at reasonable cost. A full engineering design would still need to be done.

The comparative performance study of 'platinum detectors' should be pushed to a conclusion. Efficiency vs charge confusion background for the electron channel for different setups (MECC, TAsD or LAr) needs to be understood and compared.

The monitoring of the muon beam angular divergence in the storage ring is for the moment a very challenging concept (a He Cherenkov with extremely thin windows) that needs to be turned into a demonstrably feasible object. It is not clear that a permanent device can be devised or if a different system needs to be invented.

The near detector concepts and the near detector area for the neutrino factory needs to be defined, including in a coherent way the necessary shielding and of the purely leptonic detector and DIS-charm detector.

Once a site is considered a study of the matter content of the beam line will be mandatory.

For what concerns the low energy beta-beam and superbeam detectors:

The priority is rightly given to understanding the feasibility and cost of the Mton-class water Cherenkov detector, in order to exploit the synergy with proton decay and supernovae neutrino detection.

How shallow can a LArTPC be operated? This was recently studied [74] for shallow depths (< 200 m depth) but it would be good to understand the status for surface operation.

Whether a giant LArTPC can usefully compete in this energy range should be ascertained more quantitatively, while the cost and infrastructure/safety implications of it is largely uncertain.

The design and even the concept of the near detector station { and the problems related to the relative normalization of the beta-beam and superbeam when used in combination { have not really been addressed and constitute one of the major pending issues in addressing the physics capabilities of this option. There are also fundamental issues associated with doing physics with low energy events: the effects of lepton mass, nuclear effects, Fermi motion and binding energy are some, but the different topologies and their effect on relative acceptance for ν_μ vs ν_e events remains largely untouched. At this point in time any claim of normalization errors (even relative) below 5% remains unestablished.

2 Beam instrumentation

2.1 Flux Control and Resulting Constraints on the Decay Ring Design for the Neutrino Factory

One of the most significant qualities of the Neutrino Factory, and more generally of a system where one stores a beam of decaying particles (such as the beta beam) is the potential for excellent neutrino flux control. The main parameters that govern the systematic uncertainties on the neutrino fluxes are as follows.

- The monitoring of the total number of muons circulating in the ring,

- Theoretical knowledge of the neutrino fluxes from muon decay, including higher-order radiative effects,

- Knowledge of the muon beam polarisation,

- Knowledge of the muon beam energy and energy spread,

- The muon beam angle and angular divergence.

Beam shape parameters are crucial for the measurement of oscillation length, while the absolute normalization is essential for the measurement of the mixing angle. The relative normalization of the two muon charges plays a crucial role in the measurement of CP asymmetries.

2.1.1 Neutrino fluxes from muon decay

The neutrino energy spectra from negative muon decay at rest follow the following distributions:

$$\frac{d^2N}{dx d\theta} / \frac{2x^2}{4} [(3 - 2x) + (1 - 2x)P \cos \theta] \quad (1)$$

$$\frac{d^2N}{dx d\theta} / \frac{12x^2}{4} [(1 - x) + (1 - x)P \cos \theta] \quad (2)$$

where $x = 2E_\nu/m_\mu$, P is the muon polarisation, and θ is the angle between the muon polarisation vector and the neutrino direction. In a long baseline experiment the detector is located on the same axis as the Lorentz boost and its size is negligible relative to the baseline. In this case the neutrino energy spectrum in the laboratory frame is given by the same formula as above but with $x = E_\nu/E_\mu$.

2.1.2 Absolute flux monitoring

Monitoring the total number of muons in the ring can be done in a number of ways. The total beam current can be estimated using a Beam Current Transformer (BCT), the total number of decay electrons can be estimated using an electron spectrometer, the product of the flux and cross section can be inferred from a near-by detector and, finally, the absolute normalisation can be obtained from semi-leptonic neutrino interactions in a nearby detector.

The operation of a BCT in the decay ring could provide fast-response monitoring of the muons in the ring. There are, however, a few potential difficulties that could limit the precision of such a device, which could normally reach the 10^{-3} level. The first one is the presence of decay electrons in the ring, along with the muons. Since all muons decay, the number of accompanying electrons could potentially be much larger than the remaining muons after a few muon lifetimes. A study of such decay electrons has been made [4], with the conclusion that for 50 GeV muon momentum, the decay electrons are lost in the beam elements (or the collimators placed to protect them) after less than half a turn, either because they are momentum-mismatched or because they lose energy in the arcs by synchrotron radiation. Consequently their number should be always less than about 2×10^{-3} of the remaining muons. In addition, most of the losses arise in the straight sections or in the early part of the arcs, so that a BCT situated just at the beginning of a straight section would see an even smaller fraction of them. Another worry could be the existence of a moving electron cloud created by beam-induced multipacting, or by ionization of the residual gas or of the chamber walls. This has been studied in [5], with the conclusion that the electron cloud will be several orders of magnitude less than the muon flux itself. In the absence of a significant parasitic current, it can be concluded that the BCT readings should be precise to the level of a few 10^{-3} , or better. This seems the most practical way to compare the flux induced from μ^+ and decays.

The decay electrons will be used to measure the polarisation of the beam with a spectrometer as described below, and in Fig. 1. The same device could in principle be used to monitor the number of muon decays in an absolute way, especially if one selects the momentum bite where the electron spectrum is insensitive to the muon polarisation. Certainly this will be a useful tool, as a cross-check or for monitoring, but a very detailed study of the dependence of the acceptance of this device on the beam parameters must be performed before a conclusion can be reached.

Knowledge of the flux does not provide knowledge of the cross sections folded with the detector acceptance. This task is traditionally delegated to a near detector. The high flux should make things very easy. Given the high importance of precision measurements in the Neutrino Factory, it is likely that a near detector will be an important tool for beam normalisation. Unlike the situation with conventional pion decay beams, the near detector will in fact be able to measure absolute cross sections for a large number of exclusive and inclusive processes.

It is worthwhile mentioning, finally, the possibility offered by the measurement of purely leptonic interaction processes, which have been discussed in [6]. Of practical interest for normalisation is the measurement of $\mu^+ \rightarrow e^+ \nu_\mu + e^-$, which appears as a low-angle forward-going muon with no recoil. Using the standard electroweak theory, this purely leptonic charged-current process can be calculated with high precision, and could be measured with a dedicated detector aimed at measuring also the $e^+e^- \rightarrow e^+e^- \nu_e + e^-$ and $e^+e^- \rightarrow e^+e^- \nu_e + e^-$ processes. The weakness of this method is that it only applies to the decay beam, but it

muon polarimeter

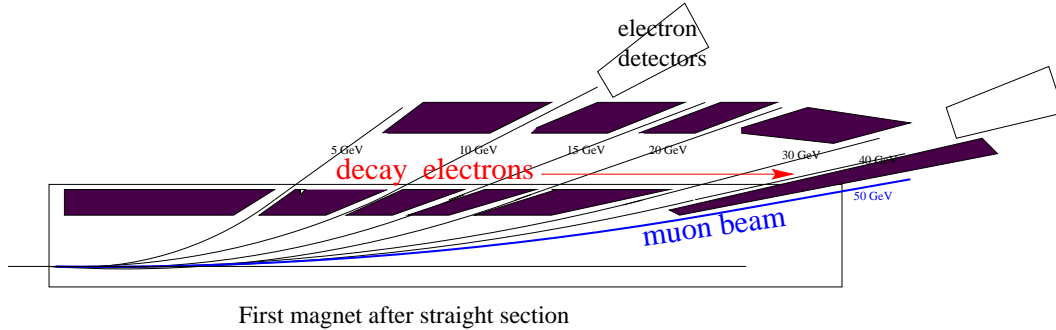


Figure 1: A possible muon polarimeter design. The momenta of the decay electrons accumulated in a short straight section are analysed in a bending magnet in the muon decay ring. Slits in the shielding define the acceptance of a number of momentum bins.

could be seen as an overall absolute normalisation process for the muon flux.

To conclude, there are many tools to monitor and control the absolute flux normalisation in a neutrino factory, so that the near detectors should be able to provide very accurate measurements of inclusive and exclusive cross sections, within the detector acceptance. A flux normalisation at the level of a few 10^{-3} seems an achievable goal. The relative normalisation of the μ^- and μ^+ decay beams should be known with similar precision.

2.1.3 Theoretical knowledge of the neutrino fluxes from muon decay

The expressions given above for the neutrino flux in muon decay, (equations 1 and 2), do not include QED radiative corrections, which have been calculated in [7] (see Fig. 2). The dominant source of corrections is, as can be expected, related to photon emission from the decay electron. For the electron energy distribution, the corrections are of the order of 1% due to terms proportional to $-\ln(\frac{m}{m_e})$. It turns out that the neutrino spectrum is insensitive to the electron mass, i.e., the integration over the system of electron and photons cancels mass singularities. It can be seen that, in the forward direction, an overall decrease of the neutrino flux of about $4 \cdot 10^{-3}$ is observed, with a larger decrease near the end point. The global decrease can be understood by the overall softening and angular widening of the neutrino decay spectrum due to photon emission. Since the overall size of the corrections is small, one can certainly trust the calculated spectrum to a precision much better than 10^{-3} .

2.1.4 Muon polarisation

Muons are naturally polarised in pion decay. In the $\pi^+ \rightarrow \mu^+ \nu_\mu$ rest frame, both the μ^+ and ν_μ have negative helicity. In the laboratory frame, the resulting average helicity of the muon, or longitudinal polarisation, is reduced from -100% for a pion at rest to $\langle h \rangle = -18\%$ for pions above 200–300 MeV momentum [13]. For a pion of given momentum, muon polarisation is correlated with muon momentum. It has been argued in [14] that monochromatisation of the pions followed by i) a drift space to separate muons of different momenta, and ii) collection

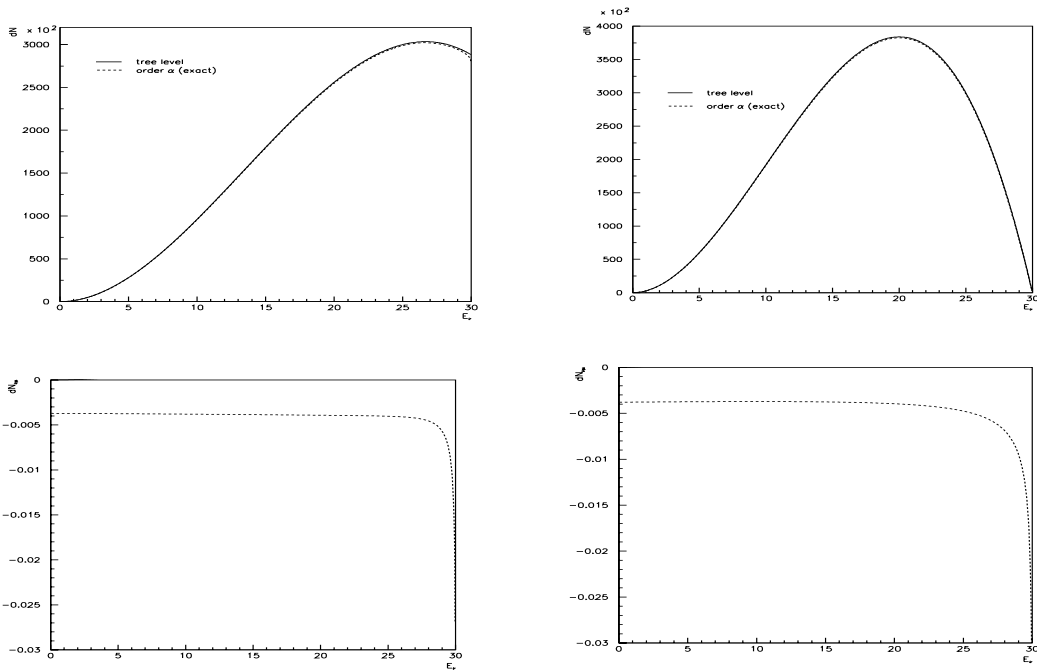


Figure 2: Radiative corrections to the muon neutrino (left panels) and electron anti-neutrino (right panels) fluxes in muon decay. Top panels: the resulting energy distribution at zero angle. Bottom panels: the relative change due to the $O(\alpha)$ correction. The overall reduction of muon neutrino flux is due to the additional energy taken away by photons, which slightly widens the angular distribution of the neutrinos. In order to avoid infinities at the end point, the quantity plotted is $\frac{O(\alpha) - 0}{(O(\alpha) + 0)}$.

in successive RF buckets, should allow separation in different bunches of muons of different polarisations. This does not change the average polarisation, but creates bunches of different polarisation (up to 50%), that can be of use for physics, as long as the times of neutrino interactions are recorded with a precision of a few nanoseconds.

The muon spin precesses in electric and magnetic fields that are present during cooling and acceleration, but the muon spin tune (the number of additional spin precessions happening when the muon makes a complete turn) is very low:

$$a = \frac{g - 2}{2} \frac{E_{\text{beam}}}{m} = \frac{E_{\text{beam}} \text{ (GeV)}}{90.6223(6)} :$$

It has been evaluated [13] that 80 to 90% of the original polarisation will survive all muon handling up to the injection into the storage ring. Its orientation will depend on the number of turns that the muons encounter along the accelerator chain, and can be arranged to be longitudinal by an appropriate choice of geometry and of the energies in the recirculating linacs [12]. As we will see, this is not necessarily important.

What will happen to the muon polarisation in the decay ring depends in the first instance on whether its geometry is a ring (race track or triangle) in which the muons undergo one rotation per turn, or a bow-tie, in which the muon undergoes zero net rotation at each turn.

In the case of a ring, the polarisation will precess. The orientation of the polarisation vector will be rotated with respect to the muon direction by an angle which increases each turn by 2π . Unless the energy is chosen very carefully, it will not be aligned, and reduced on average by a factor 2. At a muon energy of precisely $E = 45311 \text{ GeV}$, the spin tune is 0.5 and the polarisation flips during each turn. This would allow the most powerful use of the polarisation for physics purposes, but absolutely requires that the orientation is correctly chosen at injection, a condition which is otherwise unnecessary in a ring geometry. If no special measure is taken, however, depolarisation will occur, since particles of different energies will have their spins precess with different spin-tunes.

The muon polarisation can be monitored by momentum analysis of the decay electrons, as discussed in [8], in a polarimeter that could look like that sketched in Fig. 1. One can expect that this measurement will be difficult: the relative normalisation of electron rates in the different energy bins will depend on various muon beam parameters such as its exact angle and divergence, and on a precise modelling of the beam-line geometry. In a ring geometry, the device will be exposed to a succession of negative and positive helicity muon bunches, so it will have to perform relative measurements. These should be sensitive to small effects, with a relative precision of a few percent.

The spin precession in a storage ring provides a means of high precision (10^{-6} or better) for energy calibration [9]. As shown in [8], the measurement of the depolarisation can be used to measure the energy spread with high precision. In this case, the combined effect of precession and depolarisation ensure that the muon polarisation integrated over all averages out to zero with an excellent precision: simulations show that any residual polarisation is less than 4×10^{-4} .

Depolarisation can be avoided, if the storage ring is equipped with an RF system that ensures that the muons undergo synchrotron oscillations [12]. By doing this, one loses the possibility to measure the energy spread from the depolarisation, but one can maintain the muon polarisation. The average is still essentially zero, but by recording the exact time of neutrino events, one can infer their bunch number and turn number, and deduce the polarisation of the decay muons. In a ring geometry either mode of operation is left open, if one can run with the required RF system on or off.

In the case of a bow-tie, the muons will not depolarise: spin precession is zero no matter what the muon energy is. This configuration is not as convenient as the ring for several reasons.

In a bow-tie geometry, there will be no spin precession, so the energy and energy spread of the muon beam will not be calibrated.

The polarisation will not average to zero and one will have to measure it based on the measured electron spectrum. A few percent absolute accuracy seems to be very challenging in this case, which means that the flux determination will be affected by a sizeable uncertainty, due to the beam polarisation error.

It will be difficult to change the sign of the muon beam polarisation.

Unless the geometry is very carefully chosen, the beam polarisation will be different for the two long straight sections.

For these reasons, and despite the fact that in principle the useful beam polarisation is higher in the bow-tie geometry, the ring geometry is preferred from the point of view of beam control.

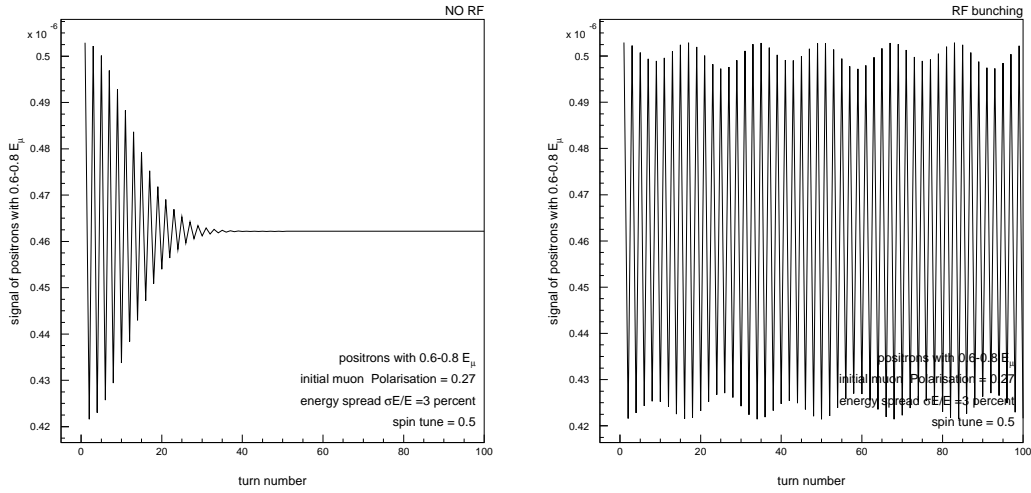


Figure 3: Oscillation with turn number in a plot of the number of electrons in the energy range $0.6-0.8 E_{\mu}$, normalised to the total number of muon decays during the given turn. The oscillation amplitude is a measure of the beam polarisation, its frequency a measure of the beam energy, and, if there is no RF bunching, its decrease with time is a measure of energy spread. The muon lifetime corresponds here to 300 turns. The beam energy is $E_{\mu} = 45.311 \text{ GeV}$ and the energy spread is 3×10^{-2} . On the left, there is no bunching RF in the muon storage ring, on the right there is RF bunching with $Q_s = 0.03$.

2.1.5 Neutrino fluxes and muon polarisation

Neutrino spectra with different beam polarisations are given by equations 1 and 2. In a long-baseline experiment, one is at extremely small angles, so that $\cos \theta = 1$. In this case, the $\bar{\nu}_e$ component of the beam is completely extinct for $P = 1$. This is due to spin conservation in the decay: a left-handed muon cannot decay at zero angle into a right-handed $\bar{\nu}_e$.

Event numbers can readily be obtained by multiplying by the cross section. They are shown in Fig. 4 for a 10 m radius detector 20 m long situated 730 km away. Since the neutrino and anti-neutrino cross sections are in the ratio 1/0.45, negative muons provide enrichment in $\bar{\nu}_e$ and positive ones in ν_e .

It is clear from Fig. 4 that the combination of muon sign and polarisation allows large variations in the composition of the beam, in a controlled way. Since detector studies show that the muon sign can easily be determined in a charged-current (CC) (anti)neutrino event, but that the electron sign is much more difficult, we have tried to use the variation of electron neutrino flux with muon polarisation to infer a signal of ν_e oscillations to be compared (for a T-violation test) with the $\bar{\nu}_e$ oscillation measured with the wrong-sign muons. Unfortunately, even for 40% beam polarisation, the improvement in the sensitivity to CP/T violation is no more than the equivalent of a factor of 1.5 to 2 in statistics. Certainly, it appears that polarisation is more useful as a tool to measure the beam properties than as a physics tool. Nevertheless, these statements might be parameter-dependent, and should be revisited once the oscillation parameters are better known.

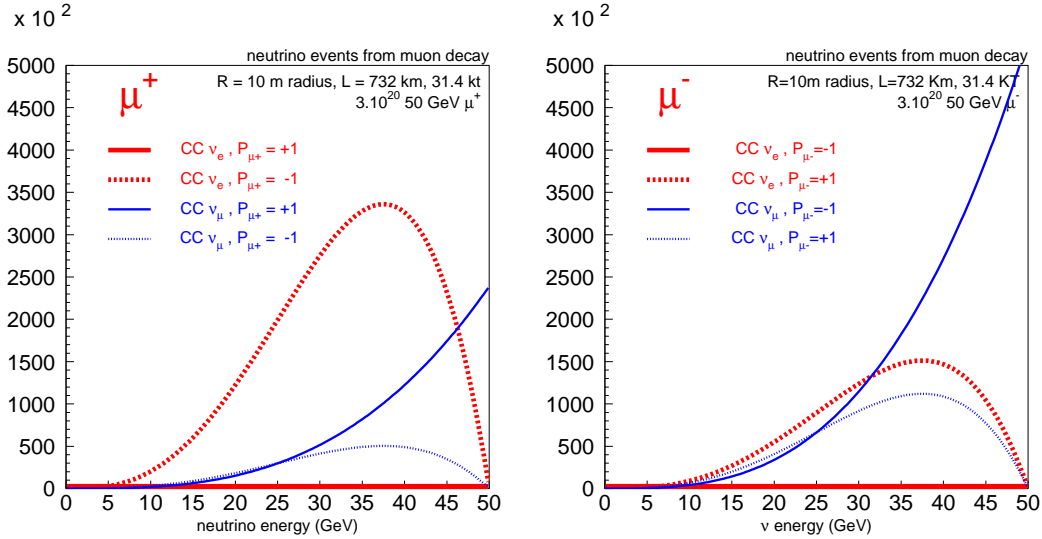


Figure 4: Event numbers for a detector of density 5 with 10 m radius that is 20 m long, situated 732 km away from the muon storage ring, for μ^+ (left) and μ^- (right) beams of 50 GeV. Full lines show the spectra for the ‘natural’ helicity $P = +1$ for μ^+ , and dashed ones for the opposite case. The $CC \nu_e$ for μ^+ with $P = +1$ and $CC \nu_e$ for μ^- with $P = -1$ are not visible, because the fluxes are almost exactly zero. The vertical axis gives event numbers per bin of 250 MeV. This plot assumes no muon beam angular divergence and no beam energy spread.

2.1.6 Effect of beam divergence

The opening angle of the neutrino beam is typically $\theta = \frac{m}{E}$, where $m = E \theta$. As soon as the beam divergence is comparable with this natural opening angle, a large fraction of the flux will be lost. This is shown for 45.311 GeV muons in Fig. 5. It is clear that beam divergence results in a loss of events, and in a sizeable distortion of the spectra and of their muon polarisation dependence. A beam divergence not larger than $\theta_x = \theta_y = 0.2m/E$ seems to be desirable, if one wants to avoid a large sensitivity of physics results upon the experimental determination of the muon beam parameters.

This effect has been studied more precisely in [10], where event numbers are calculated for various polarisations and divergences. The impact of the muon beam divergence on the neutrino event rate can be seen in Fig. 6. The first conclusion one can draw from these plots is that, for a given number of muons, the highest flux is obtained for smallest muon beam divergence. In order to keep the event rate loss due to the muon beam divergence below 5%, the divergence should be close to $\theta = 0.1m/E$.

From the curves in Fig. 7, one can determine the relative error of the predicted event rate, given the uncertainty in the knowledge of the beam divergence itself. For example, if the beam divergence is $\theta = 0.1m/E$ and is known with a relative precision of 10%, the ν_e and ν_μ event rates can both be predicted with an accuracy of about 0.75%. For a divergence of $\theta = 0.2m/E$, the uncertainty on the flux would be 2.5%. As we will see, however, the knowledge of the beam divergence is unlikely to be a constant relative fraction.

One can turn the argument around, and request that the beam divergence be $\theta = 0.1m/E$ and

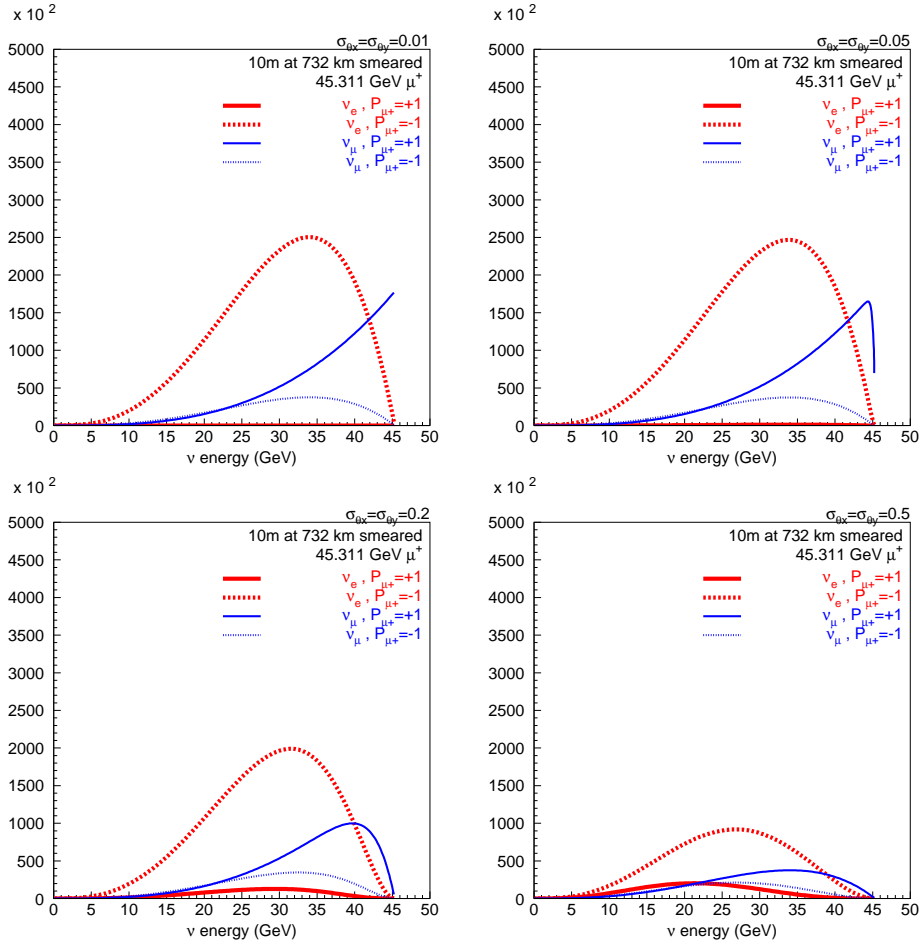


Figure 5: Neutrino event spectra for different beam divergences; Upper left: $\sigma_x = \sigma_y = 0.01 \text{ m} = E$; upper right: $\sigma_x = \sigma_y = 0.05 \text{ m} = E$; lower left: $\sigma_x = \sigma_y = 0.2 \text{ m} = E$; lower right: $\sigma_x = \sigma_y = 0.5 \text{ m} = E$. It is clear that beam divergence results in a loss of events, and in a sizeable distortion of the spectra and of their muon polarisation dependence.

known to a relative precision of 1.5% , so that the corresponding uncertainty on μ_x is only 10^{-3} . It is clear that in this case the muon beam divergence will need to be measured. For a beam of 50 GeV , the beam divergence is 200 micro-radians and the requirement is that it should be known to 3 micro-radians.

As a measurement device, one could imagine a gas Cherenkov detector focusing the Cherenkov radiation in such a way as to make an image of the muon beam direction, as sketched in Fig. 8. This has been studied in [11], with the conclusion that for 200 micro-radians divergence, a precision of a few % can be achieved. The additional multiple scattering introduced by the device leads to a growth of emittance during the muon fill, by a few tens of micro-radians, which is small and will be measured. Since the resolution is dominated by optical imperfections, diffraction effects and heating effects in the gas of the Cherenkov detector, they act as an additional experimental smearing σ_{exp} added in quadrature to the true beam divergence σ_{beam} . In the scheme of Fig. 8, the largest effect is optical diffraction,

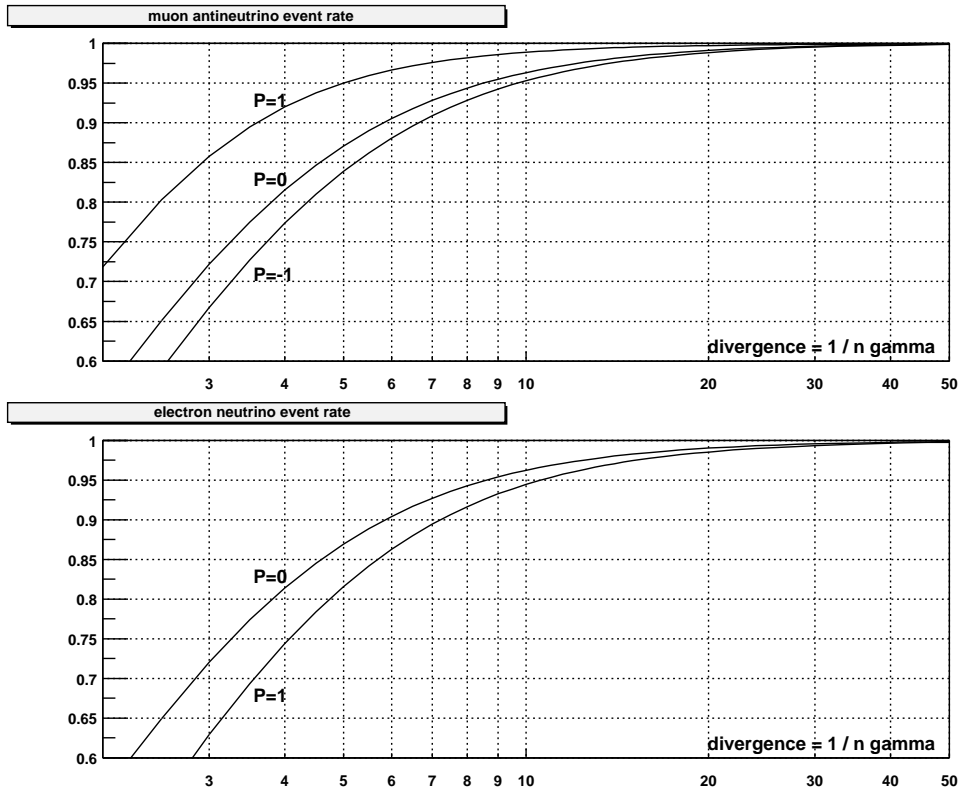


Figure 6: The relative event rates for muon anti-neutrinos (top) and electron neutrinos (bottom), for various polarisation values as a function of the beam divergence, parametrised as $1/n$.

which amounts to 30 micro-radians. It is easy to show that the correction for experimental resolution is $\frac{\text{beam}}{\text{beam}} = \frac{\text{exp}}{\text{exp}} \frac{\text{exp}}{\text{beam}}^2$;

This makes the beam divergence progressively harder to measure as it becomes smaller. Assuming that the experimental error is 30 micro-radians and is known with a precision of 30% of its value, the above gives a flux uncertainty of $5 \cdot 10^{-4}$, more or less independent of the beam divergence in the range of 0.05 to 0.2.

In conclusion, the requirement that the beam divergence be no greater than 0.1 ensures that the corrections and uncertainties to the neutrino fluxes remain small (below 1%), even if one should rely on the accelerator properties themselves. In order to achieve a higher precision a direct measurement of the beam divergence will be necessary (and is probably feasible). If relaxing this condition would allow a larger muon flux, a divergence measurement device becomes mandatory, and would ensure that the uncertainty on the neutrino flux remains well below 10^{-3} .

2.1.7 Summary of uncertainties in the neutrino flux

A first look has been given to the sources of systematic uncertainties in the neutrino fluxes and their possible cures.

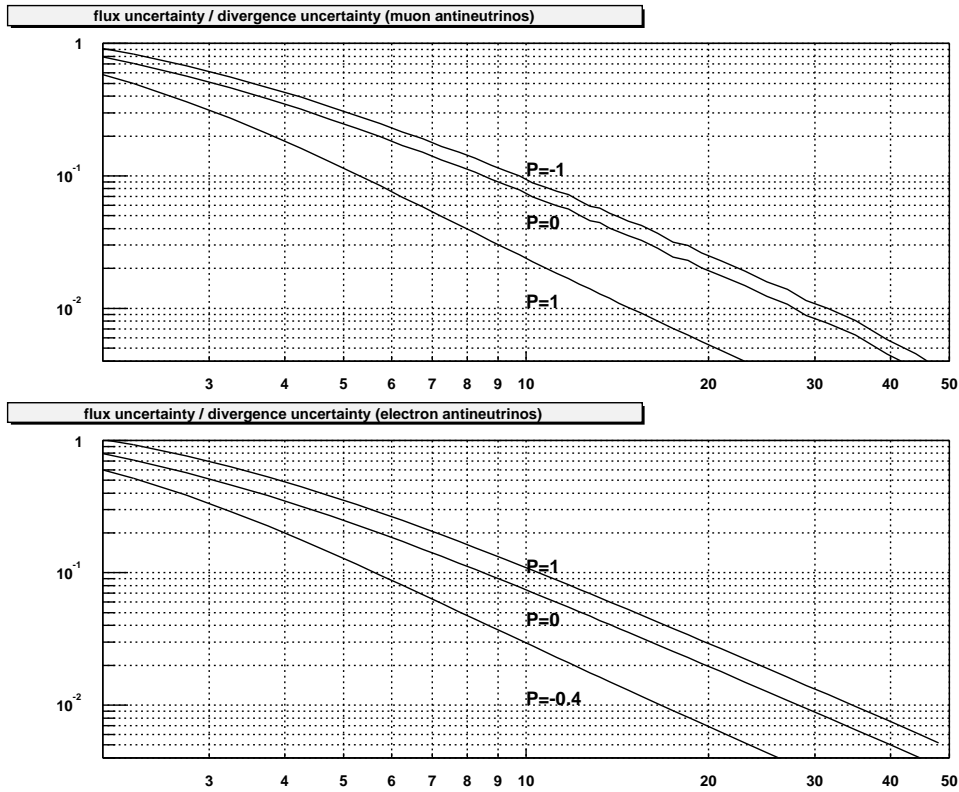


Figure 7: The ratio of the uncertainty in the event rate over the uncertainty in the muon beam divergence as a function of the beam divergence, parametrised as $l=n$. The top (bottom) plot corresponds to muon anti-neutrinos (electron neutrinos).

The monitoring of the total number of muons circulating in the ring can be inferred from a Beam Current Transformer with a precision of the order of 10^{-3} or better. The decay electrons vanish quickly and are not a problem.

The theoretical knowledge of the neutrino fluxes from muon decay is not an issue. Radiative effects have been calculated: they amount to around $4 \cdot 10^{-3}$, with an error that is much smaller [7].

The muon beam polarisation determines the flux directly, both in shape and magnitude. It seems delicate to determine its value with a precision much better than a few %. In a ring geometry, however, polarisation precesses and averages out with high precision (a few 10^{-4}). This is a strong argument in favour of a ring geometry against a bow-tie geometry.

The event rate varies like the muon beam energy to the third power, but the muon beam energy can be inferred very precisely from the muon spin precession. A polarimeter idea has been outlined, and the measurement should cause no difficulty. Beam polarisation can be preserved if an RF system is installed in the decay ring. The energy spread can be derived from the depolarisation pattern, in special runs with no RF if necessary.

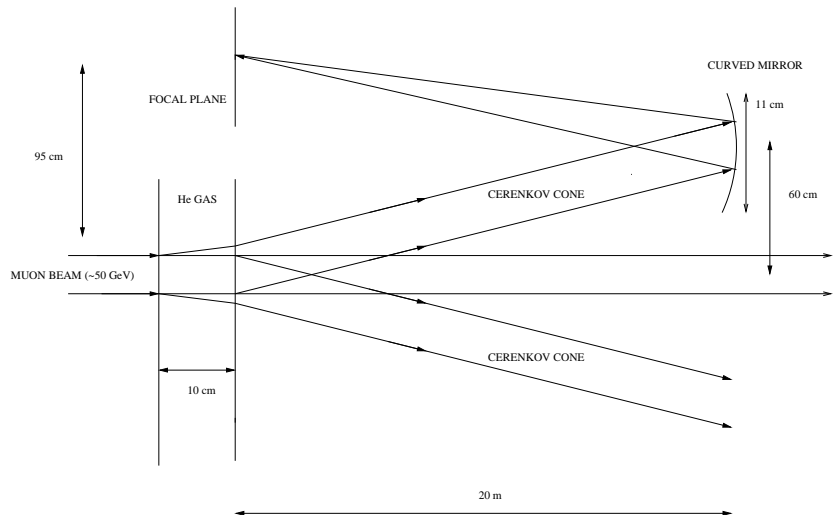


Figure 8: Schematic of a muon beam divergence measurement device. A low-pressure He gas volume is contained by windows (one of which must be transparent) within a straight section of the muon decay ring. The Cherenkov light is collected by a parallel to point optics in the direction of interest, so as to provide an image of the angular distribution of particles in the focal plane.

The muon beam angle and angular divergence have an important effect on the neutrino flux. For a given number of muons, the smaller the beam divergence, the higher the flux. Thus the beam divergence in the straight section of the muon decay ring should be made as small as possible, but should not constitute a limit on the number of stored muons.

Measurement devices for the beam divergence will be necessary, but they can probably be designed and built to ensure a flux uncertainty below 10^{-3} .

In addition, the near detector stations should allow measurements of cross sections with high precision. The inverse muon decay reaction $\mu + e \rightarrow \nu + e + \nu$ offers the possibility of an absolute normalisation of the flux.

We conclude that, provided the necessary instrumentation is foreseen, the Neutrino Factory flux should be known with a precision of the order of 10^{-3} .

2.2 Flux control for Beta Beams and Super Beams

The International Scoping Study did not explicitly look at flux control and beam instrumentation for Beta beam and Super Beams. However, some of the concepts developed in the context of a Neutrino Factory are applicable to a Beta Beam. Similar requirements for flux control are needed at a Beta beam facility as for a Neutrino Factory. Polarization of the beam is not an issue in a Beta Beam, but the number of radioactive ions in the storage decay ring can be determined with a Beam Current Transformer. The divergence of the beam would need to be measured as well. A Cherenkov detector as proposed above for a Neutrino factory would be able to measure the divergence of a Beta Beam, provided that it did not affect the

stability of the beam. In addition to these beam monitoring devices, a near detector would also be needed (see section 3).

There is extensive experience in the design of conventional beams of neutrinos from pion decay, so understanding the flux control requirements for these beams will determine the parameters needed for beam monitoring at a Super Beam. Recent examples include the MINOS beam line [17], the CERN to Gran Sasso (CNGS) beam [15] and the beam line for the T2K experiment [20].

The NUMI beam at Fermilab [17] that supplies neutrinos for the MINOS experiment [16] contains a system for flux monitoring of the neutrino beam. The monitoring system presently consists of ionization chambers [18] placed at the end of the decay pipe, to measure muons, undecayed mesons, and protons that did not react in the target, and in three alcoves dug into the dolomite rock to measure fluxes of muons that are produced along with the neutrinos. These chambers provide information to determine the neutrino beam alignment and as a beam monitor, to ensure target integrity and horn focusing.

The CERN to Gran Sasso (CNGS) neutrino beam, with an average energy of 17.4 GeV [19], is well matched to the appearance experiments at the Laboratori Nazionali del Gran Sasso (LNGS), OPERA [90, 91] and Icarus [67]. A misalignment of the horn by 6 mm or the rector by 30 mm, or if the proton beam is off-target by 1 mm, or if the CNGS beam is misaligned by 0.5 mrad, may cause a drop in neutrino flux of 3%. Monitoring of these parameters is achieved by the Target Beam Instrumentation Downstream (TBID) and the muon ionization chambers installed in the muon pits downstream of the beam stop. The TBID contains secondary emission monitors, consisting of 12 μ m thick titanium foils, and check the efficiency of the target conversion (by comparison with an upstream station) and the alignment of the beam. The muon ionization chambers measure the muon intensity, the muon profile and the centre of the beam. There are 17 fixed monitors in a cross, and one moveable chamber for relative calibration. Since OPERA and Icarus plan to perform an appearance search for tau neutrinos, it is not as important to measure the flux with a similar precision to a disappearance measurement. Hence, a near detector at the CNGS was not deemed to be an essential component of the beam line and was not built given the cost of a near cavern.

The T2K experiment [20] exploits an off-axis beam at angles between 2 and 3. It monitors the muon flux on-axis, downstream from the beam dump, and serves as a real-time status monitor sensitive to the proton intensity, proton beam position on target and the performance of the horn. The detectors will be a combination of He gas ion chambers and semiconductor detectors. In addition, there will be an on-line neutrino flux monitor, in the form of an array of iron-scintillator stacks, to determine the centre and profile of the on-axis neutrino beam. From the on-axis muon and off-axis flux monitors, one can deduce the off-axis flux, which will be compared with the ND 280 (Near Detector at 280 m from the target) [21, 22]. A similar strategy would probably have to be adopted for any other off-axis super beam scenario.

3 Near detectors

3.1 Aims

In order to perform measurements of neutrino oscillations at a neutrino facility, it is necessary to establish the ratio of neutrino interactions in a near detector with respect to the far detector.

Hence, the careful design of a near detector and of the beam instrumentation is crucial to measure the flux, energy and cross-sections of the incident neutrinos [23] to be able to reduce the long baseline neutrino oscillation systematic errors.

The present generation of near detectors (e.g. for K2K and MINOS) have been concentrating on disappearance measurements, which require the near-to-far detector comparison of the main component of the beam. Life appears to be somewhat easier when searching for the appearance measurement, at least at first, when the statistics in the appearance channel are limited. However, the physics of the golden channel is to measure precisely the appearance probability and to compare it between neutrinos and anti-neutrinos, or neutrinos of different energies or baselines, to establish CP violation and/or matter effects. All of a sudden the ratio to worry about is not only near-to-far, but electron-to-muon neutrino cross-sections. Indeed, when measuring the CP asymmetry

$$A_{CP} = \frac{P(\nu_e \rightarrow \nu_e) - P(\bar{\nu}_e \rightarrow \bar{\nu}_e)}{P(\nu_e \rightarrow \nu_e) + P(\bar{\nu}_e \rightarrow \bar{\nu}_e)}; \quad (3)$$

a troublesome quantity will appear, the double ratio:

$$DR = \frac{R_{\nu_e}}{R_{\bar{\nu}_e}}; \quad (4)$$

where R_{ν_e} really means B_{ν_e} including correction for efficiency and background B . Although it would seem that many systematic errors would cancel in this ratio, this is only partially true. The effects that ensure a deviation of this quantity from unity are quite difficult to master:

the muon mass effect;

Fermi motion and binding energy;

the non-isoscalarity of the target (this is particularly relevant for water where anti-neutrinos and neutrinos interact very differently on the free protons);

the different neutrino and antineutrino y distributions; and

the different appearance of the final state lepton in the detector.

These effects are particularly relevant for the low energy neutrinos, as discussed in Appendix D.5. Experimental certification will require a dedicated design of the beam line and near detectors, and probably measurement of cross-sections for all channels quoted above, either at the absolute level or in relation with one of the four channels.

The shape and technology of a near detector depends on the type of facility to be considered (whether Super Beam, Beta Beam or Neutrino Factory). The main requirements of near detectors are that they should measure and control the neutrino flux, the beam angle and direction, the neutrino energy, all the relevant cross-sections and the background to the far detector. Backgrounds differ depending on the far detector technology and the energy of the neutrino beam, so the requirements of a near detector for each of the facilities will be different in each case. In the following sections, we will look at the requirements for a near detector at a Beta Beam, a Super beam and a Neutrino Factory.

3.2 Near detector at a Beta beam and Super Beam

The near detector at a Beta Beam or a Super Beam was not considered in detail by the International Scoping Study. However, the average energy of the neutrino beam in these two scenarios will be low and a detector that is capable of observing low energy neutrino interactions, as discussed in appendix D.

For Super Beams, the detector will need to have a magnetic field to be able to distinguish neutrinos from anti-neutrinos as in the Near Detector currently being designed for T2K [21]. The average energy of the neutrinos will be typically from 500 MeV to a few GeV, so the dominant interactions will be charged current quasi-elastic and neutral current elastic interactions, neutral and charged current single and multi-pion production, and coherent pion production. At these energies, it is extremely important to have a detector target with the same nuclear mass (A) as the far detector, or, at least, to understand the dependency of the cross-section with the nuclear mass. Other nuclear effects at low energy, such as Pauli blocking or Fermi Motion are very important to be taken into account so, typically, one would aim to measure these in light nuclei. These data will be better known from the Minerva experiment [31], but the near detector at a high intensity Super Beam or Beta Beam should be able to carry out these measurements with improved accuracy.

For Beta Beams, there is only one species of neutrino, so a magnetic field is not essential in the near detector. All other considerations of cross-section measurements at low energy remain the same as in the Super Beam case.

3.3 Near detector at a Neutrino Factory

For a neutrino factory, we have discussed the beam instrumentation that will measure the beam angle, the divergence and the polarization of the muons in the storage ring. In addition, a near detector will need to be able to measure the neutrino flux, the neutrino beam angle and its divergence, the neutrino energy, the neutrino cross-sections and a measurement of the background to the oscillation signal at the far detector, which includes a high statistics measurement of the charm background from neutrino interactions.

There is also a rich physics programme that can be carried out at a near detector [24, 25]. Deep inelastic, quasi-elastic and resonance scattering reactions can be studied with unprecedented accuracy. Other measurements include the determination of the weak mixing angle $\sin^2 \theta_w$ from the ratio of neutral to charged current interactions, measurements of the parton distribution functions (both polarized and unpolarized) in a region of phase space that is complementary to those determined by HERA, a measurement of the strong coupling constant and other effects such as nuclear reinteractions and nuclear shadowing. The large sample of charm events reconstructed for the neutrino oscillation background studies can be used to measure the charm background to the oscillation signal but can also be used to measure the CKM matrix element V_{cd} , and to search for CP violation in $D_0 - \overline{D}_0$ mixing. More accurate measurements of θ polarization might shed more light on the spin content of nucleons.

This varied physics programme requires a near detector (or detectors) with high granularity in the inner region that subtends to the far detector. The active target mass of the detector does not need to be very large. With a mass of 50 kg, one would obtain 10^9 charged current neutrino interactions per year in a detector at a distance of 30 m from the muon storage ring, with the straight decay sections being 100 m long.

There are a number of technological choices for a near detector at a neutrino factory, to achieve the general aims stated above. Due to the nature of neutrino beams, one may choose to build a multi-purpose detector that will carry out the physics programme, or instead have a number of different more specialised detectors for individual topics. However, some of the features needed in a near detector include high granularity, to compare the subtended angle between near and far, a magnetic field for charge separation, and muon and electron identification for flavour determination. More specific needs also include excellent spatial resolution to be able to carry out measurements of charm events, the possibility of including different targets for nuclear cross-section determination and maybe the possibility to polarize the target for measurements of polarized parton distribution functions.

3.3.1 Flux normalization and control

Neutrino fluxes from muon decay are given by Eqs. 1 and 2. These fluxes are readily calculable, with small theoretical uncertainties (an accuracy of better than 10^{-3}), as was shown in section 2.

A neutrino factory offers the possibility of having an unprecedented number of neutrino interactions in a near detector. The position of the near detector at the end of the straight decay section of the muon storage ring is a crucial parameter to determine the rate and spectrum of the neutrino interactions. The systematic errors in the ratio of fluxes between the near and far detector are reduced when the spectrum in the near detector is similar to the spectrum at the far detector. For example, a far detector at 2500 km, with a radius of 20 m subtends an angle of less than 8 mrad. The flux of $\bar{\nu}_\mu$ (left panel) and ν_e (right panel) from the decay of 50 GeV μ^+ for this configuration, with average energies of 35.0 GeV and 30.0 GeV is shown in figure 9.

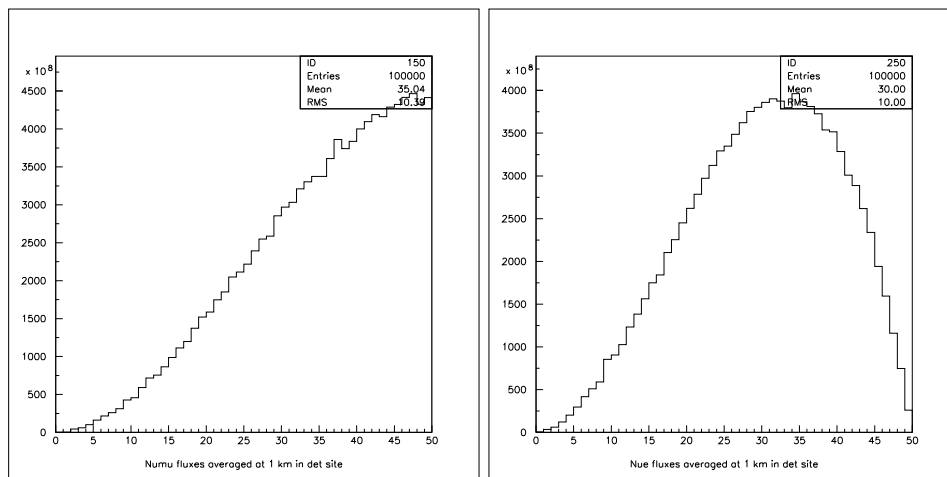


Figure 9: Flux of $\bar{\nu}_\mu$ (left panel) and ν_e (right panel) at a detector 2500 km from a neutrino factory with a 20 m radius, subtending an angle of 8 mrad, from the decay of 50 GeV μ^+ .

At the near detector, one needs to be able to subtend a similarly small angle, and this can be achieved by varying the distance to the source or by improving the spatial resolution of the detector. For example, as shown in figure 10, at a distance of 130 m from the decay point of the 50 GeV μ^+ , one obtains distributions that are quite different to the far detector (average

energies for $\bar{\nu}_\mu$ and ν_e of 21.6 GeV and 18.5 GeV), while at a distance of 1 km from the decay point of the μ^+ , the distributions now look quite similar to those of the far detector (average energies for $\bar{\nu}_\mu$ and ν_e of 34.1 GeV and 29.2 GeV). The difference in the spectra between near and far detector can be a source of systematic error in predicting the far detector flux from the migration of the near detector flux. If the near and far detector fluxes are similar, then the systematic error in the extrapolation from near to far can be reduced.

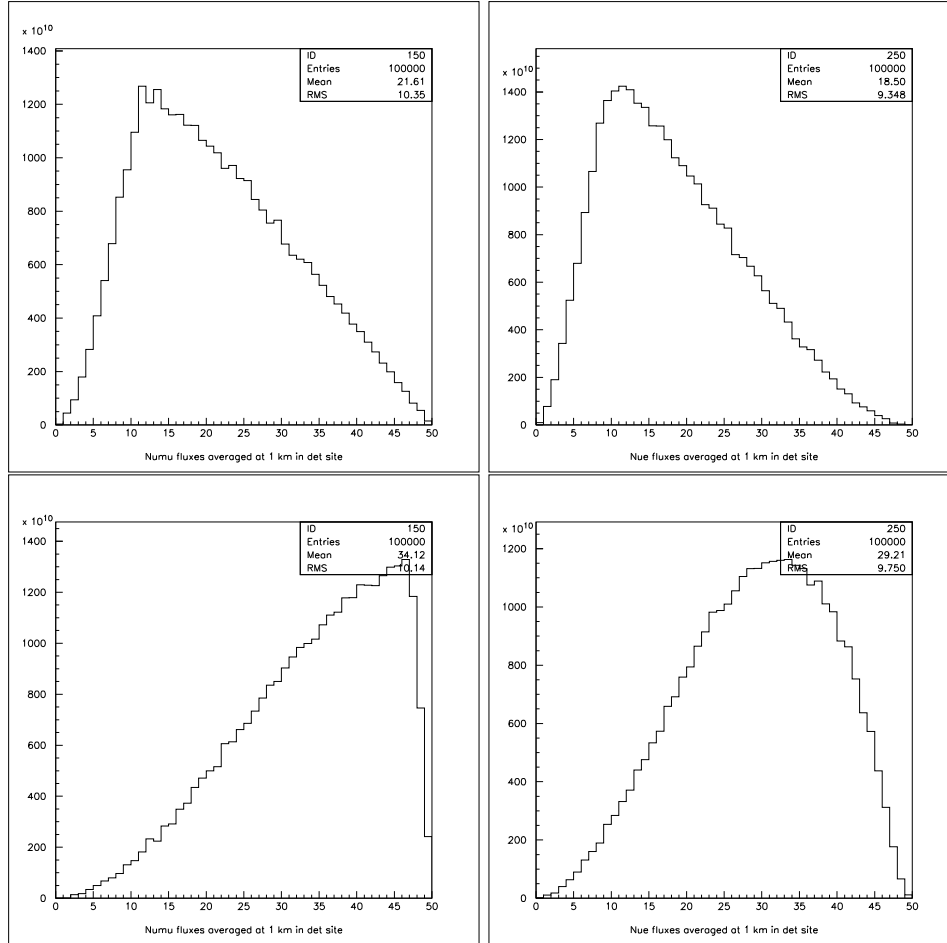


Figure 10: Flux of $\bar{\nu}_\mu$ (left panel) and ν_e (right panel) at a near detector with a 0.5 m radius, 130 m from the decay of a μ^+ (top). Flux of $\bar{\nu}_\mu$ (left panel) and ν_e (right panel) at a near detector with a 0.5 m radius, 1 km from the decay of a μ^+ (bottom).

Another source of difference between the far and near detectors is that the far detector effectively sees a point neutrino source, while the near detector sees a line source, from the decay of the muons along the decay straight in the muon storage ring. For example, let us assume we have a straight section of length 500 m, and we place the near detector at a distance of 500 m from the end of the straight section. We assume that the muons decay uniformly along the decay section, that the angular distribution is Gaussian with $\sigma = 0.5 \times 10^3$, and that the energy of the muons is 40 GeV with $E_\mu = 80$ MeV. If negative muons decay, we obtain the flux distributions shown in Figure 11, for 10^5 muon decays simulated. We will

assuming 10^{21} muon decays in one year of operation of the neutrino factory.

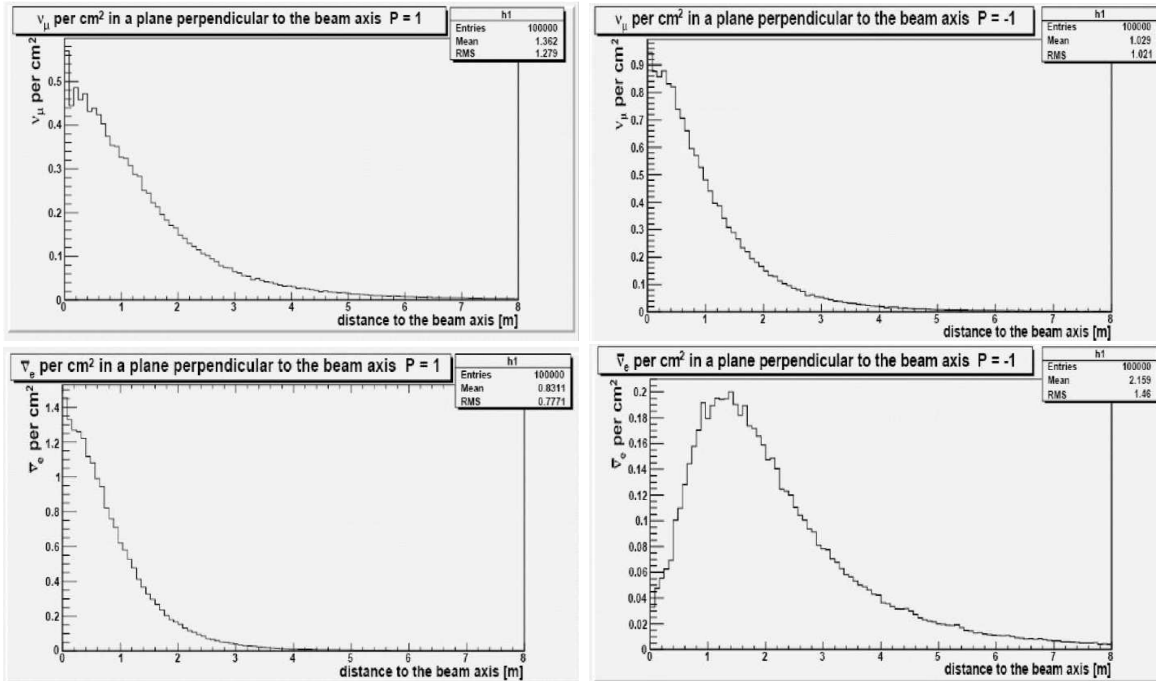


Figure 11: Number of neutrinos per cm^2 per 10^5 muon decays, at 500 m from the end of a decay straight of 500 m at a neutrino factory. Top left panel: ν_μ and $P = +1$; top right panel: ν_μ and $P = -1$; bottom left panel: ν_e and $P = +1$; bottom right panel: ν_e and $P = -1$.

One of the main issues to minimize systematic errors in the near and far detector is to determine the flux and cross-sections separately, since normally one obtains the product $\Gamma(E) \cdot \sigma(E)$. In order to separate the latter, one can use the inverse muon decay reaction: $\mu^+ + e^- \rightarrow \nu_e + \nu_\mu$, with total cross-section:

$$\sigma(\mu^+ e^-) = \frac{G_F^2 s}{s^2} \approx 1.8 \times 10^{-26} \left(\frac{s}{\text{GeV}^2}\right); \quad (5)$$

and muon production through annihilation: $\mu^- + e^+ \rightarrow \nu_\mu + \nu_e$, with the following cross-section in the Standard Model [26]:

$$\sigma(\mu^- e^+) = \frac{2G_F^2 s}{s^2} (E_e E_\mu + 1 + 3E_e E_\mu); \quad (6)$$

where $s = 2m_e E_\mu$.

The production threshold for these reactions is $E_\mu > \frac{m_e^2}{2m_e} = 10.9 \text{ GeV}$. The signature is a single outgoing muon without any visible recoil energy at the interaction point, and with a transverse momentum kinematically constrained to be $p_T \leq 2m_e E_\mu$, as was demonstrated by the measurements performed by CHARM-II [27].

Alternatively, one can also use the elastic scattering interactions: $\nu_e + e \rightarrow \nu_e + e$ and $\bar{\nu}_e + e \rightarrow \bar{\nu}_e + e$ that also have calculable rates:

$$\frac{d(\sigma_{\nu_e e})}{dy} = \frac{2G_F^2 m_e E}{2} \left[\frac{1}{2} + \sin^2 \theta_W + \sin^4 \theta_W (1-y)^2 \right] \quad (7)$$

and

$$\frac{d(\sigma_{\bar{\nu}_e e})}{dy} = \frac{2G_F^2 m_e E}{2} \left[\frac{1}{2} + \sin^2 \theta_W + \sin^4 \theta_W (1-y)^2 \right] \quad (8)$$

The signature for these neutrino-electron events is a low angle forward going lepton with no nuclear recoil. A similar signature was used by the CHARM-II [28] detector to measure $\sin^2 \theta_W$ from neutrino-electron elastic scattering. An excess of events of neutrino-electron scattering can be observed for low values of the E^2 variable over the predominant background from neutral current ν_e production and ν_e quasi-elastic scattering.

The reconstructed spectra of $\nu_e + e \rightarrow \nu_e + e$ and $\bar{\nu}_e + e \rightarrow \bar{\nu}_e + e$ can be seen in figure 12 in a detector of radius 1 m, thickness 30 cm filled with scintillator ($\rho = 1.032 \text{ g cm}^{-3}$), for a total mass of 1 tonne. The neutrinos originate from the decay of 40 GeV muons in the 500 m straight section of the decay ring at a neutrino factory and the detector is 500 m from the end of the straight section.

Table 1 shows the event rate expected from the inverse muon decay reactions. It is clear that the event rate is strongly dependent on the polarization and can be used as an independent verification of the polarization of the decay muons. Since the two reactions (ν_e and $\bar{\nu}_e$) are practically indistinguishable, the statistical error in the flux will come from the sum of the two, an accuracy of better than 10^{-3} in the flux using these reactions can only be achieved for a muon energy of more than 40 GeV within one year of data taking. However, the efficiency and the background for these reactions have not been determined yet, so the statistical significance will be diminished.

E (GeV)	Polarization	$\nu_e \rightarrow \nu_e$	$\bar{\nu}_e \rightarrow \bar{\nu}_e$	N
40	+1	$6.87 \cdot 10^5$	$5.81 \cdot 10^5$	$1.92 \cdot 10^9$
40	-1	$1.67 \cdot 10^6$	$6.97 \cdot 10^4$	$2.81 \cdot 10^9$
30	+1	$2.02 \cdot 10^5$	$1.97 \cdot 10^5$	$1.32 \cdot 10^9$
30	-1	$5.89 \cdot 10^5$	$1.60 \cdot 10^4$	$1.91 \cdot 10^9$
20	+1	$1.83 \cdot 10^4$	$1.14 \cdot 10^4$	$8.07 \cdot 10^8$
20	-1	$7.83 \cdot 10^4$	$7.76 \cdot 10^2$	$1.14 \cdot 10^9$

Table 1: Total number of muons per year from inverse muon decay reactions produced in a cylindrical detector with radius 1 m, thickness 30 cm and density 1.032 g/cm^3 (scintillator, total mass 1 ton), 500 m distant from the end of the straight section of muon storage ring (10^{21} muon decays per year). The last column shows the total number of muons per year produced in the same cylinder from inclusive CC reactions.

3.3.2 Cross-sections and parton distribution functions

The near detector will carry out a programme of cross-section measurements, necessary for the far detector [29]. Due to the experimental control of the flux, it will be possible to extract

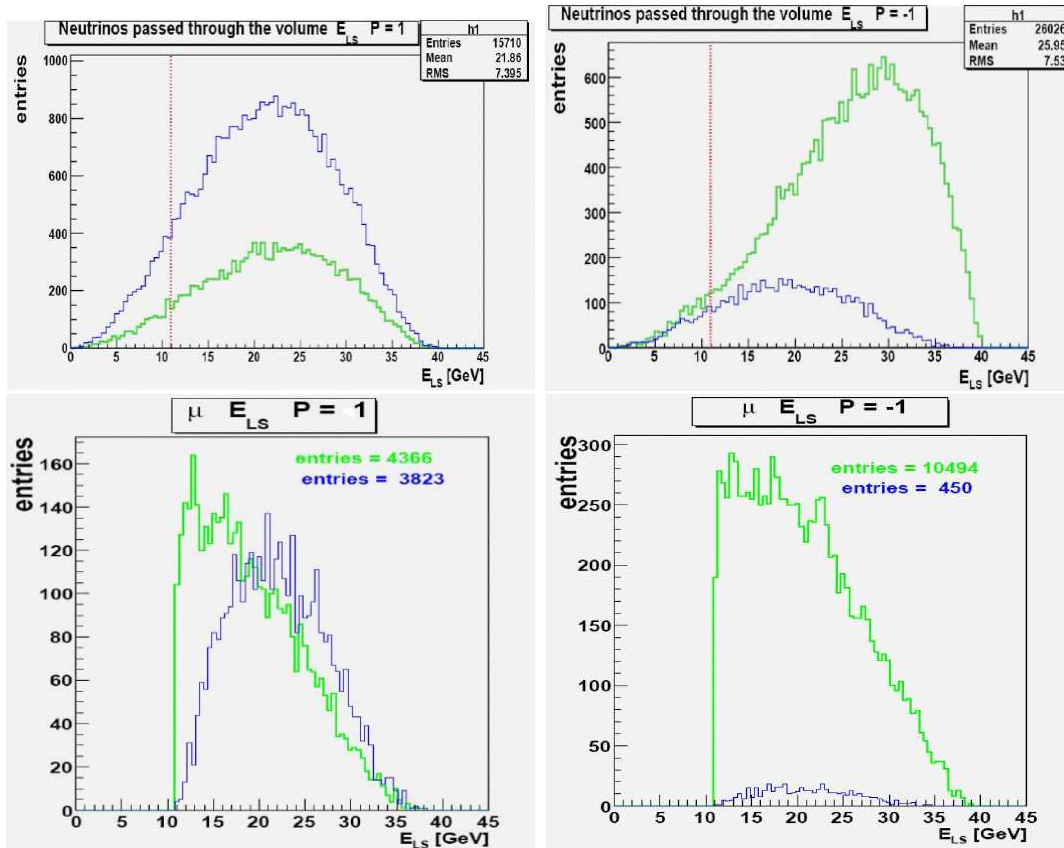


Figure 12: Energy spectrum of μ (green) and $\bar{\nu}_e$ (blue) passing through a cylinder with radius 1 m and thickness 30 cm, and at 500 m distance from the end of the straight section for polarization $P = +1$ (top left) and $P = -1$ (top right). Red line indicates the energy threshold. Inverse muon decay $\mu + e \rightarrow \bar{\nu}_e + \nu_\mu$ (green) and $\bar{\nu}_e + e \rightarrow \mu + \bar{\nu}_e$ (blue) events in a detector of radius 1 m, thickness 30 cm and density 1.032 g cm^{-2} at a distance of 500 m from the end of the straight section of the decay ring for polarization $P = +1$ (bottom left) and $P = -1$ (bottom right).

the cross-section of the different interactions to be studied, such as deep inelastic, quasi-elastic and elastic interactions, ρ^+ and ρ^{++} resonance and single and multipion production (see appendix D). The aim will be to cover all the available energy range, with particular emphasis at low energies (where quasi-elastic events dominate), since this might be needed to observe the second oscillation maximum at a far detector. At these lower energies, nuclear reinteractions and shadowing as well as the role of Fermi motion play a role, and these effects need to be determined. Very low energy interaction measurements might be achievable using a liquid argon TPC, or other very light tracking detector. We should envisage also the possibility of using different nuclear targets, as well as the direct access to nucleon scattering from hydrogen and deuterium targets.

3.3.3 Charm measurements

The wrong-sign muon signature of the neutrino oscillation "golden channel" can be identified, for example, in a magnetised iron calorimeter, by distinguishing between muons, hadrons and electrons, and measuring the charge of the lepton. The main backgrounds for this signal are due to wrong charge identification and to the production of wrong sign muons from the decay of a charm particle (for example, from a D^0), produced either in neutral current interactions or in charged current interactions where the primary muon has not been identified. The charm background is the most dangerous at high energies, but a combined cut in the momentum of the muon (P_μ) and its isolation with respect to the hadronic jet using the variable $Q_t = P_\mu \sin^2 \theta_h$, where θ_h is the angle between the muon and the hadronic shower (see section 4.1.1) can reduce the background to the $8 \cdot 10^{-6}$ level for an efficiency of 45% [47]. However, this background reduction relies on an accurate knowledge of the Q_t distribution of charm particles that should be measured at a near detector.

A near detector should be able to operate at a high rate and have very good spatial resolution, to be able to distinguish primary and secondary vertices needed to identify charm events. It should also have a small radiation length so that it may distinguish electrons from muons in a magnetic field. This can be achieved by a vertex detector of low Z (either a solid state detector, such as silicon, or a fibre tracker) followed by tracking in a magnetic field and calorimetry, with electron and muon identification capabilities [30]. A possible near detector geometry could be fit into the NOMAD dipole magnet [31], currently being used for the T2K 280 m detector [21] (figure 13).

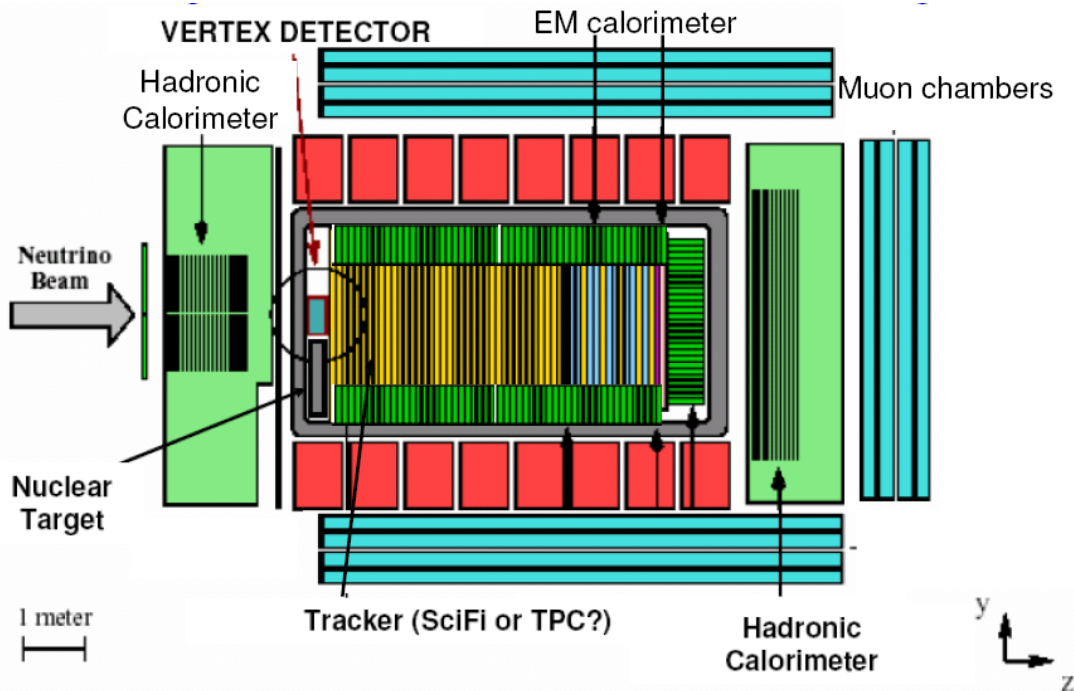


Figure 13: Possible geometry for a near detector at a neutrino factory.

A prototype silicon detector, consisting of four passive layers of boron carbide (45 kg)

and ve layers of silicon microstrip detectors (NOMAD-STAR) was implemented within the NOMAD neutrino oscillation experiment [32, 33]. Impact parameter and vertex resolutions were measured to be 33 μm and 19 μm respectively for this detector. A sample of 45 charm candidates (background of 22 events) was identified [34]. The total charm meson production rate found was $7.2 \pm 2.4\%$ of the charged current rate, at an average energy of 33 GeV, which compares well with other experiments assuming the semi-leptonic branching ratio of charm particles [35] (see figure 14). An efficiency of 3.5% for D^0 and D^+ , and an efficiency of 12.5% for D_s^+ were achieved. Even with these low efficiencies, one could obtain more than 3×10^6 charm events per year. However, using a fully active silicon pixel detector with more layers can provide further improvements. For example, 18 layers of 500 μm thick silicon of dimensions 50 \times 50 cm^2 (total silicon area of 4.5 m^2) corresponds to 52 kg of silicon. Efficiencies for reconstructing charm events should vastly improve with this geometry. Monolithic Active Pixel (MAPS) [36, 37] or DEPFET [38] detectors would be good candidates for this type of silicon technology.

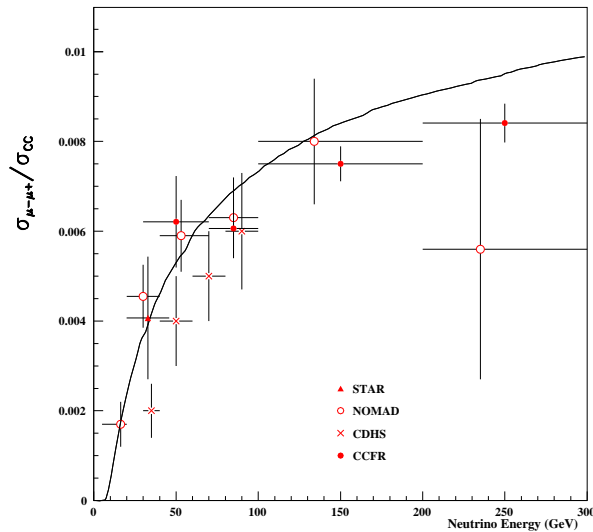


Figure 14: Opposite sign dimuon rate of NOMAD-STAR and other experiments. Overlaid is a charm mass of 1.3 GeV/c² [35].

Another possibility for a near detector dedicated to the study of charm is an emulsion cloud chamber followed by a tracking detector such as a scintillating fibre tracker (similar to OPERA [90] or CHORUS [39]). Emulsion technology has already demonstrated that it is a superb medium for the study of charm [40, 41, 42, 43, 44, 45] due to its unrivalled spatial resolution. The main issue, however, is whether it can cope with the high rate that will be observed at a neutrino factory.

In addition to the important measurement of the oscillation background, this sample of charm events can be used to determine the strange quark content of the sea, the CKM parameter V_{cd} to unprecedented accuracy and search for CP violation in D^0 - \bar{D}^0 mixing. The sign of the lepton produced at the primary vertex can be used to tag the initial charm particle, with the decay products determining whether there was any change in the flavour of the charm meson [25].

3.3.4 Outlook

The near detector at a neutrino factory is an essential ingredient in the overall neutrino factory complex, necessary to reduce the systematic errors for the neutrino oscillation signal. There are many choices for a detector technology that could be implemented. Liquid argon TPCs in a magnetic field would be able to carry out most of the near detector programme. Also, more conventional scintillator technology (similar to MINERVA [131]), a scintillating fibre tracker or a gas TPC (like in the T2K near detector [21]) would also be able to perform cross-section and flux control measurements. However, it seems likely that only silicon or emulsion detectors can achieve the necessary spatial resolution to perform the charm measurements needed to determine the background for the oscillation search. These options shall be further studied within the context of the International Design Study.

4 Far detectors

4.1 Tracking calorimeters

In a Neutrino Factory the $\nu_e \rightarrow \nu_\mu$ oscillation channel, the so-called golden channel, provides the cleanest experimental signature since it only requires the detection of "wrong-sign muons" ($\nu_\mu \rightarrow \nu_e$ muons) with the opposite charge to those circulating in the storage ring (in a detector with charge measurement capabilities). Muon reconstruction is well understood and can be performed with high efficiency keeping a negligible background level. Assuming stored positive muons, the main backgrounds for the $\nu_\mu \rightarrow \nu_e$ search are [46, 47]:

right-charge muons whose charge has been misidentified, in $\bar{\nu}_\mu$ CC events.

$\nu_\mu \rightarrow \nu_e$ muons from hadron decays and ν_μ -hadrons misidentified as muons in $\bar{\nu}_\mu$ or ν_e NC events,

$\nu_\mu \rightarrow \nu_e$ muons from hadron decays and ν_μ -hadrons misidentified as muons in $\bar{\nu}_\mu$ or ν_e charge CC when the main lepton is not identified.

A detector aiming to study the golden channel should be able to identify muons and measure their momenta and charge with high efficiency and purity. Magnetized iron calorimeters have been considered in the past [46]–[50]. The $\nu_\mu \rightarrow \nu_e$ detection efficiency can be kept above 50% for a background level of the order of 10^{-5} . This kind of detector is extremely powerful for the measurement of very small θ_{13} , reaching values of $\sin^2(2\theta_{13})$ below 10^{-4} . However, they may have trouble in studying CP violation because the high density of the detector prevents the detection of low energy neutrinos (below few GeV), which could provide very valuable information for the simultaneous measurement of θ_{CP} and θ_{13} .

An alternative to iron calorimeters, which follows the NOA experiment [58] guidelines, has been recently considered. A magnetised version of Totally Active Scintillator Detectors (TASD), could be very efficient for the $\nu_\mu \rightarrow \nu_e$ search, even for neutrino energies below 1 GeV. The non-magnetised TASD detector (as NOA) would be a good candidate for lower energy beams in the few GeV range, as WBB or Beta-Beams. The physics performance of such a detector in those scenarios has been discussed elsewhere [3]. In this section the magnetised fully active and iron calorimeters are described.

4.1.1 Magnetised iron calorimeters

The wrong-sign muon search at a neutrino factory requires a very massive detector with good muon and muon charge identification capabilities. Magnetic iron calorimeters can fulfil these requirements using well known technologies. Indeed, they are conceptually similar to the existing MINOS detector [51], but with a mass one order of magnitude larger. Several complementary studies have been conducted so far: the Magnetic Iron Neutrino Detector (MIND) [46, 47, 48] (called LMD in the past) and Monolith [49, 48]. Recently, a new option, the Indian Neutrino Observatory (INO) [50], similar to Monolith, has been proposed to study the golden channel at 7000 km.

In this section the results of the MIND study are presented. The conceptual design of the MIND detector consists of a sandwich of 4 cm thick iron plates and 1 cm thick detection layers, with transverse dimensions $14 \times 14 \text{ m}^2$. The detector has a length of 40 m and a total mass of 60 kton. The crucial mass is of the order of 50 kton.

The nature of the detection layers is not yet specified. A possible choice could be either solid (as MINOS) or liquid (as NOA) scintillator bars. The radiation length of plastic scintillator is assumed for the moment. A transverse resolution, σ , of 1 cm in both coordinates is considered. The measurement of the charge of the muon forces the detector to be magnetised. A realistic detector would use a toroidal field produced by a superconducting coil traversing the detector longitudinally (as MINOS). This implies however unnecessary complications from the point of view of the reconstruction program, at this stage of the analysis. In this conceptual design an average dipole field of 1 Tesla (1.3 Tesla in the iron plates) in the Y direction is used. From the performance point of view both are similar except by the small radial decrease of the toroidal field (see Fig. 23), which can be ignored for the moment.

To study the performance of the MIND detector a Monte Carlo simulation based on the GEANT 3 package [54] has been performed. Deep inelastic (DIS) neutrino interactions have been generated using the LEPTO package [55]. From the point of view of computing time a full simulation is not practical because background rejection has to be studied to the level of 10^{-6} , which requires more than 10^6 events for each kind of background. Thus the MIND study is based on a fast simulation in which the electronic response of the detector is not simulated and a smearing of the relevant physics quantities is used instead. The physical quantities used in the analysis are the muon momentum (P), the muon angle (θ), the hadronic energy (E_h) and the hadronic angle (θ_h). In previous analyses [46, 47, 48] all of them were smeared as in the MINOS proposal [51]. In this analysis a better hadronic angular resolution, as reported by Monolith [53], is used.

Muon identification

Neutrino interactions in such a detector have a clear signature. $\mu^+ \mu^+$ or $\mu^- \mu^-$ events are characterized by a muon, easily seen as a penetrating track of typically several metres length, and a shower resulting from the interactions of the final-state hadrons, which extinguishes at short distances. Thus, the identification of muons can be easily done by range. Fig. 15-left shows the distribution of $L = L_\mu - L_h$, where L_μ and L_h are respectively the lengths travelled respectively by the longest muon and hadron in $\mu^+ \mu^+$ events. The muon identification criterion is set as follows: a particle will be identified as a muon if it goes a given length L_{cut} to be optimised beyond any other particle in the event. Notice that this is a very conservative approach since it assumes that the muon and the hadronic shower have

the same direction.

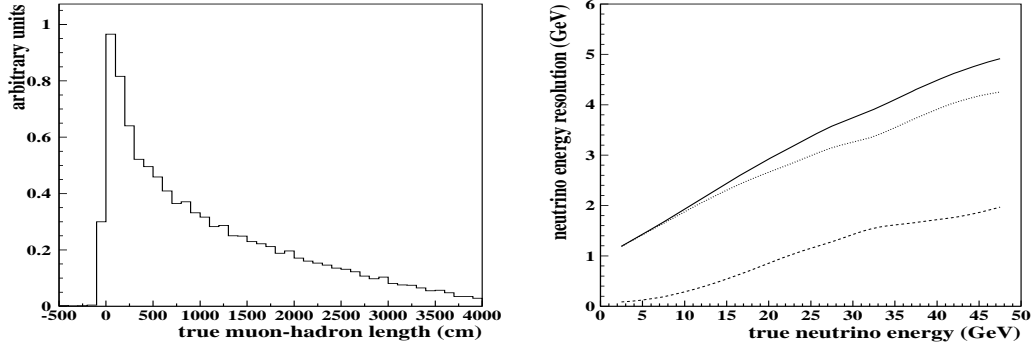


Figure 15: On the left panel, distribution of the true L . On the right panel neutrino energy resolution as a function of the true neutrino energy (solid line). The dashed line corresponds to contribution of the muon momentum measurement, while the dotted line is the hadronic energy resolution.

Energy resolution

An estimator of the neutrino energy, E_ν , is the total visible energy in the event, E_{vis} , which is the sum of the muon and hadron shower energies. The first can be estimated either by range or by curvature for fully contained muons and only by curvature when the muon escapes the detector. A momentum resolution of $(3.5P + 0.022P^2)\%$, as an approximation to the one quoted in the MINOS proposal, is used for the range measurement, while the resolution obtained by curvature is computed using the Gluckstern formula [56]. On the other hand, the hadron shower energy is computed by calorimetry, using the resolution quoted in the MINOS proposal: $E_h = E_h = 0.03 + 0.76 \frac{E_h}{P}$. Fig. 15 shows the average E_ν resolution as a function of E_ν for $\bar{\nu}_\mu$ CC events. The contributions of the hadronic shower and the muon are indicated. The former clearly dominates the E_ν resolution.

Charge identification

As mentioned above, charge misidentification of primary muons in $\bar{\nu}_\mu$ CC interactions constitutes an important background to the ν_μ signal. Fig. 16 (from Ref. [48]) shows the charge misidentification rate for different configurations of the MINOS detector assuming a constant average magnetic field of 1 Tesla (independently of the iron distribution). The muon hits have been fitted to a cubic model taking into account multiple scattering and energy loss. High angle scatters have been removed by a local χ^2 criteria. The charge misidentification rate is of the order of 10^{-6} for 5 GeV=c muons and close to 10^{-4} for 2 GeV=c muons. The distance between measurement planes seems to be the crucial parameter to be optimized. This analysis has however two main limitations: i) the average magnetic field is independent of the distance between measurement planes, which is unrealistic below some distance (≈ 5 cm) since the magnetic field is only present in the iron; ii) all interactions were generated in the center of the detector such that there were no border effects.

In principle all high angle scatters can be removed by requiring the local and global σ of the track to be within certain limits. In this case the charge misidentification rate can be computed using simple equations that assume Gaussian multiple scattering and no border effects. Fig. 17 shows the charge misidentification rate for muons of 1, 1.5 and 2 GeV=c and different detector configurations. For the default magnetic field (1.25 Tesla in iron, corresponding to 1 Tesla average), any iron plate thickness between 1 and 5 cm seems to work, being this parameter more important at lower momenta. The crucial parameter is the magnetic field. At 1 GeV=c the default performance is 0.3%. An order of magnitude less is obtained when the field in iron is increased from 1.25 to 1.7 Tesla and another order of magnitude for 2 Tesla.

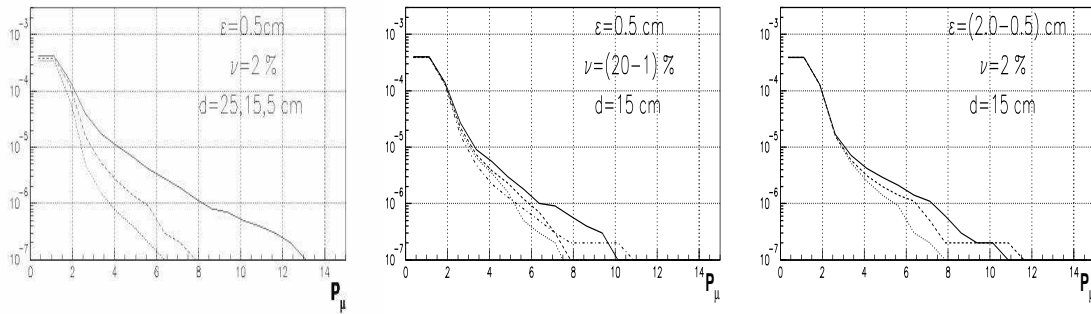


Figure 16: Charge misidentification background as a function of momentum for different configurations of MIND, assuming a constant average field of 1 Tesla. σ is the transverse resolution, ϵ is the hit finding efficiency and d the distance between measurement planes.

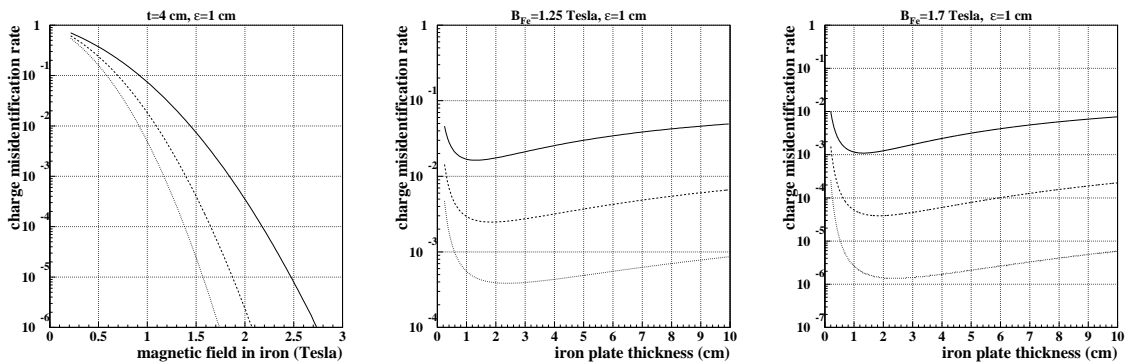


Figure 17: Charge misidentification rate for different detector configurations and for different muon momenta: 1 GeV=c (solid line), 1.5 GeV=c (dashed line) and 2 GeV=c (dotted line), assuming a Gaussian multiple scattering. t is the thickness of the iron plates (4 cm for the default setup) and σ the transverse resolution.

As it was shown in Ref. [47], muons from the decay of hadrons (mainly charm ed particles) in $\bar{\nu}_\mu$ CC interactions constitute the leading background at high neutrino energies. Fortunately, "real" wrong-sign muons (from oscillated ν_e 's) will be in general more energetic and more isolated from the hadronic jet. Thus, this background can be controlled to a reasonable level by a combined cut in the momentum of the muon (P_μ) and its isolation with respect to the hadronic jet, which is represented by the variable $Q_t = P_\mu \sin^2 \theta_h$, where θ_h is the angle between the muon and the hadronic shower. Fig. 18 shows the fractional backgrounds in $\bar{\nu}_\mu$ CC events as a function of the cuts in both P_μ and Q_t . The optimal cuts depend on the baseline since signal and background evolve differently with the distance (see Ref. [47]). For a baseline of 3500 km the optimal cuts are $P_\mu > 5$ GeV/c and $Q_t > 0.7$ GeV/c (from Ref. [48]), $P_\mu > 7.5$ GeV/c and $Q_t > 1$ GeV/c were used in [47], which give a total background rate of $8 \cdot 10^{-6}$ for an efficiency of 45%.

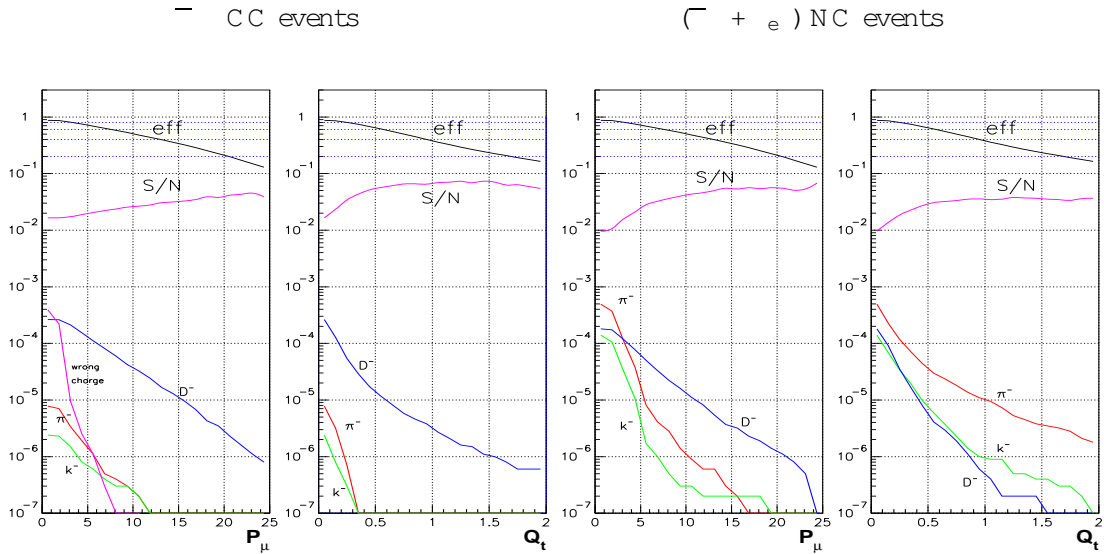


Figure 18: Fractional backgrounds from hadron decays as a function of the cuts in P_μ and Q_t for $\bar{\nu}_\mu$ CC and $(\bar{\nu}_\mu + e^-)$ NC interactions (for stored ν_μ^+ 's). The charge misidentification rate is also shown on the left for a conservative configuration: $d = 15$ cm, $\epsilon = 2\%$ and $\sigma = 0.5$ cm.

Improving the signal efficiency at low neutrino energy

The analysis presented in Refs. [47, 48] and described above was optimized for the measurement of very small θ_{13} . Values of the mixing angle below 0.2° (corresponding to $\sin^2(2\theta_{13}) < 5 \cdot 10^{-5}$) were accessible. Being the signal essentially proportional to $\sin^2(2\theta_{13})$, a very small background level was required, motivating the strong cut on the muon momentum. However, this cut led to essentially no efficiency below 10 GeV neutrino energy. This is not a problem for the measurement of θ_{13} , since this parameter enters in the oscillation probability as a normalization factor, which can be obtained at much higher energies, where the neutrino flux

and cross section are larger. However, the detection of low energy neutrinos is crucial for the simultaneous measurement of θ_{13} and δ_{CP} . Indeed, the measurement of δ_{CP} is based on the experimental capabilities to distinguish the oscillation pattern of neutrinos from that of anti-neutrinos [47]. This CP asymmetry is maximum for neutrino energies in the region of the oscillation peak (≈ 7 GeV at 3500 km) and below. Refer to the Physics Report [3] for more details.

Taking advantage of the correlation between the momentum of the muon and the total visible energy, the cuts can be optimised for both θ_{13} and δ_{CP} . Fig. 19 shows the P (top panels) and Q_t (bottom panels) distributions as a function of E_{vis} for signal (left panels) and $\bar{\nu} + \nu$ CC background (right panels) events. This Fig. also shows the variable cuts: $P > (0.2=c) E_{vis}$ and $Q_t > 0.2$ GeV=c for $E_{vis} > 7$ GeV and no cuts below this energy. The resulting efficiency for the signal and the hadronic backgrounds is shown in Fig. 20.

Table 2: The list of the relevant cuts used in the analysis. Kinematical cuts are only applied for $E_{vis} > 7$ GeV=c.

Fiducial	Quality	Muon id	Kinematical
$z < 1700$ cm	$5^\circ < \theta_{rec} < 90^\circ$	$L > 75, 150, 200$ cm	$Q_t > 0.2$ GeV=c
$ x , y < 600$ cm			$P > (0.2=c) E_{vis}$

Experience from MINOS and Monolith

The hadronic energy resolution obtained experimentally by MINOS [52], $E_h = E_h = 0.55 \frac{p}{E_h}$, where E_h is in GeV, is significantly better than the one quoted in the proposal and mentioned above. This should improve the current E resolution, as shown in Fig. 21.

The MINOS experiment has also demonstrated that $\bar{\nu} + \nu$ CC identification (based mainly on muon identification) can be performed with high efficiency and purity down to 1 GeV neutrino energy [57], as shown in Fig. 22. The MINOS analysis uses a full simulation, with QE and RES interactions, and a full reconstruction, in which the effect of the pattern recognition is included. The event classification parameter shown in Fig. 22 (right panel) combines information from track length and pulse height in each measurement plane. For neutrinos above 1 GeV the signal efficiency is better than 70% while the purity approaches 98% above 2 GeV. The main problem at such low neutrino energies would be the identification of the muon charge.

Fig. 23 shows the magnetic field strength in the MINOS detector and the extrapolation to a bigger toroid of 10 m radius. A 7 m radius toroid, as the one proposed here, seems feasible.

The hadronic angular resolution (θ_h) used in the current analysis was obtained by the Monolith group in a test beam [53]. For a spacing between measurement planes of 7 cm they found $\theta_h = 10.4 \frac{p}{E_h} + 10.1 \frac{p}{E_h}$, which is significantly better than the resolution quoted in the MINOS proposal for a spacing of 4.4 cm, $\theta_h = 16.67 \frac{p}{E_h} + 12.15 \frac{p}{E_h}$. This affects the Q_t resolution, which was important for the analyses presented in Refs [46, 47, 48], since the Q_t cut was in the tail of the distribution, but it is not an issue when the cut is relaxed, as it is the case in the current analysis.

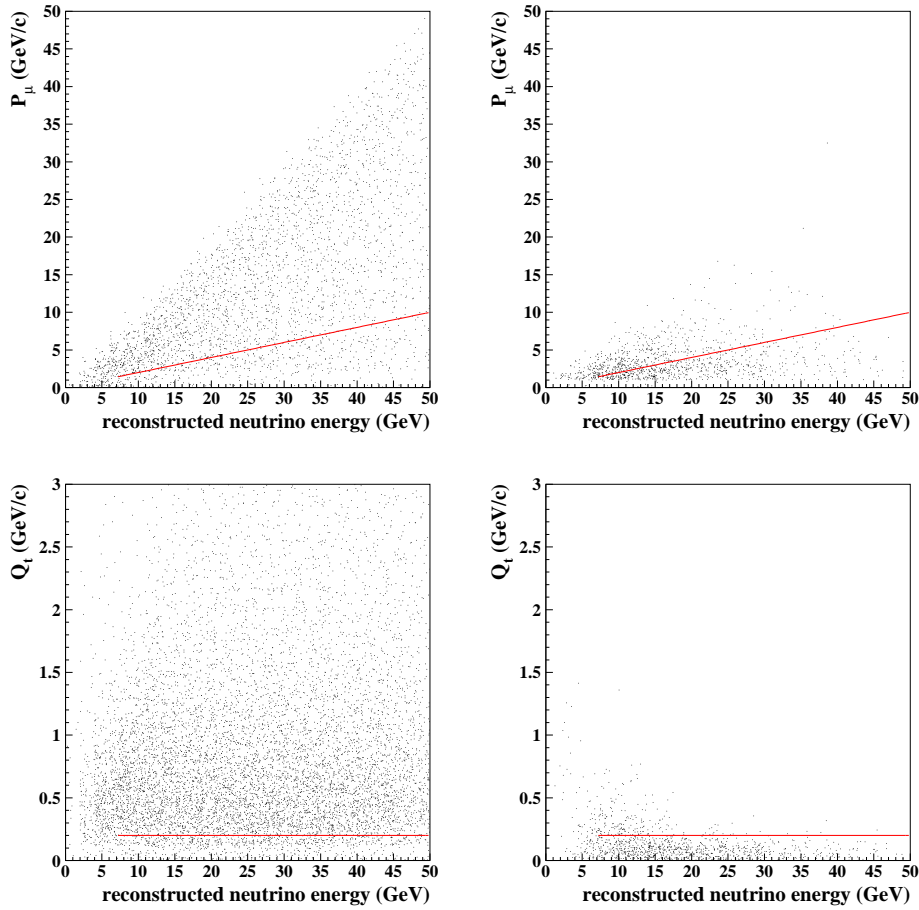


Figure 19: P_μ (top panels) and Q_t (bottom panels) distributions as a function of E_{vis} for signal (left panels) and $\bar{\nu}$ CC background (right panels) events. The kinematical cuts are also shown.

Discussion

Although a detailed study with a full simulation is still missing, the muon charge misidentification seems to be the leading background at low neutrino energies (below 10 GeV). The charge misidentification rate depends primarily on the magnitude of the magnetic field (the curvature resolution is inversely proportional to the magnetic field), which must be as high as possible. A minimum average magnetic field of 1 Tesla should be considered. The MINOS experience suggests that fields of the order of 1.5 Tesla could be achieved. As discussed previously, a small change in the field of 20% reduces the charge misidentification background by one order of magnitude. Thus, the magnetic field issue should be studied very carefully.

One of the main issues in the MINOS analysis is how well the signal efficiency can be determined at low neutrino energies. Given the high derivative of the efficiency curve below 10 GeV (see Fig. 20), the accuracy on the efficiency measurement would be highly affected by the resolution on the neutrino energy. As discussed above, the resolution assumed in this

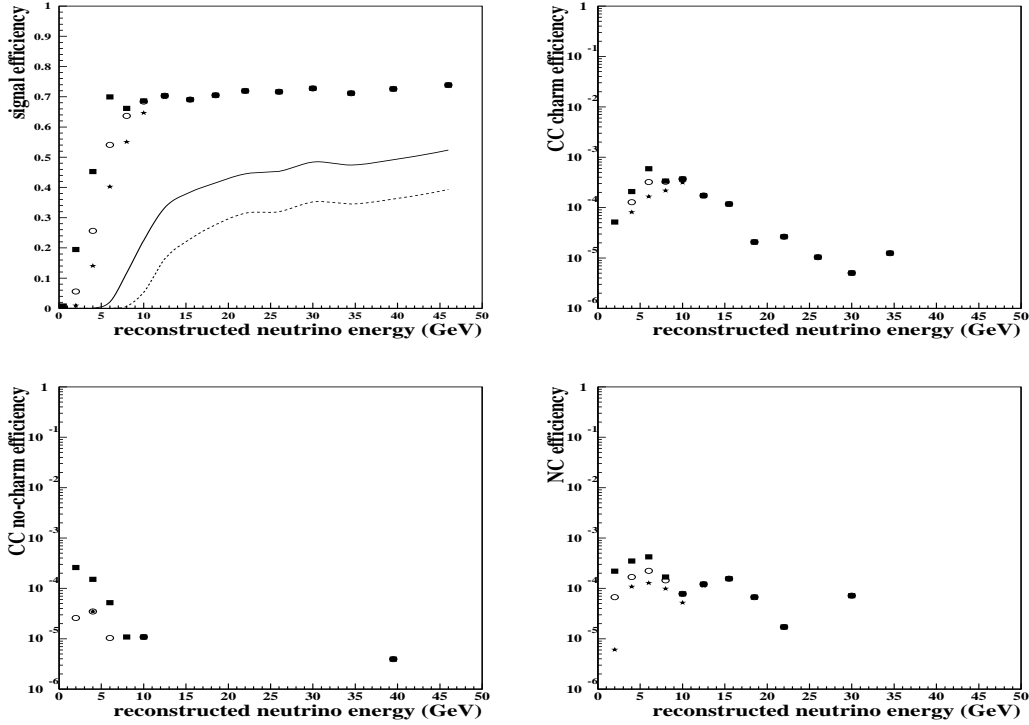


Figure 20: Signal and hadronic background efficiencies as a function of the reconstructed neutrino energy for different cuts on the muon length: 75 cm (black boxes), 150 cm (empty circles) and 200 cm (stars). top-left: $\bar{\nu}_\mu$ CC; this plot also shows the signal efficiency obtained in previous analyses: $P_\mu > 5 \text{ GeV} = c$ and $Q_\mu > 0.7 \text{ GeV} = c$ from Ref. [48] (solid line) and $P_\mu > 7.5 \text{ GeV} = c$ and $Q_\mu > 1 \text{ GeV} = c$ from Ref. [47] (dashed line). Top-right panel: $\bar{\nu}_\mu$ CC with charm decays. Bottom-left panel: $\bar{\nu}_\mu$ CC other than charm decays (mainly pion and kaon decay). Bottom-right panel: $\bar{\nu}_\mu$ NC. $5 \cdot 10^6$ events have been used both for $\bar{\nu}_\mu$ CC and NC interactions. The bin size has been chosen taking into account the E_μ resolution ($\approx 2 E_\mu$).

analysis is worst than the one obtained by MINOS (see Figs. 15 and 21).

The current simulation does not consider quasi-elastic (QE) interactions and resonance production (RES), which should dominate below 2 GeV neutrino energy. QE interactions would have a positive impact on the E_μ resolution since the neutrino energy can be directly computed from the muon momentum and angle. For these events the E_μ resolution would approach the P_μ resolution by range, which is of the order of 4% at these energies. The average resolution can be computed using the DIS and QE cross sections and the corresponding E_μ resolutions. This is shown in Fig. 21. Another possibility is to use only QE events, below a certain energy.

In the current analysis the impact of a realistic pattern recognition has been omitted. The cut in the muon length ensures that a sufficient number of muon hits are isolated from the hadronic shower. This is a reasonable approximation at high neutrino energies, since the primary muon generally escapes the hadronic shower (true for muons above $\approx 2 \text{ GeV} = c$). Low energy muons, which are lost in the current analysis, could be recovered with an improved

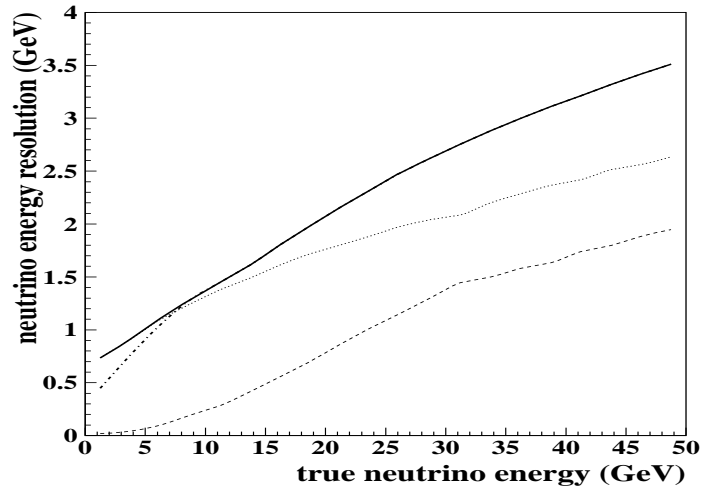


Figure 21: Neutrino energy resolution as a function of the true neutrino energy (solid line). The dashed line corresponds to contribution of the muon momentum measurement, while the dotted line is the hadronic energy resolution. The dotted-dashed line shows the improvement in the resolution when QE events are included.

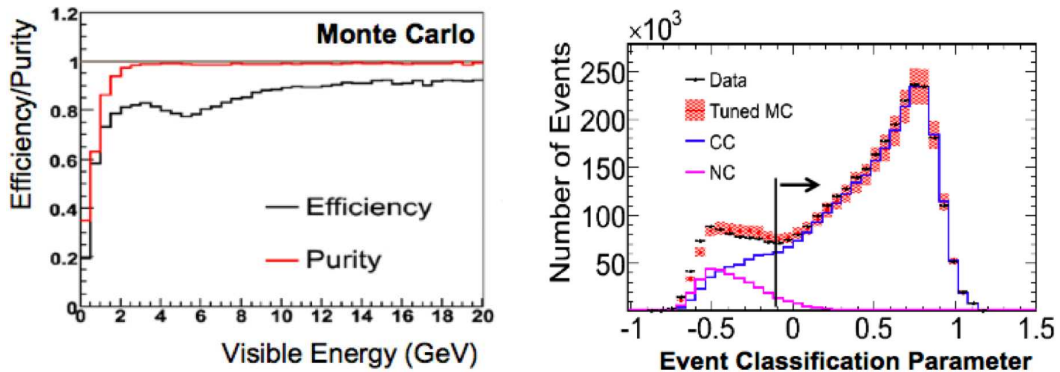


Figure 22: On the left panel CC selection efficiency and purity as a function of the reconstructed neutrino energy (E_{vis}) obtained for MC data. On the right panel comparison of the event classification parameter (likelihood function) for real data and MC.

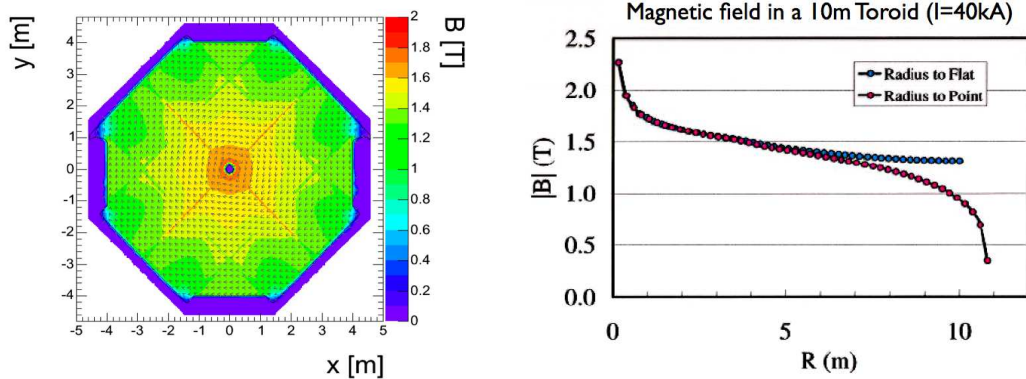


Figure 23: On the left panel, magnetic field as a function of the transverse coordinates in the MINOS far detector. On the right, extrapolation of the MINOS field to a bigger torus.

pattern recognition. The clean topologies of QE and RES events would help in this aspect. Pattern recognition should not be an issue for these kind of events, although the wrong charge assignments would be frequent for muons below 1.5 GeV/c ($\approx 2 \cdot 10^3$ for 1.5 GeV = c muons).

A satisfactory charge measurement is obtained for iron plate thickness in the range 2-5 cm. Thus, the longitudinal segmentation is mainly driven by the hadronic energy resolution and the pattern recognition efficiency. The former should improve if the number of samples increases, although the current MINOS resolution seems to be sufficient. On the other hand, an improved pattern recognition efficiency at low momentum could be very important since the cut in the muon length could be relaxed.

Transverse resolution might be important for the charge measurement at low momentum, for the Q_t resolution and for pattern recognition. Anything better than 1 cm would be sufficient for the charge and the Q_t measurements. Again, pattern recognition seems to be the main issue.

The $\bar{\nu}_\mu + \text{CC}$ identification efficiency obtained by MINOS suggests that the signal efficiency in MINOS could be much better in the energy range from 1 to 10 GeV. This is the result of using a powerful pattern recognition and event classification algorithms.

An optimised MINOS detector could reach the required performance down to neutrino energies of 1-2 GeV. A few questions remain open:

How well can the efficiency be measured at low neutrino energies?

What would be the effect of pattern recognition? This is partially answered by MINOS, although this effect should be included in the MINOS reconstruction.

What is the QE selection efficiency and purity?

What is the effect of non Gaussian effects in the charge measurement? This is one of the main issues and should be answered with a prototype.

What is the maximum magnetic field that can be afforded?

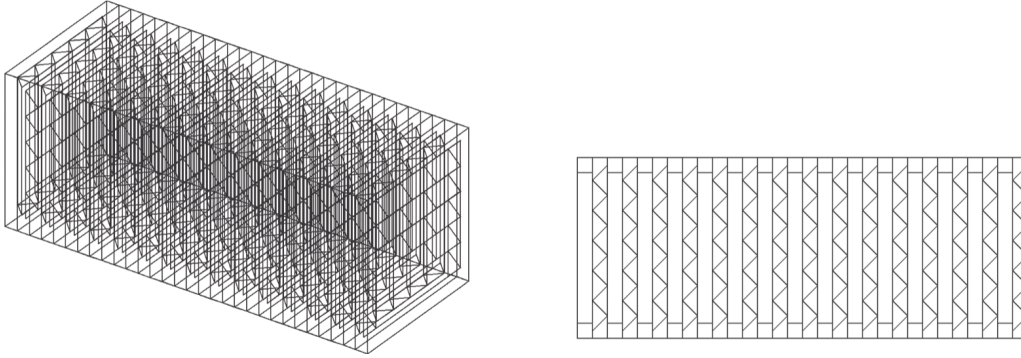


Figure 24: GEANT 4 view of the simulated TAsD detector.

4.1.2 Totally Active Scintillating Detectors

The possibility of using totally active calorimeters in a Neutrino Factory was first considered at NuFact05 [59]. A first study of the performance of this design was presented at the ISS meeting in August 2006 [60].

The detector would consist of long scintillator bars with a triangular cross-section arranged in planes which make x and y measurements in a 0.5 Tesla magnetic field. The scintillator bars considered have a length of 15 m and the triangular end has a base of 3 cm and a height of 1.5 cm. This design is an extrapolation of the MINERvA experiment [61] to produce a detector with dimensions 15 × 15 × 100 m and a mass of approximately 22.5 kton.

This detector was simulated with GEANT 4 version 8.1 (see Fig. 24) and the digitisation took into account the dE/dx in the scintillator slabs and a light yield extrapolated from MINERvA tests. The magnetic field was simulated as a uniform 0.5 Tesla field perpendicular to the beam axis. The performance of the detector was studied by simulating the passage of single muons and positrons with a momentum ranging from 100 MeV = c to 15 GeV = c . Future studies of this design will include a more realistic field map based on recent design work to achieve the large magnetic volume and the simulation of neutrino interactions.

The simulated hits were digitised with an assumed energy resolution of 2 photo electrons and the reconstruction of clusters imposed a threshold of 0.5 photo electrons before building space points and performing a track fit using the Kalman Fitting package RecPack [62].

In order to study the momentum resolution and the rate at which the charge of a muon is mis-identified, 2.3 million muons were simulated of which 1.8 million, divided equally in two momentum ranges (0.1–1 GeV = c and 1–10 GeV = c), were analysed. The position resolution was found to be approximately 4.5 mm RMS with a central Gaussian width of 2.5 mm. The momentum resolution as a function of the muon momentum is shown in Fig. 25(top-left). The tracker achieves a resolution of better than 10% over the complete momentum range studied.

A first attempt to establish the particle ID performance of the detector is summarised in Fig. 25(top-right). This figure shows the reconstructed dE/dx versus the reconstructed momentum for muons (blue/clear) and positrons (red/dark). It can be seen that above approximately 600 MeV = c it should be possible to separate muons and positrons on the basis of the reconstructed energy.

Due to the low density of the Totally Active Scintillating Detector (TAsD), it is possible

to reconstruct muons down to a few hundred MeV/c. Fig. 25 (bottom-left) shows the efficiency for reconstructing positive muons as a function of the initial momentum of the muon. The detector becomes fully efficient above 400 MeV/c.

The charge of the muon was determined by performing two separate Kalman track fits, one with a positive charge and the other with a negative charge. The charge mis-identification rate was determined by counting the rate at which the track fit with the incorrect charge resulted in a better χ^2 per degree of freedom than that with the correct charge. Fig. 25 (bottom-right) shows the charge mis-identification rate as a function of the initial muon momentum.

This first investigation of the TAsD concept has shown it to be worthy of a more detailed study. In particular, it has led to interest in the concept of a lower energy Neutrino Factory [3] (due to the lower threshold than the baseline magnetised iron detector) but more work is required in order to bring the understanding of this device to a comparable level to the baseline.

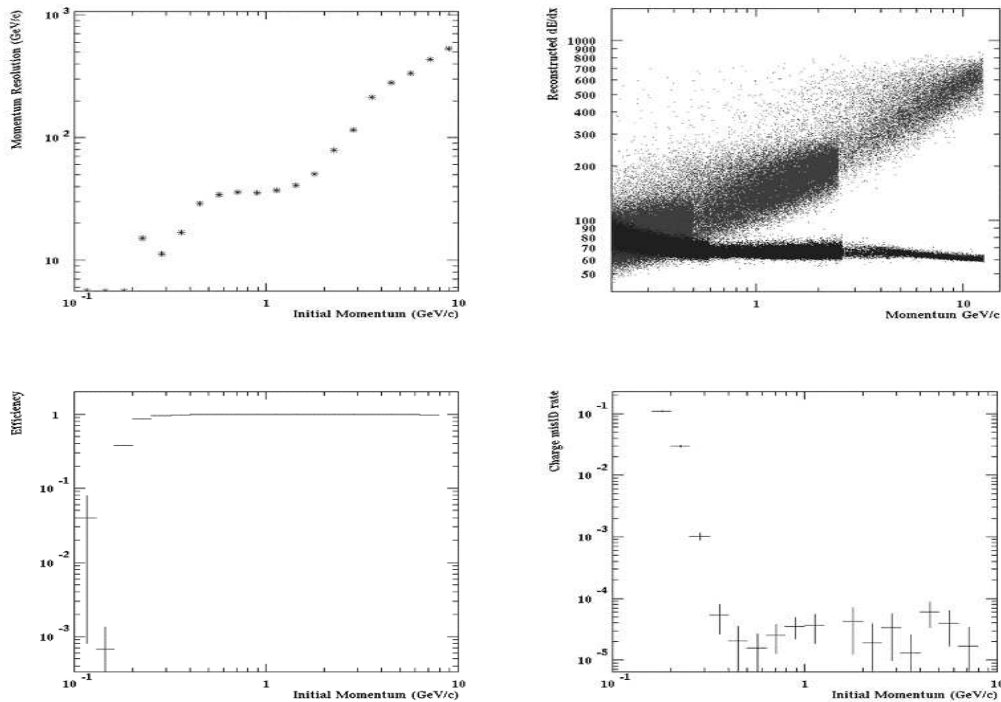


Figure 25: Performance of the Magnetised TAsD detector. Top-Left panel: muon momentum resolution as a function of the muon momentum. Top-Right panel: reconstructed dE/dx as a function of momentum for muons (blue/clear) and positrons (red/dark). Bottom-Left panel: muon identification efficiency as a function of the muon momentum. Bottom-Right panel: muon charge mis-identification rate as a function of the muon momentum.

4.2 Large Water Cherenkov detectors

Since the pioneering age of the Kamiokande and IMB detectors, and after the success of the Super-Kamiokande detector (an extension by a factor 20 with respect to previous detectors),

the physics community involved in this area is continuously growing in the three geographical regions, namely Japan, USA and Europe.

To strengthen the know-how and R&D exchanges, a series of International Workshops have been set up since 1999, the so-called NNN Workshop standing for "Next Nucleon Decay and Neutrino Detectors". The last meetings were organized at Aussois (France) in 2005, Seattle (USA 2006) and Hamamatsu (Japan 2007). As it is clearly stated in the title of this Workshop, detection techniques other than Water Cherenkov are also considered, as for instance Liquid Scintillator, Liquid Argon as well as Iron detectors.

Also, if the pioneering Water Cherenkov detectors were built to look for Nucleon Decay, a prediction of Grand Unified Theories, Neutrino physics has been the bread and butter since the beginning. Just to remind the glorious past: first detection of a Super Novae neutrino burst, Solar and Atmospheric anomaly discoveries that were explained as mass and mixing of neutrinos, the latter being confirmed by the first long baseline neutrino beams and by reactor experiments.

Nucleon decay and neutrino physics are closely linked theoretically (ie. most if not all of the GUT theories predict nucleons to decay and neutrinos to have non zero masses and mixings). Hence, these are areas of equally strong interest to motivate the R&D program extension of the next generation Water Cherenkov mass to the megaton scale (about a factor 20 more than SuperKamikande). One should keep in mind that, in addition to the physics addressed by the ISS, the physics potential of such a detector includes: nucleon decay, supernovae neutrinos from bursts, relic neutrinos, solar and atmospheric neutrinos, long baseline low energy neutrinos (beta beam, superbeam and combined with atmospheric neutrinos) and other astrophysical topics.

The physics performance [3], scalability and robustness of Water Cherenkov detectors are well established and the R&D efforts are concentrated now in two engineering aspects: the excavation of large cavities and the cost reduction of the photodetectors. The addition of Gadolinium salt, once it is demonstrated that it can be safely used in a 1 kton prototype and also in SuperKamikande, could be a decisive ingredient for the new detectors, especially for neutrinos from Supernovae.

4.2.1 The present detector design

Up to now the three geographical regions have proposed three detector designs with a fiducial mass around 500 kton. Some characteristics are presented in table 3.

The Japanese design (Fig.26) is based on two twin tunnels with 5 optically independent cylindrical compartments, each 43 m in diameter and 50 m long, each covered by about 20,000 photodetectors to realize a 40% surface coverage. The US design (Fig.27) is composed of 3 cubic optically independent compartments ($60 \times 60 \times 60 \text{ m}^3$). The inner detector regions are viewed by about 57,000 20" PMTs, with a photocathode coverage of 40% for the central compartment and 10% for the two side compartments. An outer detector serves as a veto shield of 2.5 m depth and is instrumented with about 15,000 outward-facing 8" PMTs. The European design (Fig.28) is based on up to 5 shafts (3 are enough for 500 kton fiducial mass), each 65 m in diameter and 65 m height for the total water container dimensions. The PMT surface defined as 2 m inside the water container is covered by about 81,000 12" PMTs to reach a 30% surface coverage equivalent to a 40% coverage with 20" PMTs (see sec. 4.2.3). The fiducial volume is defined by an additional conservative guard of 2 m. The outer volume between the PMT surface and the water vessel is instrumented with 8" PMTs.

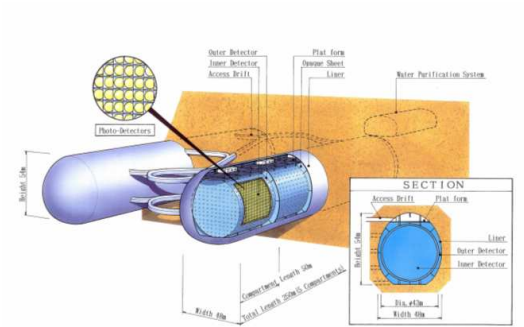


Figure 26: Sketch of the Hyper-K detector (Japan).

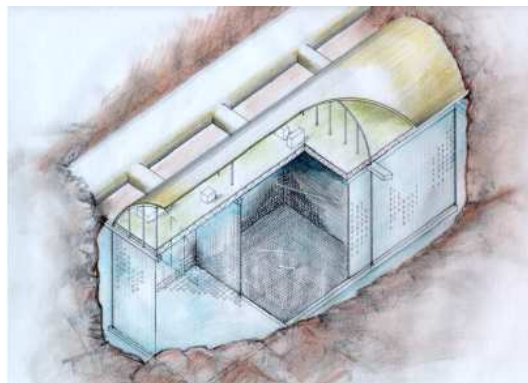


Figure 27: Sketch of the UNO detector (USA).

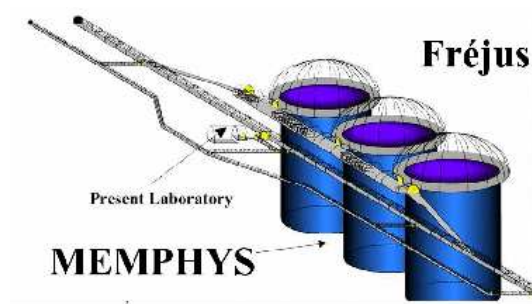


Figure 28: Sketch of the MEMPHYS detector under the Frejus mountain (Europe).

4.2.2 Large underground cavities

All the detector projects are located in underground laboratories. The water equivalent depth of the different detectors sites are: 1500 m.w.e for the Tochiobora mine in Japan, and around 4200 m.w.e for the Homestake or Henderson mines (the two remaining sites after the NSF decision for DUSEL possible site candidates) in the USA, and 4800 m.w.e for the Frejus road tunnel in Europe. A deeper site, so fewer cosmic ray induced background, is especially important in the case of relic supernovae and solar neutrinos, but in case of nucleon decay the detector segmentation may help also.

The main difficulty is the non existence yet of man-made large cavities (see Tab. 3) at the depth envisaged. But on an other hand, there are no a priori indications that one could not built such large cavities and engineering studies are undertaken in the three geographical regions. In Japan, a preliminary survey of the candidate place for Hyper-K is already done, and the rock properties at the Tochiobora mine have been checked. The cavity model has been analyzed in a real environment. The egg transversal shape and the twin tunnel scenario is envisaged as baseline for Hyper-K. In the US, various engineering models have been used by different consultants. It turns out that, with the present knowledge, the UNO cavity seems feasible, although more re-need work, with experimental inputs from rock quality measurements and geological fault knowledge in situ is needed to go further in the project design. In Europe, a pre-study has been performed by the Italian and French companies involved in the building of the existing road tunnel. These companies have taken advantage of the numerous measurements made during the excavation of the present road tunnel and (relatively small) LSM Laboratory to establish a valid estimation of the rock quality as input for simulations. The main outcome of this pre-study is that very large cavities with a "shaft" shape are feasible, while a "tunnel" shape looks disfavored. The next step that can be undertaken in an European Funding framework, is to validate the rock quality at the exact detector location and to finalize the detailed shape of the cavities and access tunnels in close conjunction with the detector design optimization.

Beyond the cavity shape and excavation scenario optimization, there is the need of an extensive R & D on water containers (vessels versus multi-liners). This is an important aspect for radioactivity background suppression and also in detector mechanical design with its associate impacts on detector cost.

4.2.3 Photodetector R & D

The surface coverage by photodetector is not yet optimized as more feedback is needed from the analysis from the SuperKamokande I-II and III phases and from Monte Carlo studies of the foreseen detectors. Nevertheless, one may already state that the very low energy neutrino events (Super Novae neutrinos, ^8B Solar Neutrinos) as well as the search of 0 in Nucleon Decay or the $^0=e$ separation in e appearance experiment, all demand good coverage.

In all the detector design there are at least one order of magnitude more photodetectors than SuperKamokande I (or III). The R & D is largely shared among the three regions and in very close contact with the two manufacturers, namely Hamamatsu in Japan and Photonis in Europe and USA (since July 05, Photonis has acquired the DEP and Burke companies).

The research axis on large HPDs in Japan has been mainly driven by the need to get a lower price for a new photodetector than the presently available Hamamatsu 20" PMTs, especially to get rid of the dynode amplifier system which is introduced manually in such a

tube. Their measured characteristics are encouraging: single photo-electron sensitivity, wide dynamic range limited only by the readout, good timing and good uniformity over the large photo-cathode. But these HPD need to be operated at 20kV High Voltage and a low noise fast electronics. So, the cost per channel is a real challenge.

In Europe, Photonis is very competitive on 12" PMTs and argue that the main parameter to optimize is the cost=($\text{cm}^2 \cdot \text{QE} \cdot \text{CE}$), including electronics. Some French laboratories are involved with Photonis in a joint R&D programme concerning the characteristics of the 12" measurements and improvements and also concerning the integrated electronics front-end. The main idea is to adopt smart-photodetectors which provide directly digitized data. The front-end requirements are: a high speed discriminator for autotrigger on single photo-electron, a coincidence logic to reduce dark current counting rate (to be defined by MC studies), a digitization of charge over 12 bits with a dynamical range up to 200 p.e, a digitization of time of arrival over 12 bits to provide nano-second accuracy, and a variable gain to equalize photomultiplier response and operate with a common high voltage (cost reduction). This electronics R&D takes advantage of the R&D from previous years and concrete realizations for OPERA, LHCb and W Sicalorimeter for ILC among others.

Another R&D line which is pursued at CERN in collaboration with Photonis is on the so-called X-HPD, an almost spherical phototube with a cylindrical crystal scintillator anode mounted in the centre of the sphere and read out by a small conventional PMT (1"). The concept which is a modern implementation of Philips' SMART tube and the QUASAR tube (Lake Baikal experiment), has been demonstrated with a 208 mm prototype tube [63, 64] and promises excellent performance in terms of viewing angle ($\sim 3^\circ$), quantum efficiency ($\sim 40\%$ peak), collection efficiency and timing. The radial field geometry makes the X-HPD immune to the earth magnetic field. The X-HPD is operated around 20 kV. Due to the pre-gain of the scintillator stage of about 30-40, gains in excess of 10^7 are easily reached. A design for a 15" tube exists.

4.3 Liquid Argon TPCs

The Liquid Argon Time Projection Chamber (LAR TPC) [65, 66] is a powerful detector for uniform and high accuracy imaging of massive active volumes. It is based on the fact that in highly pure Argon, ionization tracks can be drifted over distances of the order of meters. Imaging is provided by position-segmented electrodes at the end of the drift path, continuously recording the signals induced. The absolute timing of the event is given by the prompt scintillation light, providing the T_0 reference signal for the TPC. Such a device allows real-time imaging of events with bubble chamber quality, with a longitudinal granularity of the order of a percent of a radiation length. An example of a simulated neutral-current event in a LAR TPC detector can be seen in Fig. 30.

The use of the LAR TPC in high energy physics was pioneered by the ICARUS collaboration [68, 69, 70]. The successful operation of the ICARUS T600 half-module (~ 300 tons) demonstrated the feasibility of the technique on this mass scale [67]. Building very large mass LAR TPCs necessary for long-baseline neutrino physics will require new techniques.

Two different R&D efforts are described in the next two sections. The GLACIER project investigates a scalable concept based on an industrial Liquefied Natural Gas (LNG) tank to build very large LAR TPCs with masses up to 100 kton. It includes feasibility studies to magnetize a LAR TPC of a few 10 kton, allowing for charge discrimination { a necessary requirement at a Neutrino Factory. The North American LAR TPC effort, again based on the

Parameters	UNO (USA)	HyperK (Japan)	MEMPHYS (Europe)
Underground laboratory			
location	Henderson / Homestake	Tochibora	Frejus
depth (m.e.w. 5%)	4500/4800	1500	4800
Long Baseline (km)	1480 2760 / 1280 2530	290	130
	FermiLab BNL	JAERI	CERN
Detector dimensions			
type	3 cubic compartments	2 twin tunnels 5 compartments	3-5 shafts
dimensions	3 (60 60 60)m ³	2 5 (= 43m L = 50m)	(3 5) (= 65m H = 65m)
ducial mass (kton)	440	550	440 730
Photodetectors ^y			
type	20" PMT	20" H(A)PD	12" PMT
number	38,000 (central) & 2 9500 (sides)	20,000 per compartment	81,000 per shaft
surface coverage	40% (central) & 10% (sides)	40%	30%
Cost & Schedule			
estimated cost	500M \$	500 Oku Yen?	161M € per shaft (50% cavity) + 100M €-infrastructure
tentative schedule	10 yrs construction	10 yrs construction	t ₀ + 8 yrs cavities digging t ₀ + 9 yrs PMTs production t ₀ + 10 yrs detectors installation Start of Non Accelerator Prog. as soon as a shaft is commissioned

Table 3: Some basic parameters of the three Water Cherenkov detector baseline designs. ^y: Only inner detector photodetectors are mentioned in this table. *: Target cost, no realistic estimate yet. **: The t₀ date envisaged is 2010.

industrial LNG tank concept, is towards the design of an unmagnetized detector for use in experiments involving a "standard" neutrino super-beam.

4.3.1 The GLACIER project

A very large LArTPC with a mass ranging from 10 to 100 kton would deliver extraordinary physics output owing to the excellent event reconstruction capabilities. Coupled to future Super Beams [71, 72], Beta Beams or Neutrino Factories it could greatly improve our understanding of the mixing matrix in the lepton sector with the goal of measuring the CP-phase. At the same time, it would allow to conduct astroparticle experiments of unprecedented sensitivity [73]. Preliminary simulations show that a "shallow depth" operation at about 200 m rock overburden would not significantly affect the physics performance, including the astrophysical observations [74].

The possibility to complement the features of the LArTPC with those provided by a magnetic field would open new possibilities [75, 76]: charge discrimination, momentum measurement of particles escaping the detector (e.g: high energy muons), and precise kinematics. The magnetic field is required in the context of the Neutrino Factory [75]: (1) a low field, e.g: $B = 0.1 \text{ T}$, for the measurement of the muon charge (CP-violation); (2) a strong field, e.g: $B = 1 \text{ T}$ for the measurement of the muon/electron charges (T-violation).

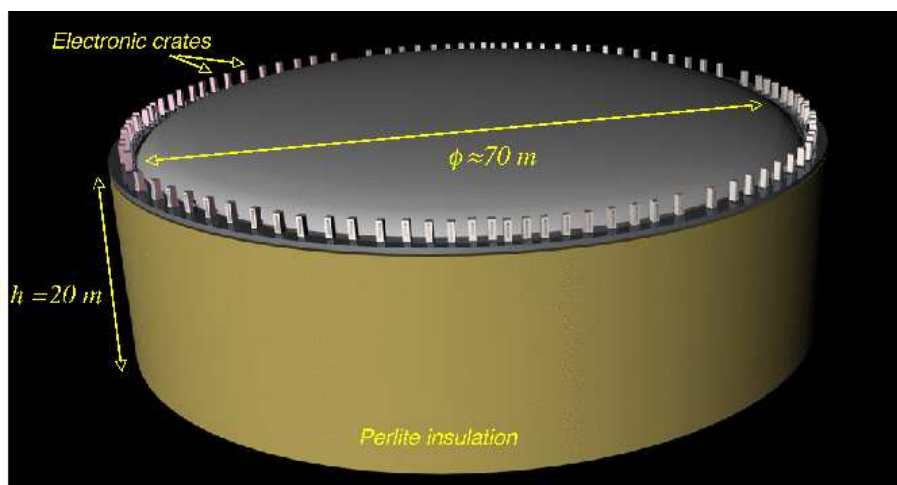


Figure 29: Tanker for a 100 kton LArTPC based on industrial LNG technology

A concept for a LArTPC, scalable up to 100 kton (see Fig 29), has been proposed [77]. It relies on (a) industrial tanks developed by the petrochemical industry (no R & D required, readily available, safe) and their extrapolation to underground or shallow depth LAr storage, (b) novel readout method for very long drift paths with e.g. LEM readout, (c) new solutions for very high drift voltage, (d) a modularity at the level of 100 kton (limited by cavern size) and (e) the possibility to embed the LAr in a magnetic field.

Such a scalable, single LAr tank design is the most attractive solution from the point of view of physics, detector construction, operation and cryogenics, and finally cost. The first experimental prototype of a magnetized LArTPC has been operated [78, 79]. These encouraging results allow to envision a large detector with magnetic field [80]. Beyond the

basic proof of principle, the main challenge to be addressed is the possibility to magnetize a very large mass of Argon, in a range of 10 kton or more. The most practical design is that of a vertically standing solenoidal coil producing vertical field lines, parallel to the drift direction, by immersing a superconducting solenoid directly into the LAr tank.

A rich R & D program is underway with the aim of optimizing the design of future large mass LArTPC detectors [81] and is briefly summarized below.

The development of suitable charge extraction, amplification and collection devices is a crucial issue and related R & D is in progress. A LEM-readout is being considered and has been shown to yield gains up to 10000 with a double stage LEM in gaseous Ar at cryogenic temperature. Experimental tests are presently ongoing on charge extraction from the LAr phase, coupled with a LEM-based amplification and collection in gaseous argon.

The understanding of charge collection under high pressure for events occurring at the bottom of the large cryogenic tank is also being addressed. For this purpose, a small chamber will be pressurized to 3-4 bar to simulate the hydrostatic pressure at the bottom of a future 100 kton tank, to check the drift properties of electrons.

Another important subject is the problem of delivering very high voltage to the inner detectors trying to avoid the use of (delicate) HV feedthroughs. A series of device prototypes were realized based on the Reinacher or Cockroft-Walton circuit allowing the feeding into the vessel of a relatively low voltage and operation of the required amplification directly inside the cryogenic liquid. Tests reaching 120 kV in cold have been successfully performed.

The realization of a 5 m long detector column will allow to experimentally prove the feasibility of detectors with long drift path and will represent a very important milestone. The vessel for this detector has been designed by a collaboration of the University of Bern, ETH Zurich and University of Granada and will be mounted in Bern in 2007. The device will be operated with a reduced electric field value in order to simulate very long drift distances of up to 20 m. Charge readout will be studied in detail together with the adoption of possible novel technological solutions. A high voltage system based on the previously described Reinacher approach will be implemented.

For the immersed magnetic coil solenoid, the use of high-temperature superconductors (HTS) at the LAr temperature would be an attractive solution, but is at the moment hardly technically achievable with the 1st generation of HTS ribbons. We have started a R & D program to investigate the conceptual feasibility of this idea [82] with BSCCO HTS wires from American Superconductor [83] and are now investigating the performance of second generation YBCO wires from American Superconductors and from SuperPower, Inc. [84].

Technodyne International Limited, UK [85], which has unique expertise in the design of LNG tanks, has produced a feasibility study in order to understand and clarify all the issues related to the operation of a large underground LAr detector. The study led to a first engineering design, addressing the mechanical structure, temperature homogeneity and heat losses, LAr process, safety, and preliminary cost estimate. Concerning the provision of LAr, a dedicated, likely not underground but nearby, air-liquefaction plant was foreseen.

The further development of the industrial design of a large volume tank able to operate underground should be pursued. The study initiated with Technodyne should be considered as a first "feasibility" step meant to select the main issues that will need to be further understood and to promptly identify possible "show-stoppers". This work should proceed by more elaborate and detailed industrial design of the large underground (deep or shallow depth) tank also including the details of the detector instrumentation. Finally, the study of logistics, infrastructure and safety issues related to underground sites should also progress,

possibly in view of the two typical geographical configurations: a tunnel-access underground laboratory and a vertical mine-type-access underground laboratory.

In parallel, a program to study the technical feasibility of a large scale purification system needed for the optimal operation of the TPC is being planned in collaboration with the cryogenic department at Southampton University (UK) and the Institut für Luft und Kältetechnik (ILK, Dresden, Germany).

The strategy to eventually reach the 100 kton scale foresees an R&D program leading to the detailed design study for a tentative 100 kton non-magnetized and 25 kton magnetized detector, including cost estimates. A 1 kton engineering module could be foreseen to investigate the tank concept, large scale purification, shallow depth operation, etc. A 10 kton detector would have complementary physics reach to the Superkamiokande detector currently in operation.

In addition to a successful completion of the technological R&D, in the medium term a measurement campaign on charged particle beams is envisaged with the goal to demonstrate $e = \bar{\nu}_e$ separation. Also a 100 ton LArTPC is being considered for the T2K 2km site, which will provide a high statistics sample of neutrino interactions.

4.3.2 0-axis NuMI or Wide-band Superbeam Detector

The purpose of future long-baseline neutrino experiments is to observe $\nu_\mu \rightarrow \nu_e$ transitions. While this doesn't give a direct measurement of $\sin^2(2\theta_{13})$ or the mass hierarchy, a combination of results from experiments with different baselines and results from reactor neutrino experiments could allow for the extraction of the neutrino parameters. In the United States there is the NuMI facility [86] at Fermilab which provides a ν_μ beam for the MINOS experiment located 732 km away in a mine in the state of Minnesota. The beam has been operating since January 2004.

The ultimate background to a ν_e appearance experiment is the inherent ν_e content of the beam. The other serious background to the ν_e appearance signal (i.e., electron appearance from charged-current ν_e interactions) is ν_μ 's produced in neutral-current events. Reducing this puts a premium on detectors that can differentiate electrons from photons. The image of a simulated neutral-current event with a 1 GeV ν_μ ($\nu_\mu + n \rightarrow \nu_\mu + \gamma + \dots + \nu_\mu + n$) in a LArTPC detector, as simulated by a GEANT3-based Monte Carlo, is shown in Fig. 30. The lower photon shower is clearly identifiable in LAr based on the displacement from the vertex and the high pulse height at the shower start. The efficiency for detecting ν_e s in a LArTPC is 80(90% with a negligible neutral-current ν_μ event background).

A group of physicists from some North American universities and Fermilab have collaborated over the past several years in an effort to design a large (15 to 50 kton) LArTPC as the detector for a long-baseline $\nu_\mu \rightarrow \nu_e$ appearance experiment [87]. In the baseline 15 kton detector, the LAr argon is stored in a large, cylindrical, industrial Liquefied Natural Gas (LNG) tank. The tank is 29.1 m in diameter and 25.6 m high. The design employs 8 distinct drift regions with 3 metres between cathode planes and signal wires. The drift field is 500 V/cm giving a drift velocity of 1.5 m/μs and a maximum drift time of 2 ms. Following ICARUS, each signal "plane" contains three wire planes (a vertical collection plane and two induction planes strung at 30° to the vertical). The wire pitch is 5 mm. There are also a number of new ideas, including utilizing wire-wrapped "panels" instead of wire planes, which are described in Ref. [88].

A schematic of the R&D programme that was proposed in the fall of 2005 is shown in

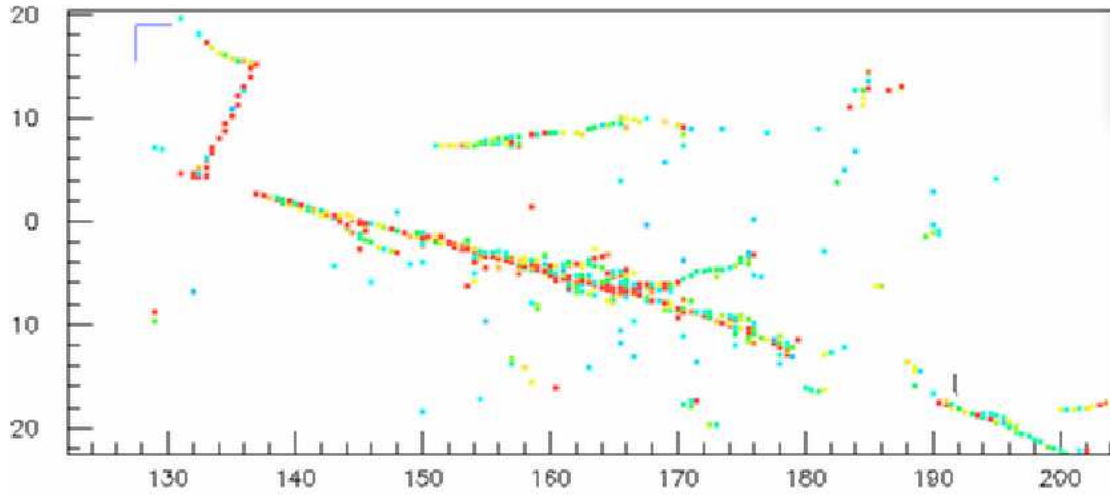


Figure 30: A simulated neutral current event with a 1 GeV ν_e ($\nu_e \rightarrow \nu_\mu + \nu_\tau + \nu_e + n$). Sampling rate is every 3.5% of a radiation length in all three views.

Fig. 31. The programme included:

1. A series of technical test setups directed to answering specific questions pertaining to a massive LArTPC (e.g., long drift, argon purity, wire tensioning, etc.). A number of these have been accomplished, as described in Ref. [88].
2. The construction of a 30-50 tonducible mass (100-130 ton total argon mass) detector in which electron-neutrino interactions can be fully reconstructed and a range of 2 GeV neutrino interactions studied. This detector will operate where it can obtain a sizeable number of neutrino interactions from the Fermilab NuMI and/or Booster Neutrino beams. This is still in the proposal stage.
3. The construction and partial outfitting of a commercial tank of 1 kton capacity using the same techniques as proposed for the 15-50 kton tank. This will serve as the test-bed to understand the issues of industrial construction.

In conclusion, there is a vigorous programme under way in North America towards the design and testing of a large liquid argon TPC for use in long-baseline neutrino physics. Specially, the LArTPC is the ideal detector for a ν_e appearance experiment as it is very efficient for reconstructing ν_e events while allowing for almost complete rejection of the neutral current background.

4.4 Emulsion Cloud Chambers

4.4.1 Introduction

An ideal detector for a Neutrino Factory should be able to exploit all the oscillation channels that are available with the well defined neutrino flux composition: ν_e (the so-called golden channel), ν_μ (the so-called silver channel), ν_τ (the so-called platinum

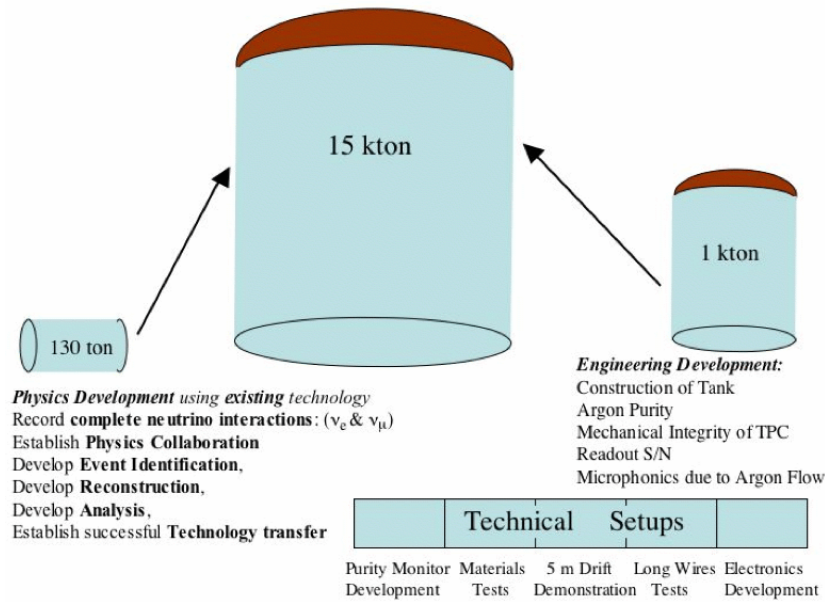


Figure 31: Proposed R & D programme towards realization of a large LArTPC.

channel) and μ^+ when a μ^+ circulates into the decay ring and their CP conjugates in the case of a μ^- circulating. Therefore, an ideal detector should perform a complete and accurate kinematical reconstruction of neutrino events and be able to:

- measure the momentum and the charge of the leptons (muons and electrons);
- identify the decay topologies of the leptons.

So far, the previous tasks have been separately tackled by using different techniques. A magnetized iron calorimeter is being optimized for the study of the golden channel requiring the muon detection and the charge determination with a high efficiency and a small pion to muon misidentification probability (Sec. 4.1.1). The task of identifying electrons and of measuring their charge is very tough and so far only a study based on a magnetized liquid argon detector has been presented (Sec. 4.3.1), although totally active scintillating detectors are potentially able to do it (Sec. 4.1.2).

A detector like OPERA [90, 91], based on the Emulsion Cloud Chamber (ECC) technique [92, 93], has been proposed to search for the silver channel through the direct detection of the muonic decay thanks to the microscopic space resolution of the nuclear emulsions [94, 95].

Here, the idea of using an ECC detector placed in a magnetic field (Magnetized ECC, MECC) is discussed. This combination provides good charge reconstruction and momentum determination capabilities, while providing at the same time the microscopic space resolution and compactness of an ECC. Such a detector has, in principle, the ambitious aim to fulfill all the requirements for an ideal detector for a Neutrino Factory.

4.4.2 The Emulsion Cloud Chamber

The ECC consists of a sequence of passive material plates interspersed with emulsion films. It combines the high-precision tracking capabilities of nuclear emulsions with the large mass

achievable by employing passive material as a target. By assembling a large quantity of ECC modules, it is possible to realize a O (kton) fine-grained vertex detector for the direct observation of the μ 's produced in charged current interactions. This concept has been adopted by the OPERA Collaboration for a long-baseline search of $\nu_e \rightarrow \nu_\mu$ oscillations in the CNGS beam [96].

The basic element of the OPERA ECC is a cell made of a 1 mm thick lead plate followed by an emulsion film, which consists of 44 μ m thick emulsion layers on either side of a 205 μ m plastic base [97]. The number (15–20) of grains of metallic silver produced after the chemical development in each emulsion layer ensures redundancy in the measurement of particle trajectories and allows the measurement of their energy loss that, in the non-relativistic regime, can help to distinguish different particle masses.

Thanks to the dense ECC structure and to the high granularity provided by the nuclear emulsions, the detector is also suited for electron and μ detection, with an efficient electron/pion separation [98]. The energy resolution for an electromagnetic shower is about 20%. By measuring the number of grains associated to each track a two-track resolution of 1 μ m or even better [99] can be achieved. Therefore, it is possible to disentangle single-electron tracks from electron pairs coming from $\mu \rightarrow e \nu$ conversion in lead. The outstanding space resolution can also be used to measure the angle between subsequent track segments with an accuracy of about 1 mrad [100]. This allows the use of Coulomb scattering to evaluate the particle momentum with a resolution of about 20% [101] and to reconstruct the kinematical event variables [102].

A lead-emulsion detector has been proposed [94, 95] to study the silver channel $\mu \rightarrow e \nu$ at a Neutrino Factory, with a detector similar to OPERA but with a total mass of 4 kton. The main limitation factor of this detector is the possibility of measuring the charge only for muons, by an external magnetic spectrometer. The fraction of the μ decays which can be exploited is thus given by the muonic decay branching ratio, about 20%.

4.4.3 The Magnetized Emulsion Cloud Chamber

The MECC here envisaged has the modular structure shown in Fig. 32. The upstream part (target) is a sandwich of passive plates and nuclear emulsions. The length of the target section in terms of radiation lengths must be such to prevent the majority of the electrons to shower before their charge has been measured by the downstream modules. More work has to be done for the optimization of the passive material. Here the stainless steel is presented as a possible choice.

An emulsion spectrometer is located downstream of the target. It consists of a sandwich of nuclear emulsions and a very light material called spacer, providing gaps in between emulsion films. The function of the spacer is to provide a lever arm between two consecutive emulsion films (tracking devices) with a stable mechanical structure. A few centimeter thick Rhocell plate fulfills this requirement. The trajectory measured with the emulsion films which precede and follow the spacer provides the measurement of the charge and momentum of the particle. The target and the spectrometer could mechanically form a single brick of about 10 cm length.

Downstream of the spectrometer, an electronic target tracker has the aim of providing the time stamp of the events. The time information is mandatory in order to match the emulsion information with the information from the electronic detectors allowing the identification of charged-current and neutral-current events. The scanning of the emulsion films should be carried out without any track prediction.

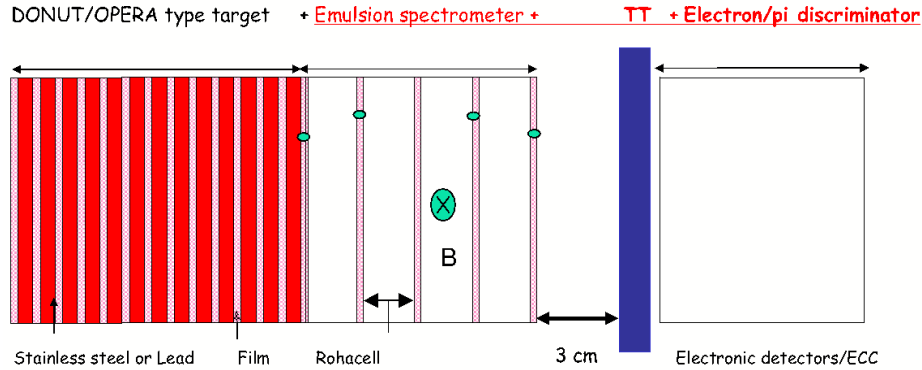


Figure 32: Schematic view of a Magnetized Emulsion Cloud Chamber.

The most downstream element of the detector is the electron/pion discriminator. Its aim is to provide the electron identification, having already measured the charge and momentum of the primary tracks in the spectrometer sector. A good electron identification with a low pion misidentification probability could be achieved at the same time either by a conventional electronic detector or by an emulsion calorimeter (emulsion-lead sandwiches). The choice between the two will be done according to a cost/effectiveness optimization.

The MECC performance both for minimum ionizing particles (MIP) and electrons has been studied by considering different parameters: particle energy in the 1 to 10 GeV range, spacer thickness in the 2-5 cm range and three values of the magnetic field (0.25, 0.5 and 1 T). The same nuclear emulsion films as used by the OPERA experiment were considered. The thickness of the stainless steel plates has been taken to be 1 mm with a total of 35 plates (about $2.5 X_0$). The number of spacers is four.

Monte Carlo simulations have been performed in order to evaluate the momentum resolution and the charge identification efficiency. The momentum and the charge of the particles have been measured with four different methods, for consistency checks: slope measurement, sagitta measurement, parabolic global fit and Kalman filter. In the following only the results obtained with the Kalman filter are shown. The muon momentum resolution has been studied in the 1-10 GeV range as a function of the detector parameters that have to be optimized: the spacer thickness and the magnetic field intensity. The results are shown in Figs. 33, 34, 35. With a spacer thickness of 3 cm (more would be better but the detector would be too long) and a magnetic field of 0.5 T, a 30% (10%) momentum resolution at 10 (1) GeV can be achieved. The charge misidentification rate, shown in Fig. 36 (left panel), is better than 1% below 10 GeV.

The electron momentum and charge measurements are strongly affected by the showering. It has been shown that only 30% of the electrons with energy in the range 1 to 10 GeV exit the target region without showering. For these events the momentum resolution and the charge identification efficiency, shown in Fig. 36 (right panel), are similar to those obtained for muons (left panel). It is worth noting that the electron reconstruction has been performed at the true hit level, i.e. without taking into account the error in the reconstruction. In this respect, it is optimistic. On the other hand, it does not take into account showering electrons for which a pattern recognition program could allow the track reconstruction, hence the charge

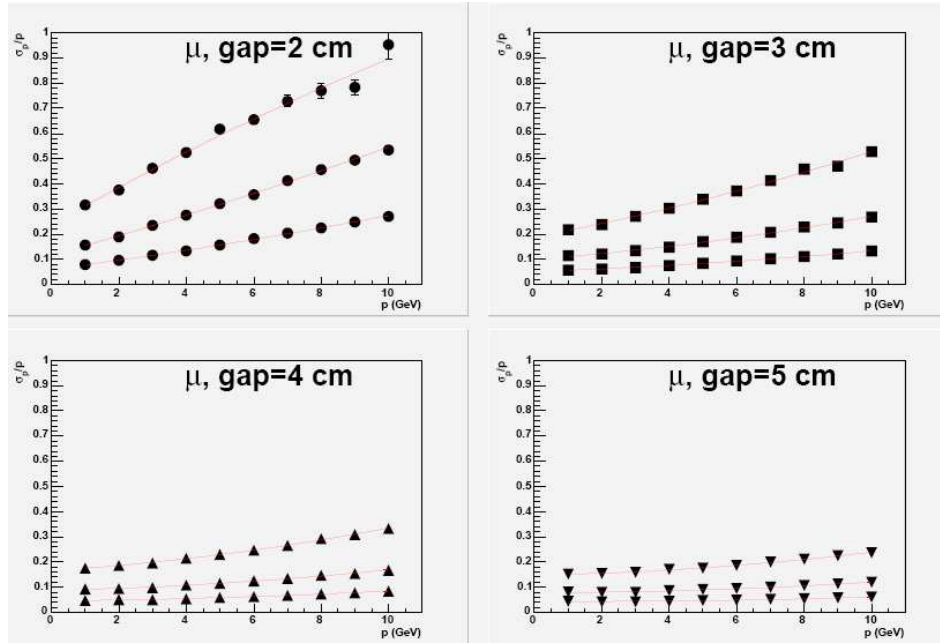


Figure 33: Muon momentum resolution as a function of the momentum for different spacer thicknesses and different values of the magnetic field: $B = 0.25$ T, $B = 0.5$ T and $B = 1.0$ T for the upper, middle and lower curves, respectively.

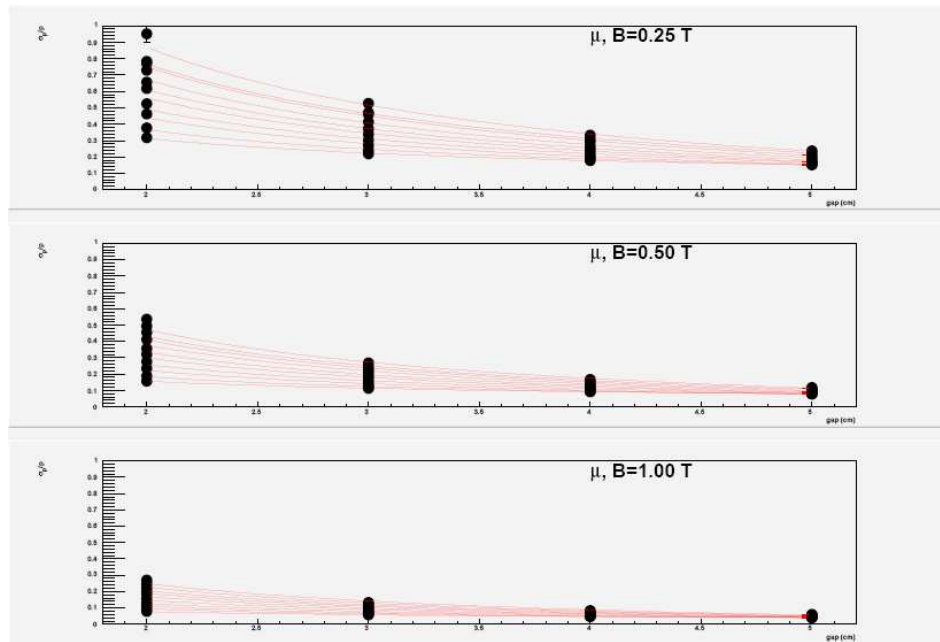


Figure 34: Muon momentum resolution as a function of the spacer thickness for different momenta (from 1 GeV to 10 GeV) and different values of the magnetic field: $B = 0.25$ T for the upper panel, $B = 0.5$ T for the middle panel and $B = 1.0$ T for the lower panel.

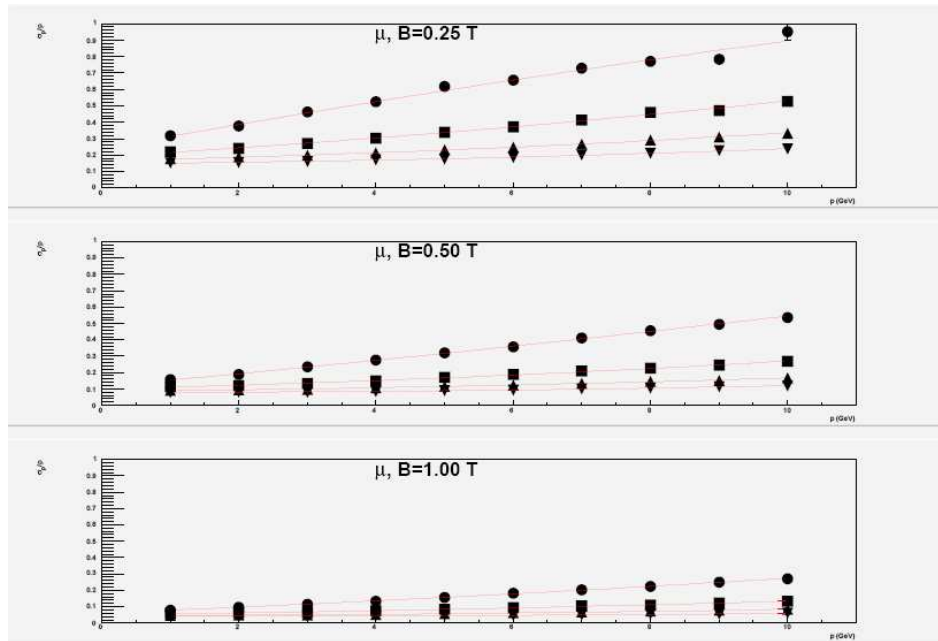


Figure 35: Momentum resolution as a function of the momentum for different spacer thickness and different values of the magnetic field: $B = 0.25$ T for the upper panel, $B = 0.5$ T for the middle panel and $B = 1.0$ T for the lower panel.

and momentum measurement.

Finally, the previous results have been obtained by considering a single emulsion spectrometer. Better results can be obtained, at least for MIP particles, by combining the information from consecutive emulsion spectrometers.

Another important issue is related to the number of interactions that can be stored in a brick preserving the capability of connecting unambiguously the events occurring in the emulsion target with the hits recorded by the electronic detectors. It has been shown [103] that by using a tracker made of 3 cm strips up to 100 events may be stored into a single brick. This is a very conservative number that ensures the capability of the detector to stay in the beam for several years.

A first test of an emulsion spectrometer exposed to a pion beam has been performed in a KEK-PS T1 pion beam [104]. The setup is shown in Fig. 37. It consisted of 2 spacers of 1.5 cm thickness sandwiched with 3 emulsion films, for a total length of 3 cm. They were located inside a 1 T permanent magnet. The emulsion spectrometer has been exposed to pion beams with momenta 0.5, 1 and 2 GeV. The beam spots in the emulsions are shown in Fig. 38. The results have been presented in [105]. The achieved momentum resolution is $\sigma_p/p = 0.14$, and almost constant in the studied energy range. This test shows that it is possible to study the performance of a MECC in a simple way, given the high modularity of the setup. Notice also that in the measurement performed, the alignment among the elements of the spectrometer is much more accurate than in the complete MECC structure (a few microns with respect to about ten microns). Conversely, the smaller number of spacers (2 with respect to 4 of the proposed MECC) and the thinner spacers (1.5 cm with respect to 3 cm of the proposed MECC) determine a worsening of the resolution with respect to the standard emulsion spectrometer.

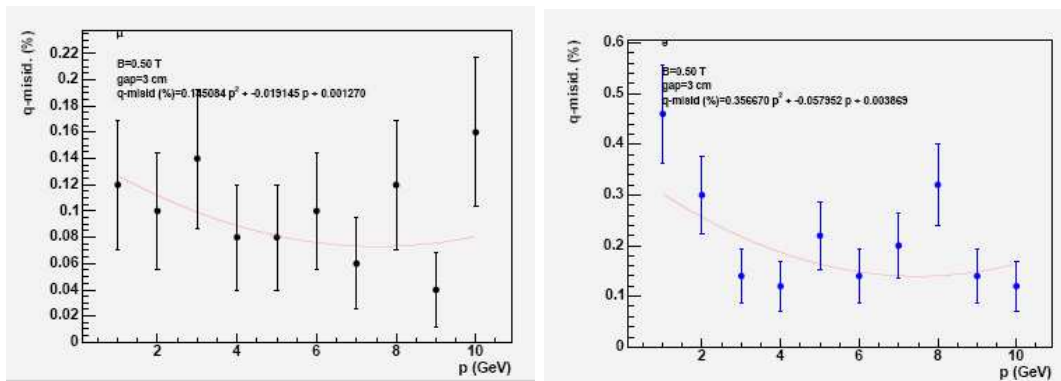


Figure 36: Charge misidentification as a function of the momentum for minimum ionizing particles (left panel) and electrons (right panel), assuming a 3 cm spacer thickness and 0.5 T magnetic field.

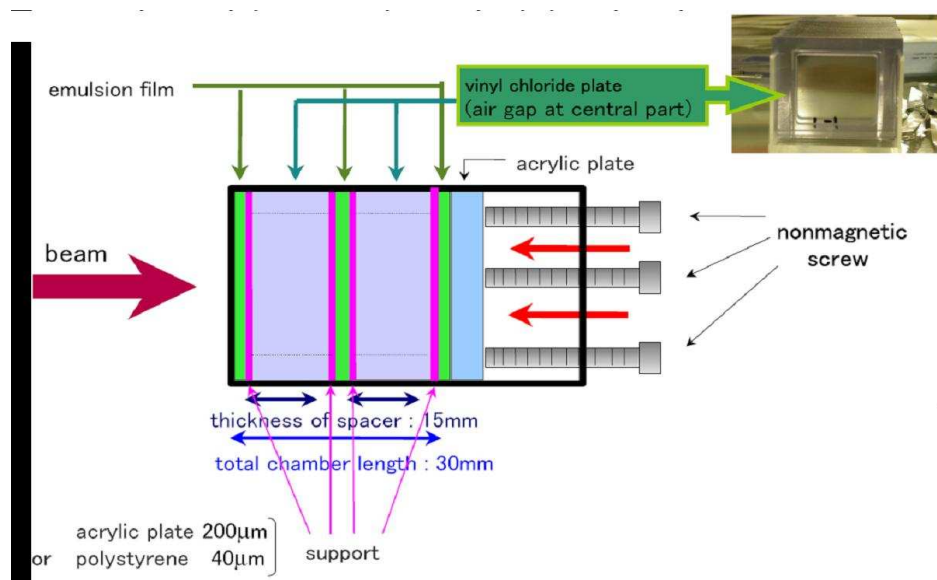


Figure 37: Schematic view of the MECC exposed at the KEK-PS T1 pion beam.

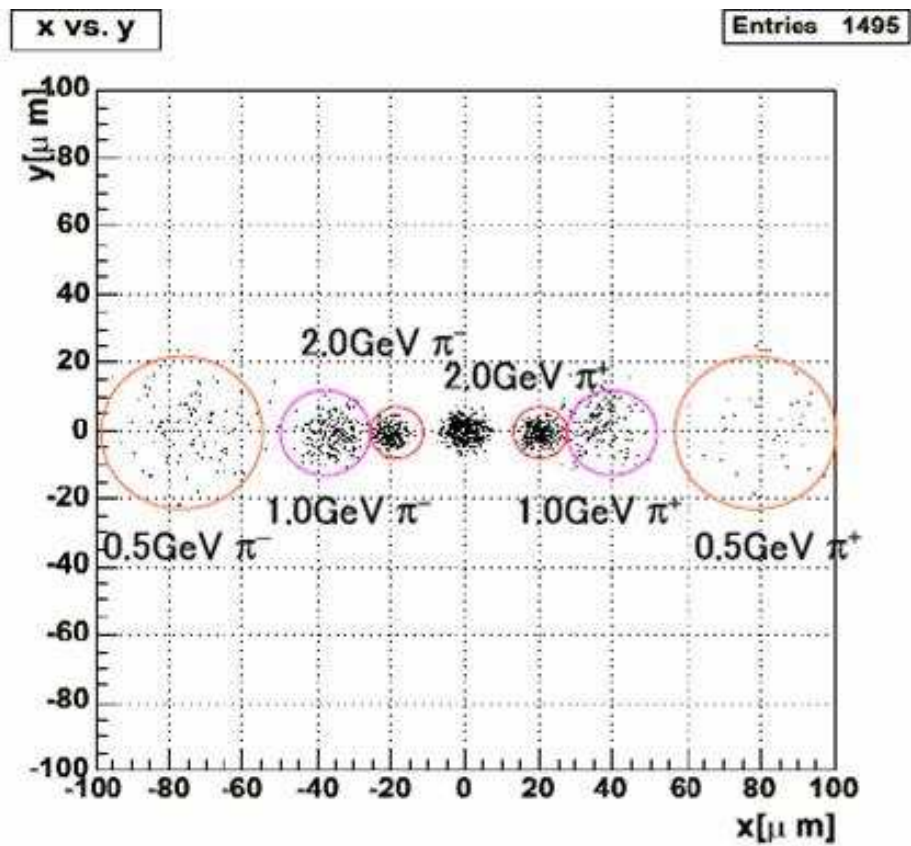


Figure 38: Spatial distribution in the transverse plane of the beam spots of different energies in pinging onto the emulsion spectrometer in the KEK-PS test.

4.4.4 Conclusion and outlook

The Magnetized Emulsion Cloud Chamber (MECC) should be able to detect τ decays measuring the charge of muons, electrons and hadrons. It should also be possible to study the golden channel by using an associated electronic detector. Before assessing its physics reach the maximum mass affordable in terms of scanning power and cost should be quantified. A smaller scale MECC detector would be suitable as a near detector.

The first tests that have been carried out gave promising results. In order to have a realistic estimate of the physics reach, in the future the following studies should be performed:

- define, also on the basis of the experience with OPERA, the maximum MECC mass that can be affordable in terms of scanning power and cost, as well the minimum mass to have good sensitivity to the silver channel;

- carry out a realistic and cost effective design of the magnet;

- study the synergy with other detectors that could act as the electron/pion discriminator. This will open the possibility to search for the golden, the silver and the platinum channels with the same detector;

- once the previous points have been studied, a full simulation with neutrino events has to be performed in order to evaluate the detector sensitivity for the golden and the silver channels, and for the oscillations that produce an electron in the final state.

4.5 Hybrid detectors

All detectors mentioned above use different technologies and are suitable for different kind of measurements. However a number of interesting synergies can be found.

In the previous section the possibility of merging an emulsion-based detector with other detectors (acting as pion/electron discriminator) has been mentioned. As described in Sec. 4.1.2, the T ASD detector could efficiently discriminate between electron and muons/pions for momenta above $0.5 \text{ GeV} = c$. In addition it could also act as a spectrometer for the measurement of the lepton momentum and charge. Thus, an ECC-T ASD hybrid would be able to measure golden (in T ASD), silver (ECC-T ASD) and platinum channels (ECC and T ASD). An important issue concerning channels involving muons (golden and silver) is the background from pion to muon decay and pion/muon mis-identification due to the low density of liquid scintillators.

The combination ECC-M IND would be interesting for the golden and silver channels, but not for platinum, since pion/electron separation in iron is very poor. The golden channel would be measured by M IND alone. For platinum, M IND would act as spectrometer for the measurement of the muon momentum and charge, and also as a muon identifier (by range), while the target and the tau vertex detection would be provided by the ECC. It is worth noting that M IND should be fully efficient and have very little background in the energy range of interest for the silver channel.

Combinations with LA rTPC s could be also considered.

An interesting combination would be the one between M IND and T ASD. In this case the detector would consist of a sandwich between M IND and T ASD modules of about 1 m thick each. M IND would provide most of the target mass, muon identification, and would act as

an hadronic shower container. T ASD would allow the measurement of the muon charge for low energy muons and the detection of electrons.

M IND would help T ASD in triggering hadronic showers, avoiding the potential background from pion to muon decay and pion/muon mis-identification. T ASD would help M IND in measuring the charge of low momentum muons.

The above arguments should be taken with the appropriate care since none of the combinations mentioned have been benchmarked with simulations yet.

5 Baseline Detectors and Conclusion

The detector group of the International Scoping Study set out to determine the baseline detector options for each of the possible neutrino beams and to define a Research and Development (R & D) plan necessary to develop those detector options (Appendix A). This programme of work will continue throughout the International Design Study in order to achieve the optimal configuration for a future neutrino facility. The baseline detectors defined by the ISS for each neutrino beam energy can be found in table 4 and are summarised below:

1. Sub-GeV Beta Beam (BB) and Super Beam (SB) A very massive (Megaton) water Cherenkov (WC) detector is the baseline option. The main R & D necessary for this detector option is the development of an inexpensive photosensor technology and the cost and engineering for the cavern and infrastructure needed for such a detector.
2. 1-5 GeV (high energy) Beta Beam (BB) and Super Beam (SB). There are a number of possibilities in this scenario, and a totally active scintillating detector (T ASD) a liquid argon TPC or a water Cherenkov detector would possibly be able to operate in this regime. The R & D for these detector options include photosensor technology once more, and the R & D for liquid argon detectors (including long drifts and wires, Large Electron Multipliers, etc.).
3. 20-50 GeV high energy neutrino factory from muon decay beams. Magnetic detectors are necessary, so the baseline is a 100 kton magnetized iron neutrino detector (M IND) for the wrong sign muon final states (golden channel), or the possibility of 10 kton of a hybrid neutrino magnetic emulsion cloud chamber (NM-ECC) detector for wrong sign tau detection (silver channel). A full physics simulation of these detectors is needed to demonstrate the efficiency as a function of energy and to determine the charge identification at low momenta.

Furthermore, there are more exciting possibilities of detectors that go beyond the baseline, which could achieve improved performance to the physics parameters in question if these detectors are found to be feasible and affordable. These are summarised in table 5. Finally, some beam instrumentation and near detector options have also been defined for each of the neutrino beams and energy ranges. These are summarised in table 6.

The International Scoping Study (ISS) has laid the foundations to proceed towards a full International Design Study (IDS) for future high intensity neutrino facilities. The aim of the community is to have a full Conceptual Design Report of a future neutrino facility by the year 2012. The detector options covered in this ISS Detector Report and the R & D programme identified in Appendix A will form a roadmap towards defining the detectors at future high intensity neutrino facilities that will be included in the Conceptual Design Report.

Beam energy	Beam type	Far detector	R & D
Sub-G eV	BB and SB	M egaton W C	Photosensors, cavern and infrastructure
1-5 G eV	BB and SB	TA SD or LA r TPC or M egaton W C	Photosensors and detectors. Long drifts and w ires, LEM s, etc
20-50 G eV	N ufact	100 kton M IND (golden) + 10 kton NM -ECC (silver)	Sim ulation + physics studies C harge at low m om enta

Table 4: B aseline detectors for each beam energy range.

Beam energy	Beam type	Far detector	R & D
Sub-G eV	BB and SB	100 kton LA r TPC	C larify advantage of LA r w ith respect to W C
1-5 G eV	BB and SB	TA SD or LA r TPC or M egaton W C	Photosensors and detectors. Long drifts and w ires, LEM s, etc
20-50 G eV	N ufact	P latinum detectors M agnetised TA SD M agnetised LA r M agnetised ECC	Engineering study. Large volum e m agnet. Sim ulations, physics. studies

Table 5: D etectors beyond the baseline for each beam energy range.

A R & D program

The Research and Development (R & D) programme for detectors at future neutrino facilities will rely on a number of international initiatives aimed at delivering the optimal technology for each of the possible neutrino beam options. The aim is to define the R & D needed over the next four years to be able to carry out a Conceptual Design Study of the combined accelerator-detector system. The following sub-sections will define the R & D tasks that need to be carried out in each of the detector systems to carry out the Conceptual Design Study and to be able to perform a critical comparison of the neutrino facilities as a whole.

A.1 Magnetized Iron Neutrino Detector (M IND) and Totally Active Scintillator Detector (TA SD)

Design, cost and engineering solutions for the magnet system for an iron calorimeter.

Design, cost and engineering solutions for the magnet system for a large volume totally active scintillation detector.

Beam energy	Beam instrumentation Near Detectors	R & D
Sub-G eV	T 2K concept	Concept simulations, theory.
1-5 G eV	No a concept for precision measurement	Concept simulations, theory.
20-50 G eV	Beam intensity (BCT) Beam energy, polarization Beam divergence Shielding Leptonic detector Hadronic detector	Need study. Need study. Need study. Need concept. Simulation and study. Simulation, study and vertex detector R & D.

Table 6: Beam instrumentation and Near Detectors for each beam energy range.

R & D on magnetic field resistant photon detector technology, which could include testing of MultiPixel Photon Counters (MPPC), Silicon Photo-multiplier tubes (SiPM), Avalanche Photo Diodes (APD) or other similar technologies.

Feasibility and cost of long strips of extruded scintillator with fibre readout.

Building prototype scintillator-fibre detection systems of varying lengths (5-20 m) and measurements of the attenuation of the signal as a function of the length of scintillator, measurement of the number of photoelectrons collected and studying the optimal geometry for the scintillator strips (for example, a comparison of the performance of square versus triangular cross-section of the scintillator strips).

Study whether a different detector technology (such as Resistive Plate Chambers, RPC) would deliver the same performance at a reduced cost.

Build a prototype to put in a suitable test beam and test its performance inside a magnetic field.

A.2 Water Cherenkov detector

The detector R & D on large water Cherenkov devices is based on the experience of running the Super-Kamiokande detector. However, for a Megaton scale water Cherenkov device, further R & D is needed on a variety of topics:

Engineering and cost of cavern excavation for Megaton water Cherenkov detectors at different sites, including the optimal modularity of such a system.

R & D on photon detectors, such as large area Hybrid Photon Detectors (HPD), or standard Photo Multiplier tubes, including the reduction of the photon detection cost, reducing the risk of implosion, electronics readout costs and reduction of energy threshold through the selection of low activity materials for the detectors and associated mechanics.

Engineering studies of the mechanics to support the photon detectors.

Studies of energy resolution of water Cherenkov detectors, especially at low energy (ie 250 MeV).

A.3 Liquid Argon detector

The Liquid Argon R & D programme is well advanced in the USA and Europe. The main R & D issues include:

Feasibility and cost of using industrial tankers developed by the petrochemical industry and their deployment for underground liquid argon storage.

Demonstration of detector performance for very long drift paths, including liquid argon purification.

R & D on detectors for charge readout (for example, with a Large Electron Multiplier, LEM).

Photon detector readout options (for example, wavelength shifting coated photomultiplier tubes).

R & D on ASICs for electronics readout and data acquisition system.

Development of new solutions for drift in a very high voltage (such as the Cockcroft-Walton style Greinacher circuit).

The possibility to embed the liquid argon in a B-field has been conceptually proven. However, the magnetic field strength needs to be determined by physics requirements and the feasibility and cost of the magnetic field design for large liquid argon volumes needs to be established. Study of high temperature superconducting coils to operate at liquid argon temperatures is an essential R & D task to demonstrate this feasibility.

Dedicated test beams to study prototype detectors and to perform tracking and reconstruction of clean electron and π^0 samples.

A.4 Emulsion Cloud Chamber

There has been a significant amount of R & D done on the use of emulsion for particle physics experiments, such as CHORUS, Donut and, more recently, OPERA. The main issues associated with the emulsion cloud chamber that need to be addressed in further R & D are:

Improvement to the automated scanning stations to reduce the overall scanning time and to improve the scanning accuracy.

Further R & D on operating emulsion-iron sandwich systems in a magnetic field and adapting the scanning algorithms to recognise tracks inside a magnetic field.

A.5 Near Detectors

Silicon vertex detector for the study of the charm background at a neutrino factory: study a comparison of performance and cost of pixel versus strip detectors. Possible solutions could include standard hybrid strip or "stripixel" detectors, hybrid pixel detectors, Monolithic Active Pixels (MAPS) or DEPFET pixel detectors. The latter are currently being studied in the context of the linear collider, so could provide useful synergy between the two projects. Study whether layers of passive material (boron carbide, graphite or other low Z material) are necessary as a neutrino target.

Tracking device: determine the tracking medium at a near detector. A possibility could be to use a scintillating fibre tracker that serves both as a target and a tracking medium. Determine its performance, feasibility and cost. Are there any other options for the tracker such as drift chambers or a gas Time Projection Chamber (TPC)?

Determine the performance needs for the other sub-detectors within the near detector. For example, what is the required energy resolution for a calorimeter? Is particle identification necessary in the near detector? An example of a particle identification system could be the use of a DIRC (Detection of Internally Reflected Cherenkov Light) [106] such as the one used in Babar. What detector technology should be used for the muon chambers of the near detector?

Determine the accuracy of the neutrino flux measurement using the near detector design and determine whether it meets the specification of 0.1% flux error. Perform a study of the charm background for the wrong sign muon signal, and measure the effect of a Q_t cut to reduce the charm background.

Determine the accuracy of cross-section measurements as a function of energy. Above 5 GeV, where it is dominated by deep-inelastic scattering, the aim is to perform a measurement at the 0.1% level. For less than 5 GeV, determine ways of measuring the different components. The near detector should be able to go to an energy threshold, at least as low as the far detector.

B Large magnetic volumes

B.1 Introduction

All detector concepts for the Neutrino Factory (NF) require a magnetic field in order to determine the sign of muon (or possibly the electron) produced in the neutrino interaction. For the baseline detector, this is done with magnetized iron. Technically this is very straightforward, although the 100 kT baseline detector does present challenges because of its size. The cost of this magnetic solution is felt to be manageable. Magnetic solutions for the other NF detectors become much more problematic. No serious consideration has been given to magnetizing a MT water Cherenkov detector, but we have considered magnetizing volumes as large as 60,000 m³ for a liquid Argon detector or a totally-active sampling scintillator detector (TASD). In addition the magnetic emulsion cloud chamber (MECC) would also require a relatively large magnetic volume. We have considered the following technologies:

Room Temperature Coils (Al or Cu)

Conventional Superconducting Coils

High T_c Superconducting Coils

Low Temperature Non-Conventional Superconducting Coils

For the cases of the T ASD , the M ECC , and the LAR approach currently being studied by a US-Canadian group providing the required magnetic volume using 10 solenoids of roughly 15m diameter 15m long has been considered with the solenoids configured into a magnetic cavern as shown in Fig. 39. We have considered a number of field strengths, but chose the baseline to be 0.5T. For the LAR concept being developed by the Glacier collaboration, field coils could be wound inside the large LAR tank. In addition, we have also considered a dipole configuration for a T ASD based on a concept that would use coils similar to those used in the Atlas toroids.

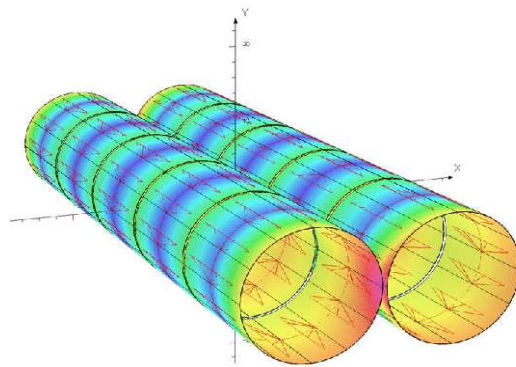


Figure 39: Magnetic cavern configuration

B.2 Conventional Room Temperature Magnets

In order to get adequate field strength with tolerable power dissipation, conventional room-temperature coils would have to be relatively thick. We first considered Al conductor operating at 150K. We then determined the amount of conductor necessary to produce a reference field of 0.1T. In order to keep the current density at approximately $100\text{A}/\text{cm}^2$, 10 layers of 1cm^2 Al conductor would be required for our 15m diameter, 15m long reference solenoid. Using a \$20/kg cost for conventional magnets [107], the estimated cost for 1 solenoid is \$5M. The power dissipation (assuming $R = 1 \cdot 10^8 \text{ Ohm}\cdot\text{m}$) is approximately 1 MW. Ten magnets would then be \$50M and we felt that this number would be acceptable for a large NF detector. However, the operating costs for 10 MW of power would be \$13M/year (based on typical US power costs). The cost of the magnet system including 10 years of operation is thus \$180M. If the cost of cooling the coils to 150K is included, the costs increase substantially. Studies have shown [108] that there is little cost benefit to operating non-superconducting (Al or Cu) coils at low temperature vs. room temperature. If we consider that the power dissipation at room temperature for Al coils triples (vs. 150K operation), then the operating cost for conventional room temperature magnets of this size will be unmanageable. Obviously trying to reach our baseline goal of 0.5T with room temperature magnets is totally unmanageable.

B.3 Conventional Superconducting Coils

One of the first configurations that we considered used superconducting coils similar to the coils used in the Atlas toroids to magnetize a roughly 30 kT T ASD as shown in Fig. 40. In this configuration, 10 coils are used along each side of the detector. We estimated that the coil cost (extrapolated from the Atlas experience) would be on the order of \$120M and was considered acceptable. The field strength for this design was chosen to be 0.15T and at this field a 5 sigma determination of muon sign could be obtained at a muon momentum of 2 GeV/c. However, we determined that the field quality in this configuration was not adequate. In addition, the amount of iron required for the return flux was quite large.

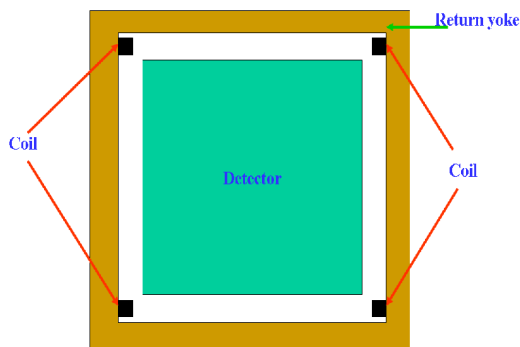


Figure 40: Magnetic dipole configuration

Conventional superconducting solenoids are certainly an option for providing the large magnetic volumes that are needed. Indeed coils of the size we are considering were engineered (but never built) for the proposed GEM experiment at the SSC. A cylindrical geometry (solenoid) does imply that a fraction of the magnetic volume will not be outside the volume of the active detector which will likely be rectangular in cross section. This is certainly a disadvantage in terms of efficient use of the magnetic volume, but would provide personnel access paths to detector components inside the magnetic cavern. It is certainly possible to consider solenoids of rectangular cross section and thus make more efficient use of their magnetic volume, but the engineering and manufacturing implications of this type of design have not been evaluated.

Technically, superconducting magnets of this size could be built, but at what cost? There have been a number of approaches to estimating the cost of a superconducting magnet and we will mention two of those here. The first comes from Green and St. Lorant [109]. They looked at all the magnets that had been built at the time of their study (1993) and developed two formulas for extrapolating the cost of a superconducting magnet: one scaling by stored energy and one scaling by magnetic volume times field. They are given below :

$$C = 0.5E_s^{0.662}$$

and

$$C = 0.4(BV)^{0.635};$$

where E_s is the stored energy in MJ, B is the field in Tesla, V is the volume in m^3 and C is the cost in M\$. The formulas given above give a cost for each 15 m diameter, 15 m long,

0.5T magnet of approximately \$20M (based on E_s) and \$38M (based on magnetic volume). As another reference point, we used the CMS coil [110] ($B = 4T$, $V = 340 \text{ m}^3$, Stored energy = 2.7 GJ, Cost = \$55M). The Green and St. Lorant formulas give costs for the CMS magnet of \$93M and \$41M based on stored energy and magnetic volume respectively. From these data we can make "Most Optimistic" and "Most Pessimistic" extrapolations for our baseline NF solenoid. The most optimistic cost comes from using the formula based on stored energy and assume that it over-estimates by a factor of 1.7 (93/55), based on the CMS as built cost. This gives a cost of \$14M for each of our NF detector solenoids. The most pessimistic cost extrapolation comes from using the formula based on magnetic volume and conclude that it under-estimates the cost by a factor of 1.3 (55/41), based on the CMS as built cost. This then gives a cost of \$60M for each of our NF detector solenoids. There is obviously a large uncertainty represented here.

Another extrapolation model was used by Balbekov et. al. [111] based on a model developed by A. Herve [114]. The extrapolation formulae are given below :

$$P_0 = 0.33S^{0.8}$$

$$P_E = 0.17E^{0.7}$$

and

$$P = P_0 + P_E$$

where P_0 is the price of the equivalent zero-energy magnet in MCHF, P_E is the price of magnetization, and P is the total price. S is the surface area (m^2) of the cryostat and E (MJ) is the stored energy. This model includes the cost of power supplies, cryogenics and vacuum plant. From the above equations you can see that the model does take into account the difficulties in dealing with size separately from magnetic field issues. Balbekov et. al. used three "as-builts" to derive the coefficients in the above equations:

$$\text{ALEPH } (R = 2.65\text{m}, L = 7\text{m}, B = 1.5\text{T}, E = 138\text{MJ}, P = \$14\text{M})$$

$$\text{CMS } (R = 3.2\text{m}, L = 14.5\text{m}, B = 4\text{T}, E = 3\text{GJ}, P = \$55\text{M})$$

$$\text{GEM } (R = 9\text{m}, L = 27\text{m}, B = 0.8\text{T}, E = 2\text{GJ}, P = \$98\text{M})$$

The GEM magnet cost was an estimate based on a detailed design and engineering analysis. Using this estimating model we have for one of the NF detector solenoids: $P_0 = 0.33(707)^{0.8} = 63 \text{ MCHF}$, $P_E = 0.17(265)^{0.7} = 8.5 \text{ MCHF}$. The magnet cost is thus approximately \$57M (which is close to our most pessimistic extrapolation given above). One thing that stands out is that the magnetization costs are small compared to the total cost. The mechanical costs involved with dealing with the large vacuum loading forces on the vacuum cryostat assumed to be used for this magnet are by far the dominant cost.

B.4 High Tc magnets

We did not explore in detail the possibilities of building a NF detector solenoid with high Tc superconductor, but we recognized the potential in this area. Currently the cost of high Tc superconductor is 100-200 times [112] that of conventional SC for the same field and there are many engineering issues that would have to be investigated first if we are to conclude

that this technology was applicable (cost + manufacturability) to our application. However since the technological status of high T_c superconductor is moving so fast, we did do some zeroth-order estimates regarding one of these NF detector solenoids fabricated with high T_c superconductor. We assumed a low-temperature operation of 35K. This might still allow for a non-vacuum insulated (foam) cryostat and thus have no vacuum loading to give higher current carrying capacity. The cost of the superconductor for 10 NF detector solenoids was estimated to be \$50M. Based on studies that have been done on foam-insulated vessels for GLACIER, we estimated the cost of the cryostats also at \$50M. Assembly and engineering could not be reliably estimated in that they will depend on the particulars of the conductor being used and the currently existing manufacturing and assembly capabilities for high T_c superconducting magnets are not yet at the stage where reliable estimates can be made. However the possible cost savings afforded by using non-vacuum insulated cryostats are large and high T_c superconductor cable technology is advancing very rapidly.

B.5 Low Temperature Non-Conventional Superconducting Coils

In this concept we solve the vacuum loading problem of the cryostat by using the superconducting transmission line (STL) that was developed for the Very Large Hadron Collider superferric magnets [113]. The solenoid windings now consist of this superconducting cable which is coned in its own cryostat. Each solenoid consists of 150 turns and requires 7500 m of cable. There is no large vacuum vessel in this design. We have performed a simulation of the Magnetic Cavern concept using STL solenoids and the results are shown in Fig. 41. With the iron end-walls (1 m thick), the average field in the XZ plane is approximately 0.58 T at an excitation current of 50 kA.

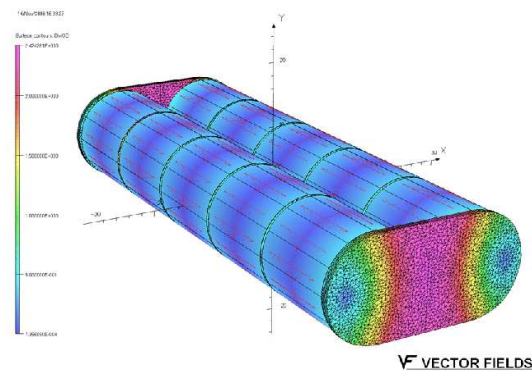


Figure 41: STL Solenoid Magnetic Cavern Simulation

The maximum radial force is approximately 16 kN/m and the maximum axial force approximately 40 kN/m. The field uniformity is quite good with the iron end-walls and is shown in Fig. 42.

B.6 Superconducting Transmission Line

The superconducting transmission line (STL) consists of a superconducting cable inside a cryopipe cooled by supercritical liquid helium at 4.5-6.0 K placed inside a co-axial cryostat. It

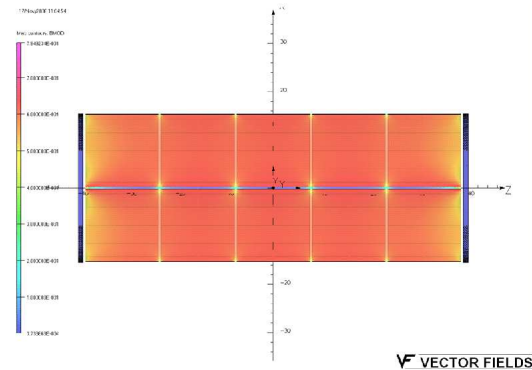


Figure 42: STL Solenoid Magnetic Cavern Field Uniformity in XZ plane

consists of a perforated Invar tube, a copper stabilized superconducting cable, an Invar helium pipe, the cold pipe support system, a thermal shield covered by multilayer superinsulation, and the vacuum shell. One of the possible STL designs developed for the VLHC is shown in Fig. 43. Its overall diameter is approximately 83 mm.

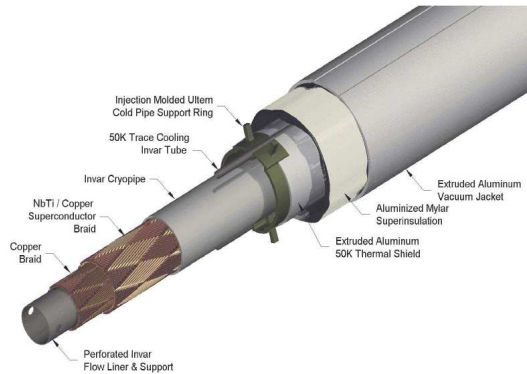


Figure 43: Superconducting transmission line

The STL is designed to carry a current of 100 kA at 6.5 K in a magnetic field up to 1 T. This provides about a 50% current margin with respect to the required current in order to reach a field of 0.5T. This operating margin can compensate for temperature variations, mechanical or other perturbations in the system. The superconductor for the STL could be made in the form of braid or in the form of a two-layer spiral winding using Rutherford cable. The braid consists of 288 NbTi SSC-type strands 0.648 mm in diameter and arranged in a pattern of two sets of 24 crossing bundles with opposite pitch angle about the tube. A conductor made of Rutherford cables consists of 9 NbTi cables that were used in the SSC dipole inner layer. A copper braid is placed inside the superconductor to provide additional current carrying capability during a quench. The conductor is sandwiched between an inner perforated Invar pipe, which serves as a liquid helium channel, and an outer Invar pressure pipe that closes the helium space. Both braided and spiral-wrapped conductors and the 10 cm long splice between them have been successfully tested with 100 kA transport current within

the R&D program for the VLHC. The STL has a 2.5-cm clear bore, which is sufficient for the liquid helium flow in a loop up to 10 km in length. This configuration allows for cooling each solenoid with continuous helium flow coming from a helium distribution box.

The thermal shield is made of extruded aluminum pipe segments, which slide over opposite ends of each support spider. The 6.4-mm diameter Invar pipe is used for 50 K pressurized helium. It is placed in the cavities at the top and the bottom of both the shield and the supports. The shield is wrapped with 40 layers of a dimpled super insulation. The vacuum shell is made of extruded aluminum or stainless steel. Heat load estimates for the described STL are:

Support system : 53 mW /m at 4.5 K and 670 mW /m at 40 K

Super insulation: 15 mW /m at 4.5 K and 864 mW /m at 40K

The estimated cost of the described STL is approximately \$500/m. Further STL design optimization will be required to adjust the structure to the fabrication and operating conditions of the desired NF detector solenoids and to optimize its fabrication and operational cost. Although what has been described here has been directed at the Magnetic Cavern concept, the STL could also be used in a very large LAr detector following the Glacier concept. The fact that the STL would be operating in liquid Argon would allow for a simplified STL design since the heat-load environment would be very different.

B.7 STL Solenoid Power

The relatively low inductance of the STL solenoids (0.3 H/solenoid) allows powering all solenoids from a single 50 kA power supply. A power supply with a voltage of 50 V will allow ramping the magnet system up or down in less than 1 hour. A single pair of 50 kA current leads is required for powering the solenoids. These could either be conventional copper leads or current leads based on High-Temperature Superconductor. The cryogenic wall power associated with the conventional 50 kA leads could be reduced by a factor of 4 with high T_c leads.

B.8 Conclusions

Magnetizing volumes on the order of 30,000 to 60,000 m³ at fields up to 0.5T presents technical challenges, but is certainly within the current engineering capabilities. The cost, however, in most scenarios is prohibitive. The use of room temperature Cu or Al conductor could provide a modest field (0.1T), but operating costs are likely to be excessive. Conventional superconducting magnet technology could provide the necessary field at acceptable operating costs, but the magnet construction costs using a conventional vacuum-insulated cryostat are not affordable. High T_c superconducting coils using foam insulated cryostats show promise, especially given the rapid pace in which this technology is developing. The current state-of-the-art in high T_c cable might present an affordable technical solution to this problem, but much more R&D on coil assembly, magnet quench performance and cryostat would need to be done. Using the STL concept presents some very interesting possibilities. It eliminates the cost driver of large conventional superconducting coils, the vacuum-insulated cryostat, and has already been prototyped, tested, and costed during the R&D for the VLHC. A full engineering design would still need to be done, but this technique has the potential to deliver

the large magnetic volume required with a field as high as 1T with very uniform field quality and at an acceptable cost. Developments with high T_c superconducting cable could also have an impact on the STL design concept, with potential cost savings.

C Matter effects

The matter effect causes different oscillation patterns for neutrinos and antineutrinos, depending on the mass hierarchy. Observing this difference is the most feasible way to determine the mass hierarchy. The difference may be observable with baselines longer than about 1000 km, depending on the quality and quantity of achievable data and oscillation parameters.

The difference is most visible at the MSW resonance, where the oscillations of one channel are enhanced and those of the other suppressed. For the usual neutrino parameters the resonance energy is about 10 GeV in the lithosphere, about 7 GeV in the mantle at depths relevant for the magic baseline, and about 3 GeV in the core. (The uncertainties of neutrino parameters cause an uncertainty of about 20% at θ_{13} for this prediction.) For energies much higher than the resonance energy all oscillations are suppressed, and for energies well below the resonance energy the oscillations can be treated as in vacuum.

The detailed simulation of the propagation of neutrinos through the Earth requires a sufficiently accurate knowledge of the density profile along the baseline. The uncertainties of the density profile cause correlations in the parameter space that complicate the analysis and reduce the accuracy of results. For a large θ_{13} the density uncertainty of 5% may cause rather large errors while 1% accuracy would make the correlations ignorable. With smaller θ_{13} the requirements for the accuracy are milder, and with $\sin^2 2\theta_{13} < 10^{-3}$ the dominant error comes from elsewhere and any reasonable density model will be sufficiently accurate. The correlations can be also reduced by a suitable choice of multiple baselines and channels [115].

Within first order, one can use the average density uncertainty of the baseline as an indicator of goodness. Uncorrelated local variations around the average mostly smooth out for realistic density profiles, when not in resonance, and all small-scale density variations with a scale up to a few kilometres are completely irrelevant. However, a better error analysis in a variable density requires numerical treatment, as different densities contribute differently, and particularly the resonance case should be studied with more care.

According to geophysical studies, the difference between the density of the Earth and the density defined by a standard spherical Earth model (e.g. PREM [116]) does not exceed 5%.² The uncertainties are due to both global or systematic effects for the average density distribution and unknown local variations. The local variations can be rather large, particularly for complicated zones like active mountains, subduction zones, hot spots, plumes or superplumes. Such variations may extend down to the border of the inner core. Also it is to be noted that the inner core is in rotation relative to the mantle, even its axis deviates from the rotation axis of the Earth. The detailed models for the inner parts are not yet free from inconsistencies, and therefore must be treated with care.

Using the data of local and regional geophysical measurements one can construct local models much better than the 1-dimensional PREM model. Specific local and regional models

²The errors here and throughout this section do not correspond to Gaussian distributions, but are rather "axial reasonable deviations". For any decisions on the location of experiments we need more than 1 certainty.

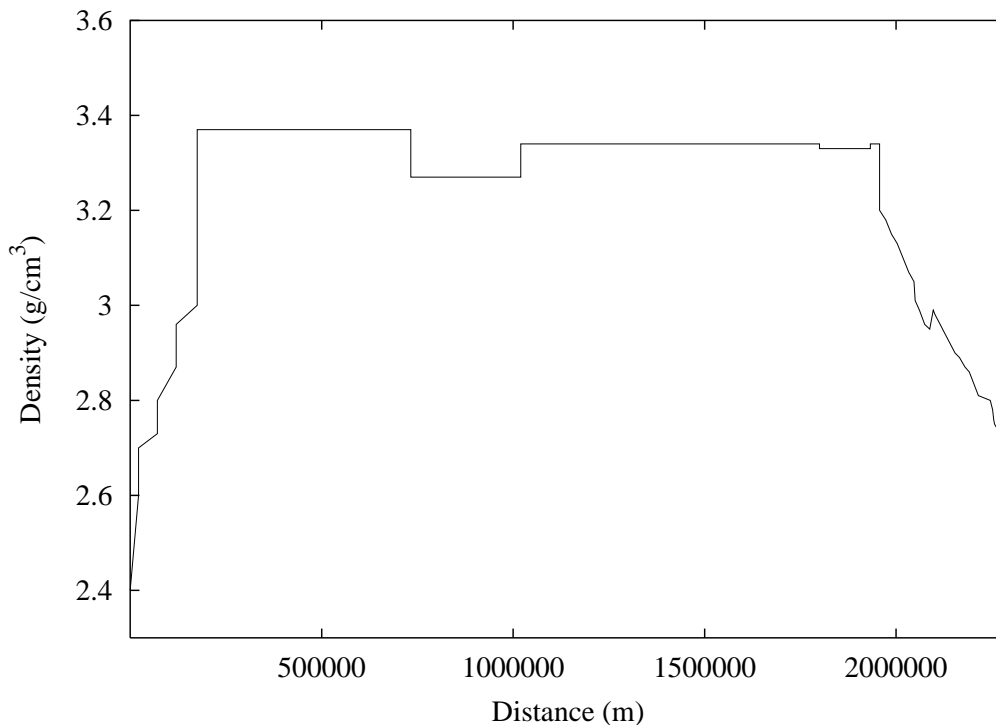


Figure 44: The estimated density profile for the baseline CERN-Pyhasalmi (Finland).

may reach up to 1% accuracy. With good geophysical measurements one can obtain knowledge to define the density profile even for complicated regions. Nevertheless, for most part of the Earth, particularly oceans, sufficiently accurate measurements cannot be done, and one has to rely on general models. The models for ocean crust are usually very simple, but one should be careful when using such models as the simplicity may be due to our ignorance.

A specific model for the baseline CERN-Pyhasalmi was constructed in Ref. [117] (Fig. 44). For this specific baseline there are abundant geophysical data, and a realistic density profile can be built up, despite some parts of the baseline being rather complicated. The most challenging part is the upswelling asthenosphere under Germany which causes the largest uncertainty. It was concluded that one can reach about 1% accuracy in estimating regional density variations (e.g. density inhomogeneities of more than several dozens kilometers) for baselines from CERN to Pyhasalmi. All later geophysical studies support the previous view, and no surprises have occurred.

It was shown explicitly in Ref. [117] that the uncertainties in this model do not cause any significant error in the interpretation of the data, with realistic experimental scenarios.

Similar studies for other baselines would be welcome (see [118] for a study in Japan). While waiting for other studies, we can extrapolate the experiences from modelling of the above baseline and from general considerations, to predict the accuracies of other profiles. Also, opinions different from those above have been expressed [119].

In order to get the best accuracy for the density profile, the following general conclusions can be drawn:

1. It is recommendable to use well known continental areas passing tectonically stable at regions.
2. One should avoid complicated zones like high mountains and seismically active or volcanic areas.
3. One should avoid oceans where little data are available.
4. Similarly one had better avoid baselines passing underdeveloped or politically challenging countries where geophysical measurements will be too risky.

These conditions may be rather contradictory: some of the most complicated zones are also the most studied, like Japan. On the other hand, particularly challenging zones are the Atlantic ridge and most of the Pacific that are both complicated and difficult to be studied.

To reach the best accuracy for the density profile, the favoured beam directions are:

From CERN towards North-East. Baseline lengths up to 2700 km are achievable with 1% accuracy for the density. On-going and planned geophysics measurements can improve the accuracy even more.

Across North-America. Similar accuracies are reachable for the USA when the USA array gives data. Baseline lengths up to 4000 km are possible from BNL to West Coast of the USA, and baselines up to 4000{5000 km can be achieved through Canada to Alaska.

Geophysically disfavoured directions include beams from CERN to Canary Islands, Azores, Madeira or Iceland, as well as any baseline around Japan.

For other long baselines the accuracy of density may not be better than 2{3%. The above favoured baselines cannot be extended due to geographic constraints, and hence the longer baselines necessarily must pass through complicated or worse known zones. Baselines 4500{6000 km may be particularly difficult when the baseline crosses the transition zone and touches tangentially boundary layers at the depths of 400 km and 660 km, with density jumps of 5% and 10%, respectively. In such a case a small error in the model may cause a considerable error in the baseline density profile. For the most difficult oceanic baselines one can hardly reach 5% accuracy for the average density.

When the baseline length equals the refraction length or its multiples one can do a clean measurement of the θ_{13} mixing angle, independent on the CP-phase [120, 121, 122]. These baselines are called magic, and can be solved analytically in constant density, but in varying density they must be computed numerically, for example by solving the equation:

$$\int_0^{L_{\text{magic}}} \exp(i \int_0^x V(y) dy) dx = 0; \quad (9)$$

where $V(y)$ is the interaction potential in matter, which is proportional to the electron density. Equation 9 gives a good first order approximation [123, 122] to the magic baseline. Integrating the above using the PREM model and two extreme cases with arbitrary 5% uncertainties for the density, and a 5 km uncertainty for the core-mantle boundary, the first magic length turns out to be (7300 \pm 300) km long, the second (10060 $^{+70}_{-50}$) km and the third (12280 $^{+170}_{-140}$) km. For the first magic baseline, the dominant error comes from the deep mantle, and detailed knowledge of the crust in start and end points is rather irrelevant. For the other two magic baselines the uncertainty of the length is surprisingly small, considerably smaller than for the

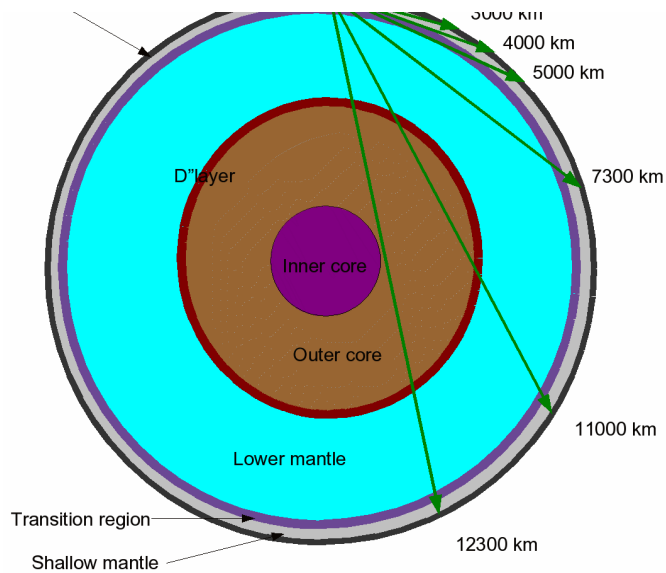


Figure 45: Several baselines projected through the model of the Earth interior (not to scale). A baseline of 5000 km may be problematic as it largely intersects with the transition zone, where the density changes quite abruptly from 4.0 to 4.4, and errors on its depth may result in large errors in the density profile. We see that the second and third magic baselines (11000 km and 12300 km) traverse through the outer core that dominates their refraction lengths.

first one. This may sound paradoxical, but is understandable from Fig. 45. These baselines pass through the dense outer core which gives the largest contribution to the total refraction length, and also to the error. For these baselines, the details of the lithosphere are completely ignorable, but the quoted 5% accuracy for the core density and particularly the 5 km accuracy for the core-mantle boundary may be rather optimistic.

The first magic baseline is not very sensitive to such uncertainties [124] (See also respective sections in ISS Physics Report for analyses and references). On the other hand, the second and particularly the third magic lengths are more sensitive to errors, which makes them less usable for neutrino studies until better certainty on the core conditions can be reached. Alternatively, it has been suggested to use neutrinos to measure the density of the mantle or core [125, 126, 127, 128, 124].

There is no geophysically optimal candidate for a magic baseline from the proposed sites of the accelerator. In any case it is safest to use continental baselines, and avoid oceans and complicated zones. Most important is to choose the baseline so that we can maximize the accuracy in the deepest parts of the trajectory, while the properties of the lithosphere at the end points are less relevant. CERN to Eastern Siberia or Northern China may be closest to optimal, and from Japan the best direction is towards Northern Europe.

We conclude that it is possible to obtain sufficient accuracy for the density profile to avoid correlations. Future measurements may improve the accuracy, and if necessary, a dedicated geophysical measurement campaign for the selected baseline can be made, at a cost which is marginal to total cost. However, in practice such measurements are possible only in limited parts of the Earth, and particularly oceanic measurements will remain unrealistic for a long time. If the mixing angle is small enough, density uncertainties are irrelevant and any baseline

is good enough. For defining the length of the magic baseline, however, uncertainties of the density are relevant for all parameters, but in practice the physics is not very sensitive to them.

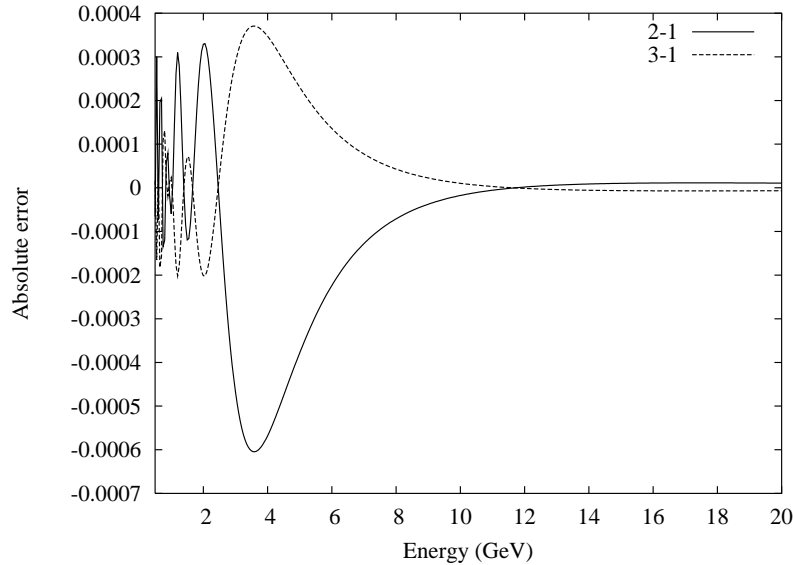


Figure 46: A sample plot presenting the effect of the uncertainties in the density profile of Fig. 44 to the muon neutrino appearance probability due to errors in density. These correspond to the absolute deviation in the probability with typical parameters.

D Low energy cross sections

Existing cross-section measurements cover properly the high-energy regime, above 5 GeV, but not the low-energy where many of the new oscillation experiments will operate. In this region, the energy is crossing several threshold of interactions. The knowledge of the cross-section in this regime is very limited, see [129] for a recent compilation. In addition to the intrinsic knowledge of the interaction, the final state particles are affected by nuclear effects like nuclear re-interactions, Pauli blocking and Fermi motion that alters the topology and kinematics of the outgoing particles.

The final state interactions could change the momentum and nature of nucleons and pions produced in the interactions. Both charged and neutral pions contribute to the background in disappearance (charged pions faking a muon) and appearance (neutral pion faking an electron) experiments and should be understood to a 10% level for the next generation of superbeams [22].

The nuclear effects also alter the kinematics of the final state muon in charged current interactions by inhibiting the reaction (Pauli blocking) or changing the center of mass energy where the reaction takes place (Fermi motion). These phenomena change basic kinematic properties of the interaction like the q^2 or the threshold of the reaction. The dependency of the cross-section with the nuclear mass (A) has to be considered, since most of the measurements are done in light nuclei (deuterium, carbon, oxygen, etc.). The measurement of

the dependency of cross-section with A is part of the experimental program of the MINER experiment [131].

The dominant neutrino interactions from 500 MeV to few GeV are :

- Charged current quasi-elastic and neutral current elastic interactions.
- Neutral and charged current single pion production.
- Neutral and charged current multipion production and more inelastic interactions.
- Neutral and charged current coherent pion production.

A compilation of actual knowledge on cross-sections is shown in Fig.47 for charged current neutrino and anti-neutrino interactions.

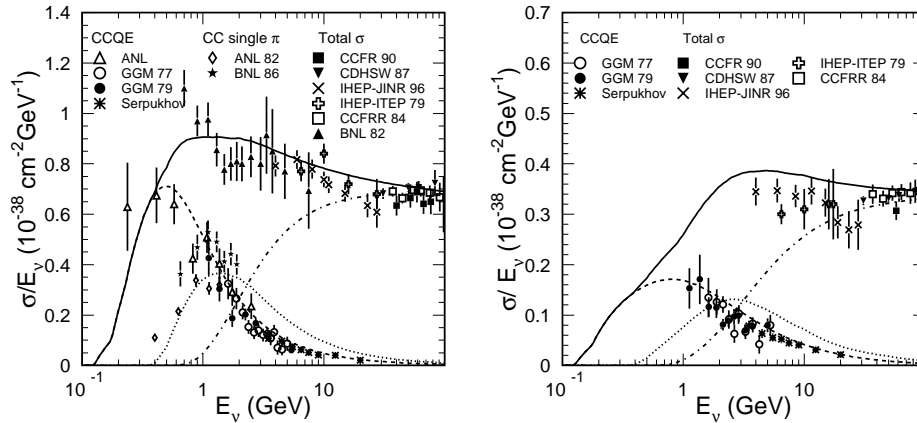


Figure 47: Cross-section experimental values as a function of the neutrino energy (left). Results are compared to NEUT [132] Monte Carlo simulation. Points show the experimental data: BNL 82 [133], CCFR 90 [134], CDHSW 87 [135], IHEP-JINR 96 [136], IHEP-ITEP 79 [137], CCFRR 84 [138], ANL 82 [139], BNL 86 [140], ANL [141], GGM 77 [142], GGM 79 [143] and Serpukhov [144]. Cross-section experimental values as a function of the anti-neutrino energy (right). Results are compared to NEUT [132] Monte Carlo simulation. Points show the experimental data: CCFR 90 [134], CDHSW 87 [135], IHEP-JINR 96 [136], IHEP-ITEP 79 [137], CCFRR 84 [138], GGM 77 [142], GGM 79 [143], and Serpukhov [144].

In general, the available data is old (from the 70's and 80's), normalized to charged current quasi-elastic using obsolete form factors and the beam spectrum and flux was based on dubious hadron production models. The nuclear corrections are also not well documented or inconsistent, the data is sparse, low statistics and sometimes inconsistent. The panorama is even worse when we consider production of more than one pion in the final state.

Note that all existing cross-section measurements above 200 MeV refer always to muon neutrinos and anti-neutrinos. The τ and e cross sections have not being measured due to the intrinsic difficulties to produce the appropriate neutrino beam and due to neutrino detection techniques. The cross-section can be safely assumed to be equal to that of muon neutrinos, except when we are close to the threshold and the mass of the final state lepton

together with the nuclear effects play an important role. This is specially critical in the case of the low-energy beams. The beam search for the transition of e to ν , the low energy version is being designed for energies from 100 MeV to 500 MeV. This is the energy region that has the largest uncertainties in the relative cross-sections between e and ν . Dedicated experiments will be needed in this case to control the systematic errors to the required level, 0.1 %.

D.1 Neutral current elastic and charge current quasi-elastic interactions

This interaction is of vital importance since it provides a method to reconstruct the neutrino energy. The actual knowledge of the cross-section is not better than 20%, Theory is based on Conserved Vector Current (CVC), Partially Conserved Axial Current (PCAC) and form factors measured in electron nucleus scattering. The axial form factor is not known and it is normally parametrized as a dipolar form factor with the axial mass as a free parameter. It should be noticed that this parameter changes the total cross-section and the q^2 of the interactions. Both methods had been used to measure the parameter, coming to contradictory results as it was noted in [130]. Future experiments [131, 22, 21] will be able to measure if the axial form factor departs from the simplistic dipole form.

The neutral current elastic scattering is not of relevant importance for oscillation experiments, although they can be used to determine the strange quark content inside nucleons.

D.2 Charge and Neutral Current resonance: single and multipion production

The production of charged and neutral pions are important backgrounds to both disappearance and appearance experiments. The knowledge of the resonance cross-section is difficult to model. To the lack of knowledge of the standard axial form factors we have to add the uncertainties on the amplitude of high mass resonances in the transition region to the deep inelastic. There are also models [145] showing that the non-resonant contributions could be relevant and affect the cross-sections very close to threshold. The non-resonant contribution is clearly present in n channels. Nieves [145] argued that it is probably necessary to depart from $C_5^A(0) = 1.2$, which is the PCAC dictated value of the leading axial form factor for the excitation.

The neutral current resonant pion production should also be measured since they are background for appearance and also disappearance experiments, with the pion being identified as a neutrino flavor tagging lepton. The nuclear reinteractions are very relevant at this stage altering the sign of the pion leaving the nucleus. The nuclear reinteraction cross-sections are known to a 20 to 30% and they are difficult to measure in standard neutrino experiments. It is possible that T2K will be able to address this measurement with the near detector that has good particle identification capabilities and momentum resolution, see [22].

D.3 Neutral and charged current multipion production and deep inelastic interactions

Deep inelastic cross-sections have been measured at high energies. The theoretical framework, based on structure functions, is well established and it has been measured in different experimental conditions. But, there are still some unclear items: nuclear effects, low q^2 region and the transition region to the resonant (single and multipion) neutrino interactions.

As an example of the situation, the implementation of the transition region in the NEUT Monte Carlo is done as a mixture of experimental results and standard Monte Carlo tools. NEUT produces pions in the final state according to FN L-7 [146] results for a region where $1.3 \text{ GeV} < W < 2.0 \text{ GeV}$ (W is the invariant mass of the hadronic current) and according to JET SET 7.4 [147] above this value.

D.4 Charge and Neutral Current coherent pion production

The neutral current coherent pion production has been measured at relatively high energies (2.0 GeV) and heavy nuclei. The values for light nuclei and low energies are not available and they might depend on the theoretical model for extrapolations. Miner a [131] and the near detector of T2K [21] will be able to provide measurements for these reactions that are very important to determine the background on ν_e appearance. Anyhow, this background will be mainly produced by interactions of high energy neutrinos.

The charged current coherent production is related to the neutral current cross-section at higher energies but the relation might be distorted at low energies as it was suggested by a recent K2K result [148] due to the mass of the muon [149].

D.5 The cross-section double ratio

As discussed already in section 3, the precise measurement of the CP asymmetry

$$A_{CP} = \frac{P(\nu \rightarrow \nu_e) - P(\bar{\nu} \rightarrow \bar{\nu}_e)}{P(\nu \rightarrow \nu_e) + P(\bar{\nu} \rightarrow \bar{\nu}_e)}; \quad (10)$$

or precise measurement of any appearance probability, will require knowledge of the cross-section, efficiency and background of both the initial channel (for the near detector normalization) and of the appearance channel. The ratio to worry about is the electron-to-muon neutrino cross-sections. Indeed, the troublesome quantity is the double ratio:

$$DR = \frac{R_{\nu_e}}{R_{\bar{\nu}_e}}; \quad (11)$$

where R_{ν_e} really means $R_{\nu_e}^B$, including a correction for efficiency and background B . Although it would seem that many systematic errors would cancel in this ratio, this is only partially true. The effects that ensure a deviation of this quantity from unity are quite difficult to master:

- the muon mass effect;

- Fermi motion and binding energy;

- the non-isoscalarity of the target (this is particularly relevant for water where anti-neutrinos and neutrinos interact very differently on the free protons);

- the different neutrino and antineutrino y distributions; and

- the different appearance of the final state lepton in the detector.

These effects are particularly relevant for the low energy neutrinos, as will be discussed here. One can legitimately wonder whether everything needs to be measured or if theory cannot help by predicting the double ratio using safe assumptions. Such an analysis was developed by Jan Sobczyk and collaborators [150]. If one concentrates on low energies, the dominant cross-sections will be quasi-elastics. The cross-sections for the four relevant species of neutrinos are shown on the top line of Figure 48.

The muon threshold effect is clearly visible. Due to the different inelasticity (or γ distribution) of neutrinos vs antineutrinos, the muon mass correction is however not the same for neutrinos and antineutrinos, by an amount that can be quite large (20%).

The next thing to worry about are nuclear effects, which are nucleus dependent and particularly relevant in water where antineutrinos can interact on the free protons, while neutrinos cannot. These can be broadly separated in two classes, binding energy and Fermi motion. The description of the effect of binding energy is considered to be quite uncertain given that the debris of the nucleus from which the struck nucleon originates probably take away some of the binding energy in the reaction, and it cannot entirely be attributed to the struck nucleon. The resulting effect on the double ratio is extremely large at low energies, because of the existence of antineutrino interactions on the free protons. The region below 250 MeV probably cannot be trusted and the region above should be seen as having an uncertainty given by the following factors.

The uncertainty on the description of Fermi motion could be evaluated with the guidance given by the difference between the Spectral Function approach and the Fermi Gas model. Around 250 MeV this leads to an uncertainty of about 2% on the double ratio.

The uncertainty due to the binding energy modelling. A shift by, say, 50% of the binding energy itself would change the double ratio by another 2%.

There is also a large uncertainty related to the Impulse Approximation (IA) used in cross section computations. The IA assumes that the relevant degrees of freedom are individual nucleons. The analysis of electron scattering data clearly shows that the IA is reliable only for momentum transfers $q > 400$ MeV [151]. On the other hand, at a neutrino energy ≈ 400 MeV, about 40% of the cross section calculated within the IA corresponds to lower values of q (Fig. 49). This is a source of large uncertainty which is difficult to estimate. Of course, one can be optimistic and believe that the ratios are not affected much by the use of the IA, but it is a source of additional systematic error.

Thus from considerations on total cross-sections alone, a fundamental uncertainty of the order of 3-4% can be ascertained. The energy of 250 MeV incidentally corresponds to the oscillation maximum for the distance between CERN and Frejus. Taking into account the difficulties that will be associated with the different energy spectra and detection efficiencies for muons and electrons, it seems very unlikely that an uncertainty of less than 5% on the double ratio DR can ever be achieved at low energies from a combination of simulations and theory.

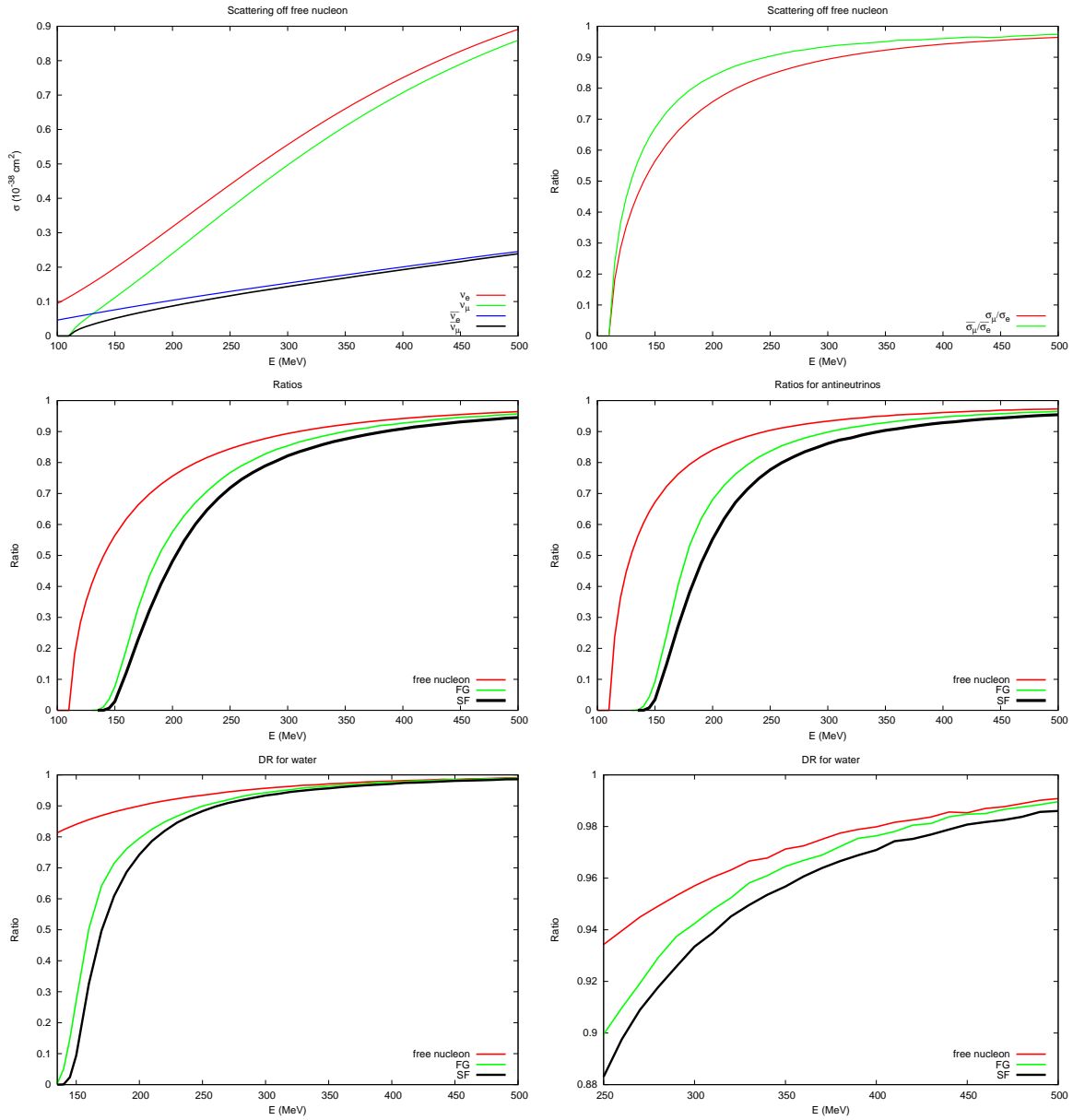


Figure 48: Top Left: quasi-elastic cross-sections on free nucleon (neutron for neutrinos and protons for anti-neutrinos) for electron and muon neutrinos and antineutrinos. The muon threshold is clearly visible. Top Right: the ν_μ to ν_e and $\bar{\nu}_\mu$ to $\bar{\nu}_e$ cross-section ratios showing the effect of the different y -distributions. Middle Left: the cross-section ratios between muon- and electron neutrinos (left) and antineutrinos (right) taking into account nuclear effects, compared to those on free nuclei. The binding energy shows up as a shift in the threshold, but the exact description of this is considered uncertain; the curves correspond to modelling the nucleus with the Fermi Gas Model (FG) or with the Spectral Function approach. Bottom Left: the double ratio in water from threshold to 1 GeV, and in the 'reliable' region above 250 MeV (right).

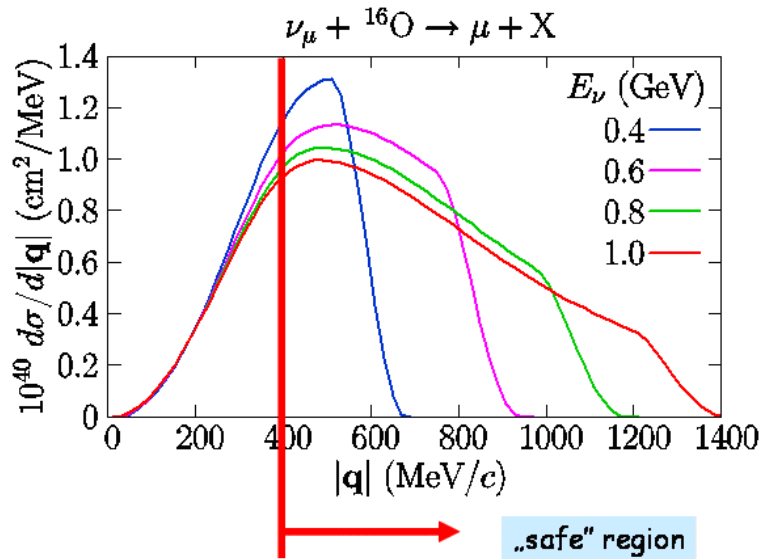


Figure 49: Differential cross section of $\nu_\mu + {}^{16}\text{O} \rightarrow \mu + X$ as a function of momentum transfer, at several values of neutrino energy. The Impulse Approximation is only reliable in the region with $|\mathbf{q}| > 400 \text{ MeV}$.

References

- [1] <http://www.lnf.infn.it/conference/2005/nufact05/>
- [2] <http://dpnc.unige.ch/users/blondel/detectors/detector-study.htm>
- [3] ISS report, Physics section, RAL-TR-2007-019, arXiv: 0710.4947 [hep-ph]
- [4] E. Keil, CERN-NUFACT Notes 54, Power Deposition due to Muon Decay Losses in a Neutrino Factory (2000) available from <http://molat.home.cern.ch/molat/neutrino/nf54.pdf>
- [5] E. Keil, CERN-NUFACT Notes 56, Electron Cloud at the CERN Muon Storage Ring (2000) available from <http://molat.home.cern.ch/molat/neutrino/nf56.pdf>
- [6] M. L. Mangano et al, Physics at the front-end of a neutrino factory. in ECFA/CERN studies of a Neutrino Factory complex, CERN report 2004-002, A. Blondel et al, eds.
- [7] A. Broncano and O. Mena, Corrections to the fluxes of a Neutrino Factory, hep-ph/0203052, May 2002.
- [8] A. Blondel, in Prospective study of muon storage rings at CERN, CERN 98-02, ECFA 99-197 (1999) p. 51-54.
- [9] R. Raja and A. Tollestrup, Calibrating the energy of a 50 GeV Muon Collider using g-2 spin precession, Phys. Rev. D 58, (1998)13005.

- [10] I. Papadopoulos, Impact of the muon beam divergence and polarisation on the prediction accuracy of the neutrino flux at a distant detector of a neutrino factory, Proceedings NUFACT00, Monterey California, (2000)
- [11] R. Pereira, Measurement of the muon beam size and divergence in the Muon storage ring of a neutrino factory, internal report, Stage de Magistere, Ecole Normale superieure de Paris, (2001).
- [12] A. Blondel, Muon Polarisation in the neutrino factory, Nucl. Instr. Meth. A 451, (2000) p. 131.
- [13] R. Femow, J. Gallardo, Y. Fukui, Muon polarisation effects in the front end of the neutrino factory, MUCOOL-note 129, (2000) http://www-mucool.fnal.gov/mnotes/public/pdf/muc0129/muc0129_abs.txt see also: A. Blondel, M. Donega and S. Gilardoni, CERN NUFACT-Note-078 (2000), <http://nicewww.cern.ch/molat/neutrino/nf78.pdf>
- [14] C. Johnson, R. B. Palmer and E. Keil, A cost-effective design for a neutrino factory Nucl. Instr. Meth. A 451, (2000) p. 265.
- [15] The CERN Neutrino beam to Gran Sasso (Conceptual Technical Design), Ed. K. Elsener, CERN 98-02, INFN/AE-98/05; Addendum to report CERN 98-02, INFN/AE-98/05, R. Bailey et al., CERN-SL/99-034(DI), INFN/AE-99/05; Update of changes to CNGS layout and parameters, M. Clement et al., SL-Note-2002-012.
- [16] MINOS Detectors, Technical Design Report, P. Adamson et al., The MINOS Collaboration, NUMINote NUMIH-337.
- [17] NUMI Technical Design handbook, http://www-numi.fnal.gov/numwork/tdh/tdh_index.html
- [18] J. McDonald et al., Nucl. Instr. and Meth. A in Phys. Res. 496 (2003) 293-304.
- [19] A. Ferrari, A. Guglielmi, P. R. Sala, Nucl. Phys. B (Proc. Suppl.) 145 (2005), 93-97.
- [20] Y. Ajima et al., "Tokai-to-Kamioka (T2K) Long Baseline Neutrino Oscillation Experiment Proposal", Program Advisory Committee for Nuclear and Particle Physics Experiments, Proposal 060611, J-PARC, Japan, <http://jparc.jp/NuclPart/pac.0606/pdf/p11-Nishikawa.pdf>
- [21] D. Karlen, Nucl. Phys. Proc. Suppl. 159 (2006), 91-96.
- [22] Y. Yamada, Nucl. Phys. Proc. Suppl. 155 (2006), 28-32 and 207-208.
- [23] P. Perez, Nucl. Instr. and Meth. A in Phys. Res. 451 (2000) 216-217.
- [24] A. Blondel (ed.) et al., ECFA/CERN Studies of a European Neutrino Factory Complex, CERN-2004-002-ECFA-04-230, CERN, Geneva, (2004), 365 p.
- [25] K. MacFarland, Nucl. Instr. and Meth. in Phys. Res. A 451 (2000) 218-228.
- [26] L. B. Okun, "Leptons and Quarks", Amsterdam, Netherlands: North-holland (1982).
- [27] P. Vilain et al., Phys. Lett. B 364 (1995), 121-126.

- [28] P. Vilain et al., *Phys. Lett. B* 335 (1994), 246-252.
- [29] See International Workshop on Neutrino-Nucleus Interactions. NUINT-04: <http://nuint04.lngs.infn.it/> and NUINT-05: <http://fphy.hep.okayama-u.ac.jp/NUInt05/>
- [30] M. Ellis, F.J.P. Soler, *Nucl. Instr. and Meth. in Phys. Res. A* 569, 127-131 (2006).
- [31] J. Aitegoer et al., *Nucl. Instr. and Meth. in Phys. Res. A* 404, 96-128, (1998).
- [32] G. Barichello et al., *Nucl. Instr. and Meth. in Phys. Res. A* 419, 1-15, (1998).
- [33] G. Barichello et al., *Nucl. Instr. and Meth. in Phys. Res. A* 506, 213-237, (2003).
- [34] M. Ellis, F.J.P. Soler, *Journal of Physics G : Nuclear and Particle Physics*, 29, (2003), 1975-1979.
- [35] P. Astier et al., NOMAD Collaboration, *Phys. Lett. B* 486 (2000), 35-48.
- [36] R. Turchetta et al., *Nucl. Instr. and Meth. in Phys. Res. A* 458, 677-689 (2001).
- [37] J.J. Velthuis et al., *Nucl. Instr. and Meth. in Phys. Res. A* 560, 40-43 (2006).
- [38] J.J. Velthuis et al., *Nucl. Instr. and Meth. in Phys. Res. A* 569, 57-60 (2006).
- [39] E. Eskut et al., *Nucl. Instr. and Meth. in Phys. Res. A* 401, 7-44 (1997).
- [40] A. Kayis-Topaksu et al., *Phys. Lett. B* 626 (2005) 24-34.
- [41] G. Onengut et al., *Phys. Lett. B* 614 (2005) 155-164.
- [42] G. Onengut et al., *Phys. Lett. B* 613 (2005) 105-117.
- [43] G. Onengut et al., *Phys. Lett. B* 604 (2004) 11-21.
- [44] G. Onengut et al., *Phys. Lett. B* 604 (2004) 145-156.
- [45] A. Kayis-Topaksu et al., *Phys. Lett. B* 549 (2002) 48-57.
- [46] A. Cervera, F. Dydak and J.J. Gomez Cadenas. *Nucl. Inst. Meth. A* 451, 123 (2000).
- [47] A. Cervera et al., *Nucl. Phys. B* 579, 17 (2000).
- [48] A. Cervera-Villanueva. *Nucl. Phys. B* 149, 201 (2005).
- [49] M. Selvi, Ph.D. thesis, Bologna University, 2002. <http://www.bo.infn.it/selvi/tesips.gz>
- [50] <http://www.inscres.infn.it/>
- [51] E. Ables et al. (MINOS Collaboration), *Fermilab Proposal P-875* (1995).
- [52] A. Cabrera and J. Hartnell *Nucl. Phys. B* 143, 569 (2005).
P. Adamson et al., *Nucl. Inst. Meth. A* 556, 119 (2006).
- [53] G. Bari et al., *Nucl. Inst. Meth. A* 508, 170 (2003).
- [54] GEANT 3.21, CERN Program Library, Long Writeup W 5013

- [55] G. Ingelman, A. Edin and J. Rathsmann, *Comp. Phys. Comm.* **101**, 108 (1997).
- [56] R.L. Gluckstern, *Nucl. Instrum. Methods* **24**, 381 (1963).
- [57] Talk by D. Harris, "Minos and Nova", at W IN 07 (Kolkata, India)
- [58] <http://www-nova.fnal.gov/>
- [59] http://www.lnf.infn.it/conference/nufact05/talks2/WG1/Nelson_Magnetic_Tracking_WG1.pdf
- [60] <http://dpnc.unige.ch/users/blondel/ISS-4/iss4-sci-20060821.ppt>
- [61] <http://minerva.fnal.gov/>
- [62] A. Cervera, J.J. Gomez and J.A. Hernandez, *Nucl. Inst. Meth. A* **534**, 180 (2004).
- [63] A. Braem, C. Joram, J. Seguinot, P. Lavoute and L. Pierre, 11th Vienna Conference on Instrumentation (VCI 2007), Vienna, Austria, 19-24 Feb 2007, *Nucl. Instrum. Methods Phys. Res. A* **581** (2007) 469-472. CERN-PH-EP-2007-007.
- [64] A. Braem, C. Joram, J. Seguinot, P. Lavoute and C. Mousant, *Nucl. Instrum. Meth. A* **570** (2007), 467-474. CERN-PH-EP-2006-025.
- [65] C. Rubbia, CERN-EP/77-08 (1977).
- [66] E. Aprile, K.L. Giboni and C. Rubbia, *Nucl. Instrum. Meth. A* **241**, 62 (1985).
- [67] S. Amerio et al., *Nucl. Instrum. Meth. A* **527** (2004) 329.
- [68] P. Benetti et al., *Nucl. Instrum. Meth. A* **332** (1993) 395.
- [69] P. Cennini et al., *Nucl. Instrum. Meth. A* **345** (1994) 230.
- [70] F. Amendo et al. [ICARUS-Milano Collaboration], *Phys. Rev. D* **74** (2006) 112001 [arXiv:physics/0609205].
- [71] A. Ferrari, A. Rubbia, C. Rubbia and P. Sala, *New J. Phys.* **4** (2002) 88.
- [72] A. Meregaglia and A. Rubbia, *JHEP* **0611** (2006) 032 [arXiv:hep-ph/0609106].
- [73] A. Rubbia, in Proceedings of the 11th International Conference on Calorimetry in High Energy Physics, Perugia 2004, p. 485-506 [arXiv:hep-ph/0407297].
- [74] A. Bueno et al., *JHEP* **04**, (2007), 041. arXiv:hep-ph/0701101.
- [75] A. Rubbia, in Proceedings of the 9th International Symposium on Neutrino Telescopes, Venice 2001, p. 435-462 [arXiv:hep-ph/0106088].
- [76] A. Bueno, M. Campanelli, S. Navas-Concha and A. Rubbia, *Nucl. Phys. B* **631**, 239 (2002) [arXiv:hep-ph/0112297].
- [77] A. Rubbia, in Proceedings of the 2nd International Workshop on Neutrino Oscillations in Venice (NO-VE 2003), p. 321-350 [arXiv:hep-ph/0402110].

- [78] A. Badertscher, M. L. Lancia, A. Meregaglia and A. Rubbia, *New J. Phys.* 7, 63 (2005) [arXiv:physics/0412080].
- [79] A. Badertscher, M. L. Lancia, A. Meregaglia, A. Müller and A. Rubbia, *Nucl. Instrum. Meth. A* 555, 294 (2005) [arXiv:physics/0505151].
- [80] A. Ereditato and A. Rubbia, *Nucl. Phys. Proc. Suppl.* 155 (2006) 233 [arXiv:hep-ph/0510131].
- [81] A. Ereditato and A. Rubbia, *Nucl. Phys. Proc. Suppl.* 154 (2006) 163 [arXiv:hep-ph/0509022].
- [82] T. Strauss, "First test of a liquid Argon TPC in magnetic field produced by a HTS coil", ETH Z diploma work. Available at <http://neutrino.ethz.ch>.
- [83] American Superconductor, <http://www.amsuper.com>.
- [84] SuperPower, Inc., <http://www.superpower-inc.com>.
- [85] Technodyne International Limited, Unit 16 Shakespeare Business Center, Hathaway Close, Eastleigh, Hampshire, SO 50 4SR, see <http://www.technodyne.co.uk>
- [86] J. Hylen et al., FERMILAB-TM-2018 (1997).
- [87] C. Bromberg et al., FERMILAB-FN-0776-e (2005).
- [88] D. Finley talk at NNN 2006 in Seattle Washington on September 21, 2006 { <http://lartpc-docdb.fnal.gov/cgi-bin/ShowDocument?docid=211>
- [89] A. Cervera, A. Donini, M. B. Gavela, J. J. Gomez Cadenas, P. Hernandez, O. Mena and S. Rigolin, *Nucl. Phys. B* 579 (2000) 17 [Erratum *ibid.* B 593 (2001) 731] [arXiv:hep-ph/0002108].
- [90] M. Güler et al., OPERA Proposal CERN/SPSC 2000-028, CERN/SPSC 2001-025; Y. Declais et al., CERN-SPSC 2002-029, <http://operaweb.web.cern.ch/operaweb/documents/index.shtml>.
- [91] R. Acquafredda et al. [OPERA Collaboration]. *New J. Phys.* 8 (2006) 303.
- [92] M. Kaplan, B. Peters and D. Ritson, *Phys. Rev.* 85 (1952) 900.
- [93] W. H. Barkas, *Nuclear research emulsions*, Academic Press, London (1963); C. F. Powell et al., *The study of elementary particles by the photographic method*, Pergamon Press, New York (1959).
- [94] A. Donini, D. Mebni and P. Migliozzi, *Nucl. Phys. B* 646 (2002) 321 [arXiv:hep-ph/0206034].
- [95] D. Autiero et al., *Eur. Phys. J. C* 33 (2004) 243 [arXiv:hep-ph/0305185].
- [96] G. Acquistapace et al., CERN 98-02 and INFN/AE-98/105 (1998); R. Bailey et al., Addendum to Report CERN 98-02, CERN-SL 99034 and INFN/AE-99/05 (1999); A. E. Ball et al., SL-Note 2000-063 (2000); CNGS project: <http://projcngs.web.cern.ch/projcngs/>.

- [97] T. Nakamura et al., Nucl. Instr. Meth. A 556 (2006) 80.
- [98] L. Arrabito et al., Journal of Instrumentation 2 (2007) P02001 [arXiv:physics/0701192]
- [99] T. Toshito et al., Nucl. Instrum. Meth. A 516 (2004) 436.
- [100] M. De Serio et al., Nucl. Instrum. Meth. A 554 (2005) 247.
- [101] G. D. Lellis et al., Nucl. Instrum. Meth. A 512 (2003) 539.
- [102] K. Kodama et al., Nucl. Instrum. Meth. A 493 (2002) 45.
- [103] P. Migliozzi, Talk given at the 2nd Meeting of the International Scoping Study for a Neutrino Factory and Super-beam Facility, January 23-25, 2006, KEK.
- [104] C. Fukushima, M. Kinura, S. Ogawa, H. Shibuya, G. Takahashi, T. Hara and K. Kodama, Study of a compact emulsion spectrometer for identification of neutrino/anti-neutrino interactions, paper in preparation.
- [105] L. S. Esposito, Talk given at the 3rd Meeting of the International Scoping Study for a Neutrino Factory and Super-beam Facility, April 24-28, 2006, Rutherford Appleton Laboratory.
- [106] I. Adam et al., Nucl. Instr. and Meth. a 538 (2005), 281.
- [107] Mike Green, Private communication.
- [108] Mike Green, Private communication.
- [109] Design study for a staged Very Large Hadron Collider, Fermilab-TM-2149, June 4, 2001.
- [110] M. A. Green and S.J. St. Lorant, Estimating the cost of Large Superconducting Thin Solenoid Magnets", Advances in Cryogenic Engineering, 39, 1994. Also LBL-35002.
- [111] A. Herve et al., Status of the CMS Magnet, IEEE Trans. on Applied Superconductivity, 12, No. 1, (2002).
- [112] Balbekov et al., MUCoolNote 216, MUC/NOTE/COOL-EXP//216, 2001.
- [113] <http://www.amsuper.com/products/htsWire/index.cfm>.
- [114] A. Herve, Private communication 2007.
- [115] A. Blondel, A. Cervera-Villanueva, A. Donnini, P. Huber, M. Mezzetto, P. Strolin, Acta Phys. Poln. B 37 (2006) 2077-2113. hep-ph/0606111
- [116] A. M. Dziewonski and D. L. Anderson, Phys. Earth Planet. Inter. 25, 297 (1981).
- [117] E. Kozlovskaya, J. Peltoniemi and J. Sarkamo, hep-ph/0305042.
- [118] L.Y. Shan, Y.F. Wang, C.G. Yang, X. Zhang, F.T. Liu, B.L. Young, Phys. Rev. D 68 (2003) 013002. hep-ph/0303112.
- [119] M. Warner, International Scoping Study presentation, <http://www.hep.ph.ic.ac.uk/uknc/iss0406/detector.html>

- [120] V. Barger, D. Marfatia and K. Whisnant, *Phys. Rev. D* 65 (2002), 073023. hep-ph/0112119.
- [121] P. Huber, W. Winter, *Phys. Rev. D* 68 (2003), 037301. hep-ph/0301257.
- [122] A. Yu. Smirnov, hep-ph/0610198.
- [123] E. K. Akhmedov, M. Maltoni, A. Yu. Smirnov, *Phys. Rev. Lett.* 95 (2005) 211801. hep-ph/0506064.
- [124] R. Gandhi, W. Winter, *Phys. Rev. D* 75 (2007), 053002. hep-ph/0612158.
- [125] T. Ohlsson, W. Winter, *Europhys. Lett.* 60 (2002), 34-39. hep-ph/0111247.
- [126] T. Ohlsson, W. Winter, *Phys. Lett. B* 512 (2001), 357-364. hep-ph/0105293.
- [127] W. Winter, *Phys. Rev. D* 72 (2005) 037302. hep-ph/0502097.
- [128] H. Minakata, S. Uchinami, To appear in *Phys. Rev. D*. hep-ph/0612002.
- [129] Jarosław A. Nowak, Jan T. Sobczyk, *Acta Phys. Poln. B* 37 (2006) 1955-1966.
- [130] K. S. Kuzmin et al., *Acta Phys. Poln. B* 37 (2006) 2337-2348.
- [131] K. S. McFarland, *Nucl. Phys. Proc. Suppl.* 159 (2006) 107-112.
- [132] J. Kamada, Published in "Kashiwa 2004, Sub-dominant oscillation effects in atmospheric neutrino experiments" 131-141.
- [133] N. J. Baker et al., *Phys. Rev. D* 25 (1982) 617.
- [134] P. S. A. Uchinoss et al., *Z. Phys. C* 48 (1990) 411.
- [135] J. P. Berge et al., *Z. Phys. C* 35 (1987) 443.
- [136] V. B. Anikeev et al., *Z. Phys. C* 70 (1996) 39.
- [137] A. I. Mukhin et al., *Sov. J. Nucl. Phys.* (1979) 30.
- [138] D. M. McFarlane et al., *Z. Phys. C* 26 (1984) 1.
- [139] G. Radecky et al., *Phys. Rev. D* 25 (1982) 116.
- [140] T. Takagaki et al., *Phys. Rev. D* 34 (1986) 2554.
- [141] S. Barish et al., *Phys. Rev. D* 16 (1977) 3103.
- [142] S. Bonetti et al., *Nuovo Cimento* 38 (1977) 260.
- [143] M. Pohl et al., *Nuovo Cimento* 26 (1979) 332, N. Arminise et al., *Nucl. Phys. B* 152 (1979) 365.
- [144] S. Belikov et al., *Z. Phys.* 320 (1985) 625.
- [145] E. Hernandez, J. Nieves and M. Valverde, hep-ph/0701149

- [146] S.J. Barish et al., *Phys. Rev. D* 17 (1978) 1.
- [147] T. Sjöstrand et al., CERN-TH-7112-93 (1994).
- [148] H. Hasegawa et al. *Phys. Rev. Lett.* 95 (2005) 252301.
- [149] D. Rein and L.M. Sehgal, hep-ph/0606185
- [150] J. Sobczyk et al. , Neutrino cross-sections in the few MeV region, ISS meeting, RAL, April 2006, unpublished.
- [151] Artur M. Ankowski, Jan T. Sobczyk, (2007) arXiv:0711.2031 [nucl-th].